A Space Communications Study

Final Report

PIB EE 68-0012

September 15, 1967 - September 15, 1968

Prepared for

National Aeronautics and Space Administration

Electronic Research Center

under

NASA GRANT NGR-33-006-020

DEPARTMENT OF ELECTRICAL ENGINEERING
POLYTECHNIC INSTITUTE OF BROOKLYN

A Space Communications Study

Final Report

PIB EE 68-0012

September 15, 1967 - September 15, 1968

Prepared for

National Aeronautics and Space Administration

Electronic Research Center

under

NASA GRANT NGR-33-006-020

Donald L. Schilling,
Associate Professor
Principal Investigator

Kenneth K. Clarke,
Professor,
Co-Principal Investigator

Raymond L. Pickholtz,
Associate Professor
Co-Principal Investigator

DEPARTMENT OF ELECTRICAL ENGINEERING
POLYTECHNIC INSTITUTE OF BROOKLYN

TABLE OF CONTENTS

Introduction.

This final report summarizes all of the research sponsored by the National Aeronautics and Space Administration under the grant NGR-33-006-020 for the period 15 September 1967 through 15 September 1968. The research supported by this grant encompasses the problem of transmitting and receiving analog and digital signals through noisy media. Frequency modulation is emphasized, with particular attention focused on the problem of threshold extension. Throughout the study, theory and experiment were worked hand-in-hand witn approximately equal effort expended on each.

Part I of this report presents the results of the threshold extension studies. These results are used to determine the output SNR of an FM demodulator when the input SNR of a frequency modulated signal is known. In addition, the probability of error obtained under FSK transmission can also be determined.

Two different techniques are employed to determine the output clicks, and hence the threshold performance and error rate of the Phase Locked Loop. Both techniques assume that the noise present at the PLL output can be represented by a smooth component, which is almost gaussian, and an impulse or click component. This model was first postulated by Schilling in 1963 and is currently being used by most investigators.

The results obtained by the independent investigations were found to be similar. Thus the studies provide an accurate determination of the threshold of 1st, 2nd and 3rd order phase locked loops. In addition, a computer program has been found which allows the threshold of any phase locked loop or FMFB to be found using 30 miniutes of computer time. Two or more threshold extension devices, if they can be modeled as the PLL and FMFB, can be compared on the basis of threshold extension using 15 minutes of computer time.

A new threshold extension device, the Frequency Locked Loop (FLL), invented by Clarke and Hess, is discussed here in detail. Threshold extension and error rate reduction is considered for the 1st and 2nd order FLL.

The "Most Likely Noise" technique employed is an extension of the one used by Schilling in the calculation of PLL threshold extension. Preliminary results are presented.

Part II of this report considers the transmission of TV signals through a noisy, fading channel. FM transmission is employed and the received picture is obtained using a FLL and a FM Discriminator Demodulator. The improvement in the clarity of the video signal when using the FLL indicates another advantage of this device over the ordinary FM Dis criminator.

Part III deals with a study of SSBFM and the characteristics of FM noise.

A SSBFM system was developed to determine whether threshold extension could be obtained and to see what advantages, if any, SSB transmission offered. SSBFM is interesting since for narrowband FM a bandwidth reduction results. In addition, the SSBFM generation employed permits an ordinary FMD to demodulate the signal. Thus, for the case of a small modulation index the same receiver currently employed can be used with a reduced IF bandwidth

Rice's results, separating the output noise of an FM discriminator into a gaussian component and a click component, are approximate. A derivation determining the spectrum of the FM noise is presented in section III. 2.

The effect of multipath on an FM signal is investigated and the results are verified experimentally.

Part IV of this report considers synchronism procedures for single channel PSK communication systems. The main purpose of this report is to compare the principles upon which practical synchronizers operate. Analytical bounds on the average probability of error are derived and it is shown that all of the "popular" synchronization systems perform comparably. This is in contrast to some previously published results.

In Part V, the recursive methods developed during the previous interval have been implemented in practice by using estimates of the signal derivatives. The computer results indicate a very rapid convergence toward the optimum for even simple derivative estimates. Further theoretical results are also indicated.

Part VI presents, briefly, some experimental results of the effects of noise on a PCM system using a new high speed A/D and D/A converter developed at PIB, and which will be used for further experimental work in this area.

The results of this grant represent a significant step forward in the theory of operation of FM analog and digital communication systems. This grant has also served to support the publication of a large number of papers, as well as the masters and Ph.D. dissertations listed in Sections VII and VIII.

Participating in this program were:

Professors R. Boorstyn

K. Clarke

D. Hess

J. Oberst

Professors R. Pickholtz

D. Schilling

Messrs. E. Hoffman

P. Osborne

A. Snider

N. Tepedelenlioglu

M. Unkauf

The final report was prepared by

Professors K. K. Clarke

R. L. Pickholtz

D. P. Schilling

I. THRESHOLD EXTENSION

1. The Phase Locked Loop

1.1 Expected Number of Spikes of Phase Locked Loop Demodulators

Summary. - A new method is presented for finding the expected number of spikes in a phase locked loop of any order, with or without modulation. The procedure can also be employed to determine the threshold of the FMFB, FM discriminators and the Maximum Likelihood Estimator. The low pass equivalent gaussian noises x(t), y(t) in the differential equation describing the system (PLL or FMFB) are replaced by the deterministic time functions (Conditional Expectations)

1) $E[x(t)/x(0), \dot{x}(0)]$

2) $E[y(t)/y(0), \dot{y}(0)]$

and solved on a digital computer. The mid spike time (t=0) is taken to be the time when x(0) (quadrature noise) = 0, and a surface or surfaces in $\dot{x}(0)$, y(0), $\dot{y}(0)$ space are determined which indicates the region A where spikes in the demodulator are obtained. From this the expected number of spikes per second is calculated.

Results are presented for the first, second, and third order phase locked loops, and for an ordinary FM discriminator (which can be shown to be equivalent to a PLL of infinite gain). The second order loop used a constant plus integral filter, while the third order loop used a constant plus integral plus double intergral filter.

Introduction. - For the past several years there has been a great deal of research to determine the theshold behavior of the phased locked loop.[1] However, there are important deficiencies in the analyses to date. These analyses have assumed that the input noise is white, and have neglected the effect of the modulation. The design of a PLL is, however, vastly different

if there is modulation than when there is no modulation.

The expected number of spikes in the output of a phase locked loop decreases as the gain of the PLL is reduced, if there is no modulation. When modulation is present, one finds that there is a minimum loop bandwidth below which distortion results. The number of spikes present in this region is large. Increasing the PLL bandwidth results in a decrease in the number of spikes. However, we know that infinite bandwidth is equivalent to using a discriminator, hence an optimum bandwidth exists which can only be found by considering the effect of the modulation.

In this paper, a Carson's rule 3dB IF bandwidth equal to $2(\beta+1)\,f_m$ Hz is employed, where β is the modulation index, and f_m the modulating frequency. Square wave modulation is considered. The square wave modulation represents a worst-case solution since the number of spikes occurring per second is proportional to the deviation Δf.[2]

Mathematical Preliminaries.

A. FM Discriminator. - The output of an IF Discriminator when integrated is:

$$V_{FMD}(t) = \Phi_m(t) + \arctan\left(\frac{x(t)\cos\Phi_m + y(t)\sin\Phi_m}{1 + x(t)\sin\Phi_m - y(t)\cos\Phi_m}\right) \qquad (1)$$

where

Φ_m = phase of the modulating signal

$x(t)$ = quadrature low pass equivalent noise

$y(t)$ = in phase low pass equivalent noise

A spike occurs when the arctan term jumps $\pm 2\pi$ (see Ref. 2).

B. Phased Locked Loop Differential Equations.

1. First Order Loop. - A block diagram of a first order phase locked loop is shown in Fig. I-1.1. The differential equation describing the loop is easily shown to be:

$$\dot{\Phi} + G\sin(\Phi-\Phi_m) = G(x(t)\cos\Phi + y(t)\sin\Phi) \qquad (2)$$

where

Φ = phase of VCO output

G = loop gain and 3dB bandwidth of PLL.

We let the modulating signal be $2\pi\Delta f$. Thus $\Phi_m(t) = 2\pi(\Delta f)t$. When considering noise, this represents a worst case solution. The solution of Eq.(2) with no noise is

$$\Phi(t) = 2\pi t\Delta f - \arcsin\left(\frac{2\pi\Delta f}{G}\right) \qquad (3)$$

For proper operation of the PLL (low distortion) the error voltage $(\Phi - \Phi_m)$ must be much smaller in magnitude than $\pi/2$, or

$$\arcsin\left(\frac{2\pi\Delta f}{G}\right) \ll \frac{\pi}{2} \qquad (4)$$

which implies that

$$G \gg 2\pi\Delta f \qquad (5)$$

2. Second Order Loop. - A block diagram of a second order constant plus integral phase locked loop is shown in Fig. I-1.2. The differential equation describing the loop is:

$$\ddot{\Phi} + 2G_1[x(t)\sin\Phi - y(t)\cos\Phi + \cos(\Phi - \Phi_m)]\dot{\Phi} + G_1G_2\sin(\Phi - \Phi_m)$$
$$= G_1[(2\dot{x} + G_2x)\cos\Phi + (2\dot{y} + G_2y)\sin\Phi + \dot{\Phi}_m\cos(\Phi - \Phi_m)] \qquad (6)$$

where

Φ is the phase of the VCO output,

$G_1(2 + G_2/s)$ is the transter function of the constant plus integral filter.

When ther is no noise and $|\Phi - \Phi_m| \ll \frac{\pi}{2}$, the PLL equation becomes,

$$\ddot{\Phi} + 2G_1\dot{\Phi} + G_1G_2\Phi = G_1G_2\Phi_m + G_1\dot{\Phi}_m \qquad (7)$$

and

$$\Phi(p) = \frac{2G_1 p + G_1 G_2}{p^2 + 2G_1 p + G_1 G_2} \Phi_m(p) \tag{8}$$

In this report $G_1 = G/\sqrt{2}$, and $G_2 = G\sqrt{2}$ (maximally flat). Equation (8) reduces to

$$\Phi(p) = \frac{\sqrt{2}Gp + G^2}{p^2 + \sqrt{2}Gp + G^2} \Phi_m(p) \tag{9}$$

The 3dB bandwidth of the PLL is $\sqrt{\sqrt{5} + 2}\,G = 2.05G$.

The better way to view this loop is to consider the transfer between the modulating phase and the error phase of the loop, since for proper operation, this error phase must be much less than $\frac{\pi}{2}$. Then

$$\Phi_e(p) = \Phi(p) - \Phi_m(p) = \frac{p^2}{(p^2 + \sqrt{2}Gp + G^2)} \Phi_m(p) \tag{10}$$

This represents a high pass filter with a 3dB lower frequency of G radians per second. For proper operation, the modulating frequencies must be considerably less than G in order to maintain a small phase error (for low distortion). Thus, the error bandwidth G is of more practical interest than the PLL bandwidth. For example, if $\Phi_m(t) = \beta \sin \omega_m t$

$$\Phi_e(t) = \frac{\beta\omega_m^2}{\sqrt{G^4 + \omega_m^4}} \sin\left[\omega_m t - \arctan\left(\frac{\sqrt{2}G\omega_m}{G^2 - \omega_m^2}\right)\right] \tag{11}$$

From Eq.(1.11,) for low distortion, G must be such that

$$\frac{\beta\omega_m^2}{\sqrt{G^4 + \omega_m^4}} \ll \frac{\pi}{2} \tag{12}$$

3. Third Order Loop. - A block diagram of a third order constant plus integral plus double integral phase locked loop is shown in Fig. I-1.3. The differential equation describing the loop is:

$$\dddot{\Phi} = G_1\ddot{e}(t) + G_1G_2\dot{e}(t) + G_1G_2G_3e(t) \tag{13}$$

where

$$e(t) = -\sin(\Phi - \Phi_m) + x(t)\cos\Phi + y(t)\sin\Phi$$

$G_1 + G_1G_2/s + G_1G_2G_3/s^2$ is the transfer function of the PLL filter.

When there is no noise and $|\Phi - \Phi_m| \ll \frac{\pi}{2}$, the PLL equation becomes,

$$\dddot{\Phi} + G_1\ddot{\Phi} + G_1G_2\dot{\Phi} + G_1G_2G_3\Phi = G_1\ddot{\Phi}_m + G_1G_2\dot{\Phi}_m + G_1G_2G_3\Phi_m \tag{14}$$

The better way to view this loop is to consider the transfer between the modulating phase and the error phase of the loop, since for proper operation, this error phase must be much less than $\frac{\pi}{2}$. In this report, $G_1 = 2G$, $G_2 = G$, and $G_3 = G/2$, which makes the above transfer maximally flat. Then

$$\Phi_e(p) = \Phi(p) - \Phi_m(p) = \frac{p^3}{p^3 + 2Gp^2 + 2G^2p + G^3}\,\Phi_m(p) \tag{15}$$

This high pass filter has a cutoff frequency of G radians per second. Again, to maintain low distortion, the modulating frequencies must be considerably less than this. If $\Phi_m(t) = \beta\sin\omega_m T$ the phase error developed is

$$\Phi_e(t) = \frac{\beta\omega_m^3}{\sqrt{\omega_m^6 + G^6}}\,\sin\left[\omega_m t - \arctan\left(\frac{2G^2\omega_m - \omega_m^3}{G^3 - 2G\omega_m^2}\right)\right] \tag{16}$$

From the above equation, it is clear that for low distortion, G must be such that

$$\frac{\beta\omega_m^3}{\sqrt{\omega_m^6 + G^6}} \ll \frac{\pi}{2} \tag{17}$$

C. Noise Model.[2] - Instead of the random processes x(t) and y(t), which are the quadrature and in phase low pass equivalent noises respectively, we shall use the following deterministic signals (conditional expectations) with random variable parameters:

$$x_1(t) = E(x(t) \,/\, x(0),\ \dot{x}(0)) \tag{18}$$

$$y_1(t) = E(y(t) \,/\, y(0),\ \dot{y}(0)) \tag{19}$$

We consider the mid spike time, t = 0, as being the time when x(0) = 0. Thus, Eq. (18) becomes

$$x_1(t) = E(x(t) \,/\, x(0) = 0,\ \dot{x}(0)) \tag{20}$$

The IF filter is assumed to consist of the cascade of two identical stages, each single tuned with a 3dB bandwidth of two radians per second. Thus the low pass noise components x(t) and x(t) have the spectrum

$$S(\omega) = \frac{4\sigma^2}{(\omega^2 + 1)^2} \tag{21}$$

where σ^2 is the variance of the random processes x(t), y(t). It then follows that:

$$R(t) = R_x(t) - R_y(t) = \frac{1}{2\pi} \int_{-\infty}^{\infty} S(\omega)\, e^{j\omega t}\, d\omega = \sigma^2 (1 + |t|)\, e^{-|t|} \tag{22a}$$

$$R_{x\dot{x}}(t) = R_{y\dot{y}} = \frac{1}{2\pi} \int_{-\infty}^{\infty} (-j\omega)\, S(\omega)\, e^{j\omega t}\, d\omega = -\dot{R}(t) = \sigma^2 t e^{-|t|} \tag{22b}$$

The conditional density of x(t) given x(0), x(0) is

$$f(x(t) \,/\, x(0),\ \dot{x}(0)) = \frac{e^{\left[\frac{-\left(x(t) - x(0)\frac{R(t)}{\sigma^2} + \dot{x}(0)\frac{\dot{R}(t)}{\sigma^2}\right)^2}{2\sigma^2\left(1 - \frac{R^2(t)}{\sigma^4} - \frac{\dot{R}^2(t)}{\sigma^4}\right)}\right]}}{\sqrt{2\sigma^2\left(1 - \frac{R^2(t)}{\sigma^4} - \frac{\dot{R}^2(t)}{\sigma^4}\right)}} \tag{23}$$

The conditional density of y(t), $f(y(t) / y(0), \dot{y}(0))$ has the same form as Eq. (23).

Usings Eqs. (22a), (22b), and (23), we find for the following conditional expectations:

$$x_1(t) = E(x(t) / y\ x(0) = 0,\ \dot{x}(0)) = \dot{x}(0)\ te^{-|t|} \tag{24a}$$

$$y_1(t) = E(y(t) / y(0),\ \dot{y}(0)) = (y(0)\ (1 + |t|) + \dot{y}(0)t)\ e^{-|t|} \tag{24b}$$

The above deterministic functions are the noise models used in the PLL analyses which follows. A typical noise trajectory is shown in Fig. I-1.4.

D. Computation of the Expected Number of Spikes per Second - Using a digital computer, and the noise model of Eq. (24), the differential equations of the PLL see(Eqs. (2), (6), (13))are solved. A fourth order Runge-Kutta starting procedure is used, with a Moultons predictor-corrector program. The solution is made over a period of time from t = -5 to t - +25 seconds. A hunting procedure on the parameters $\dot{x}(0)$, $y(0)$, $\dot{y}(0)$ is used in the program such that a "spike" surface in $\dot{x}(0)$, $y(0)$, $\dot{y}(0)$ space is determined. Values of the parameters $\dot{x}(0)$, $y(0)$, $\dot{y}(0)$ on one side of this surface cause the phase error between the phase output of the PLL VCO, and the phase of the modulation to be $\pm 2\pi$ at t = 25 seconds. Values of the parameters on the other side of this surface cause the above phase error to be zero when t = 25 seconds.

The expected number of spikes per second is simply the expected number of times the random vector $\dot{x}(0)$, $y(0)$, $\dot{y}(0)$ is in a spike region. From Rice[3], we get

$$N = \int_S |\dot{x}|\ f(x(0) = 0,\ \dot{x}(0),\ y(0))\ d\dot{x}\ dy\ d\dot{y} \tag{25}$$

where

S = spike regions

N = expected number of spikes/sec.

$f(x, \dot{x}, y, \dot{y})$ = joint gaussian density of $x, \dot{x}, y, \dot{y}$.

The integral is performed by approximating the spike surfaces by plane segments, and summing the results of Eq. (25) for each segment. A digital computer was used to perform this tedious computation.

To simplify computations, the equations were normalized. The 3dB bandwidth of the IF filter is

$$\omega'_{IF} = 2(0.643) = 1.286 \text{ radians/sec.}$$

To compare the results for this IF bandwidth with results for other bandwidths, we introduce a time scale to the phase locked loop equations:

$$t' = t/K \tag{26a}$$

This results in a new IF frequency:

$$\omega_{IF} = K\omega'_{IF} \text{ radians/sec.} \tag{26b}$$

for the first order loop

$$G = KG' = \frac{\omega_{IF}}{\omega'_{IF}} G' \tag{27}$$

while for the other loops

$$G_1 = KG'_1 \; ; \; G_2 = KG'_2 \; ; \; G_3 = KG'_3 \tag{28}$$

The number of spikes/second is then

$$N = KN' \tag{29a}$$

or

$$N' = N/K = \frac{\sqrt{\sqrt{2} - 1}}{\omega_{IF}/2} \tag{29b}$$

where

β = modulation index

f_m = modulating frequency

ω_{IF} = IF bandwidth (radians/sec.)

Results. - The spike boundary can be found for the FM discriminator by plotting Eq. (1) from t = -5 to +25 seconds instead of solving a differential equation. Figure 5 shows the resulting spike surface for a FM discriminator with a constant modulation offset of 0.6 radians per second. (This is equivalent to square wave modulation). It is interesting to note that there are multiple spike regions and that no positive spikes occure in the region shown.

The surface for the first order PLL with no modulation is shown in Fig. I-1.6. Negative spikes occur for values of $\dot{x}(0)$, $y(0)$, $\dot{y}(0)$ to the right of the surface and none to the left. The surface for positive spikes is simply a mirror image of the one shown, below the $y(0)$, $\dot{y}(0)$, plane.

The surfaces for the second and third order loops are shown on Figs. I-1.7 and 8, for the case of no modulation. Note that they have the same shape and form as the surface for the first order loop, (no modulation), and again the surface for positive spikes is a mirror image of the one shown, below the $y(0)$, $\dot{y}(0)$, plane. Also spikes are obtained to the right of the surfaces as before.

The gains of the second and third order loops were adjusted so that the phase error developed with sine wave modulation ($\beta\sin(\omega_m t)$) is the same for both loops and modulation indices (3 and 12). The lower gain loops are designed to operate with the larger β, while the higher gain loops are to operation with the lower β. Note that since the IF bandwidth is kept constant, a larger modulation index impleis a lower modulating frequency ω_m, hence a lower loop gain can be used.

The surface for the first order PLL with a constant modulation offset of .6 radians per second, is shown in Fig. I-1.9. It is very similar to the surface obtained fro the FM discriminator. This is to be expected, since the gain of the first order loop is rather high (to maintain a low distortion),

which makes the performance of this loop not very much different that that of the FM discriminator.

The surfaces for the second and third order loops with constant modulation offsets of $(3/4)\omega'_{IF}$ and $(12/13)\ \omega'_{IF}$ radian per seconds $[\beta\omega'_{IF}/(\beta + 1)]$ are shown in Figs. I-1.10 and 11. Note that only negative spikes occur, and that they occur to the right of the surface.

The expected number of spikes per second for the above surfaces was calculated using Eq. (25). The normalized results are plotted in Fig. I-1.12. The curves for the first order PLL show that spikes are approximately a thousand times more frequent with modulation than without. Also it is evident that better performance is achieved as the order of the loop is increased. It is also interesting to note that the difference in performance between the no modulation and the modulation case decreases as the order of the loops increase.

Conclusions. - The expected number of spikes, for an FM Discriminator with modulation, obtained from the spike surface of Fig. I-1.5, was found to be almost the same as that for no modulation. These results, together with a simple approach heuristically derived by Rice[3], are compared in Fig. I-1.12. The difference, in terms of carrier to noise ratio, is only 0.5 dB.

The results are also compared with experimentally obtained results, for the first, and second order loops. The agreement, in terms of carrier to noise ratio, is very good for the first order loop. The agreement for the second order loop is not quite as good, a poorer result being obtained for the experimental points. (i.e., more spikes per second.)

The theory assumes that the low pass equivalent noises x(t), and y(t), are independent. This requires the bandpass IF filter to be symmetric about the center frequency. To do this with a cascade of two single tuned

stages, requires a very high Q. In the experiment, the IF filter used had a center frequency of 455 Hz and a bandwidth of $\pm$ 4.1 Hz. The correlation of the low pass equivalent noises was indicated by the fact that symmetrical spikes were obtained with a carrier frequency 1 kcs. above the center frequency. The discrepancy between the theoretical and experimental results are expected to be due to the above problem.

It is worth noting that the method allows the comparison of different systems by comparing their respective spike boundary surfaces. If the surface of one system is closer to the origin than the other, then the first system generated more spikes than the second under the conditions for which the surfaces were computed.

References.

1. A. J. Viterbi, "Phase Locked Loop Dynamics in the Presence of Noise by Fokker Planck Techniques" Proc. IEEE - December, 1963, Vol. 51, No. 12, pp. 1737 - 1753.

V. I. Tikhonov, "The Effects of Noise on Phase Lock Oscillation Operations" Auto-matika Telemakhanika, Vol. 22, No. 9, 1959.

R. C. Tause worth, "A Method for Calculating Phase Locked Loop Performance Near Threshold" IEEE Transactions on Communication Thoery Technology, August, 1967.

2. This method was suggested in a private correspondence with S. O. Rice of the Bell Telephone Laboratories.

S. O. Rice, "Noise in FM Receivers" Time Series Analysis, Ch. 25, Wiley, 1963.

3. Schilling, Nelson, and Hoffman, "Error Rates for Digital Signals Demodulated by an FM Discriminator" IEEE Transaction on Communication Technology, August, 1967.

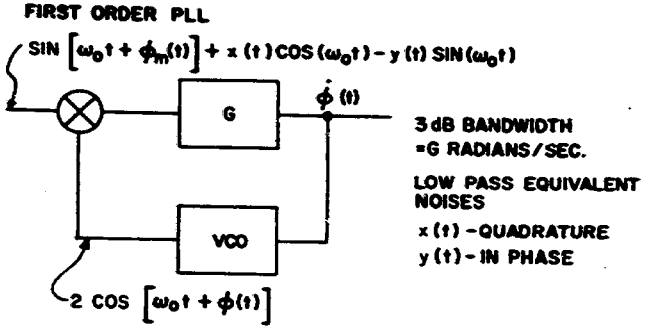

Fig. I-1.1 The First Order Phase Locked Loop

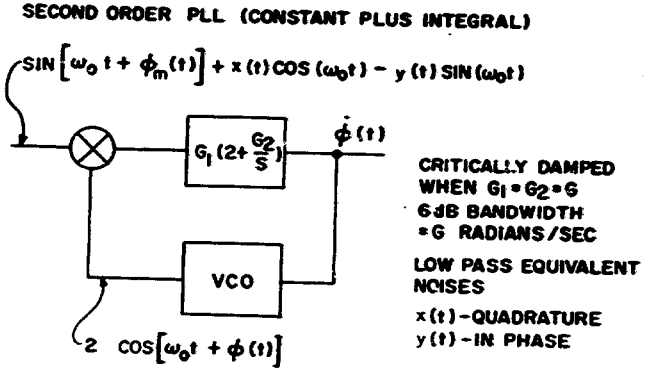

Fig. I-1.2 The Second Order Phase Locked Loop

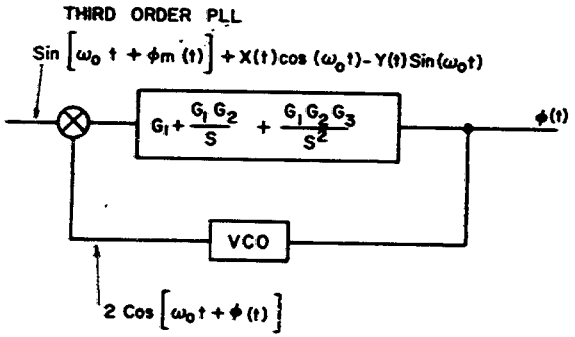

Fig. I-1.3 The Third Order Phase Locked Loop

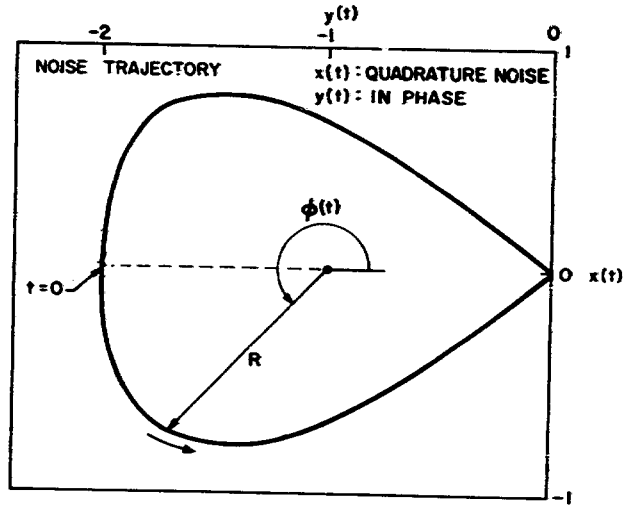

Fig. I-1.4 The Trajectory of the Most Likely Noise

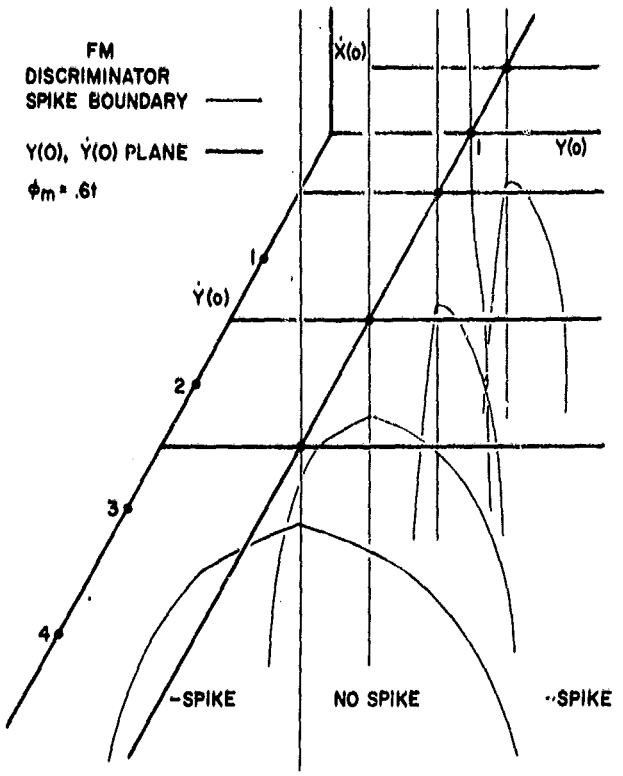

Fig. I-1.5 Spike Boundary for the FM Discriminator

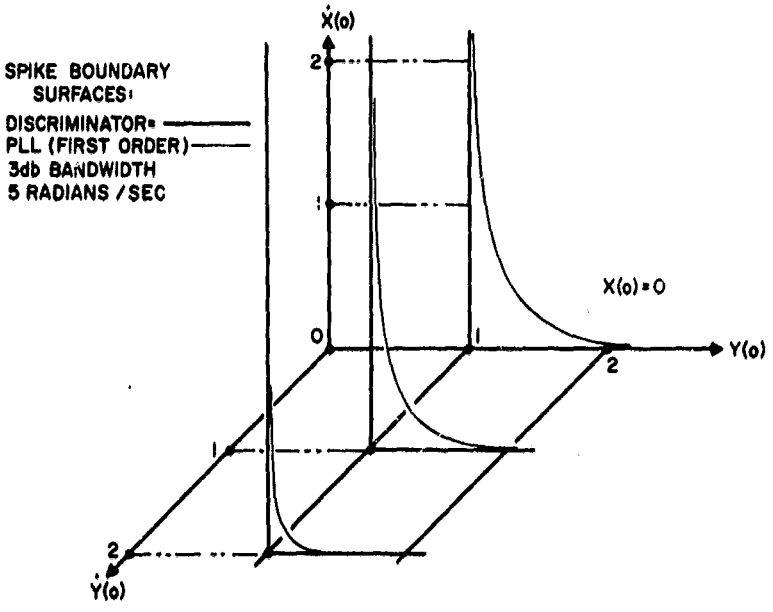

Fig. I-1.6 Comparison of the Spike Boundary Surfaces for the Discriminator and First-Order PLL - No Modulation

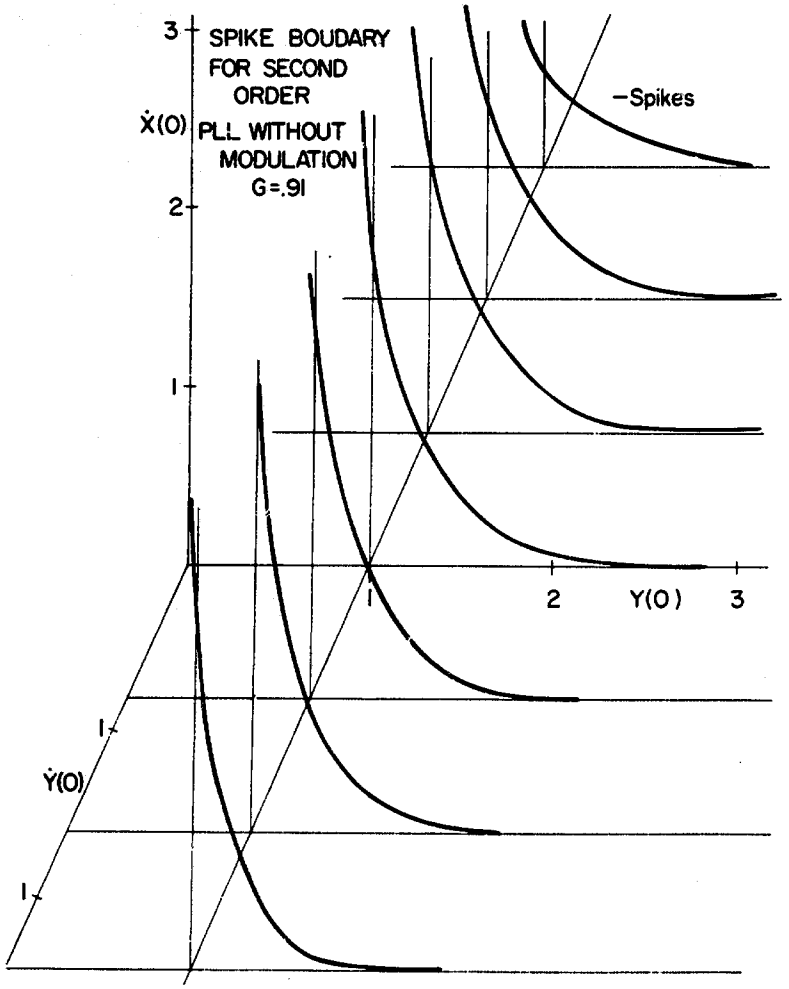

FIG. 7a

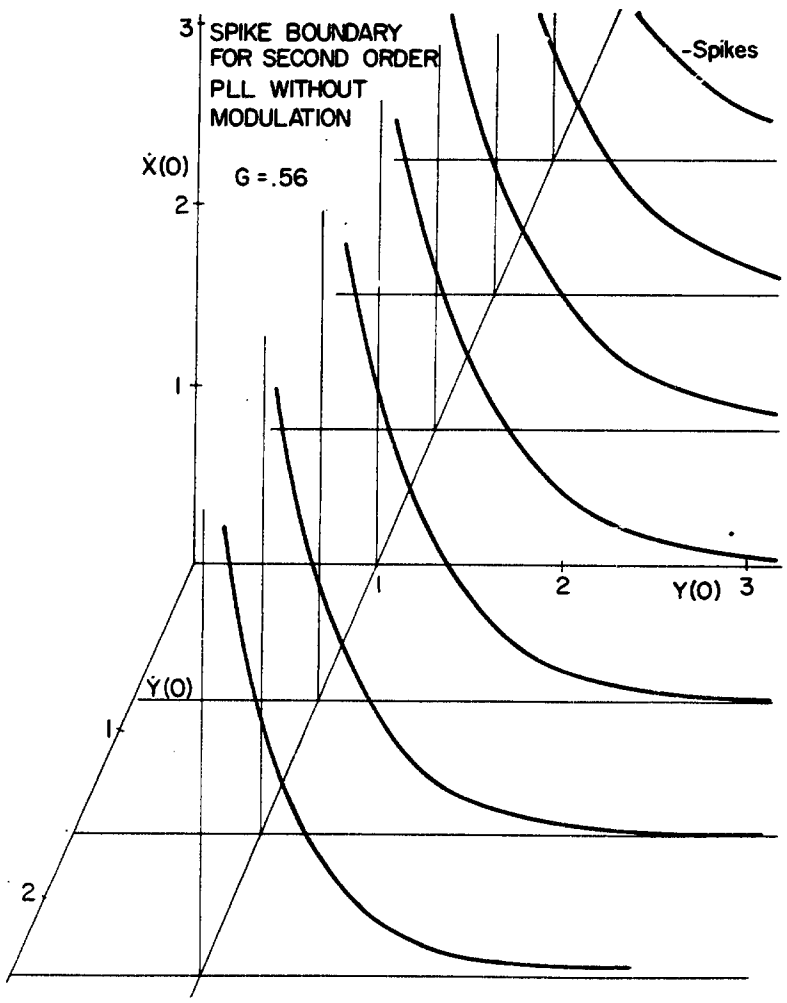

FIG. 7b

Fig. I-1.7 Spike Boundary for the Second Order PLL - No Modulation

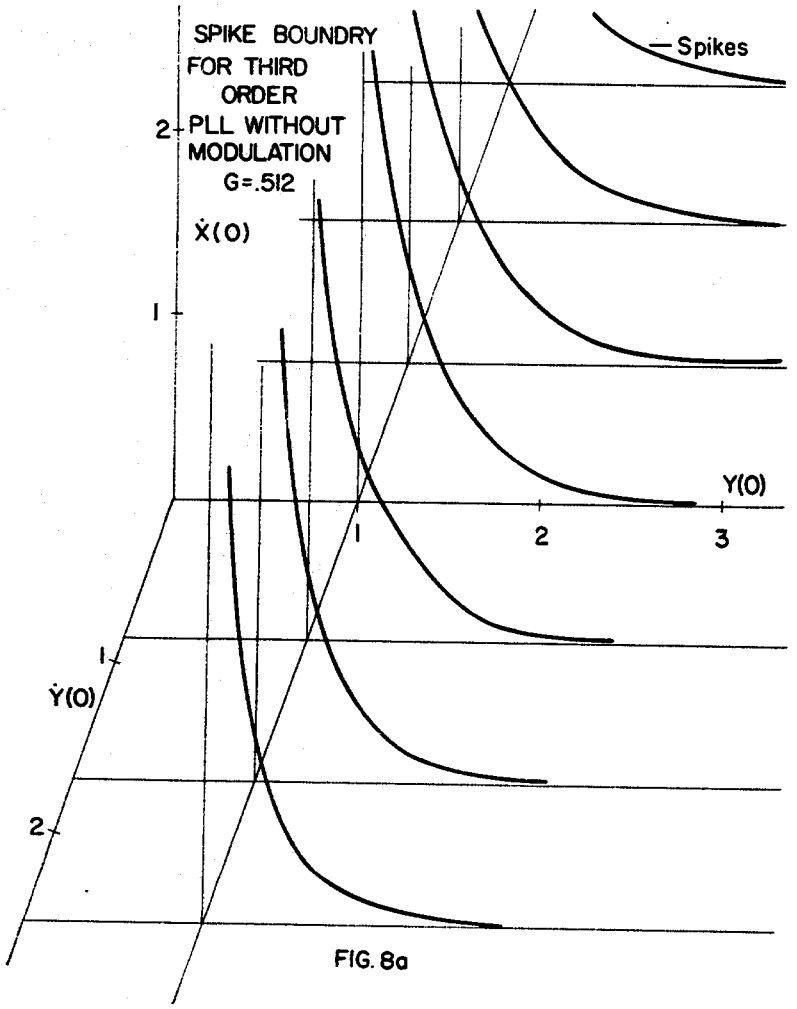

FIG. 8a

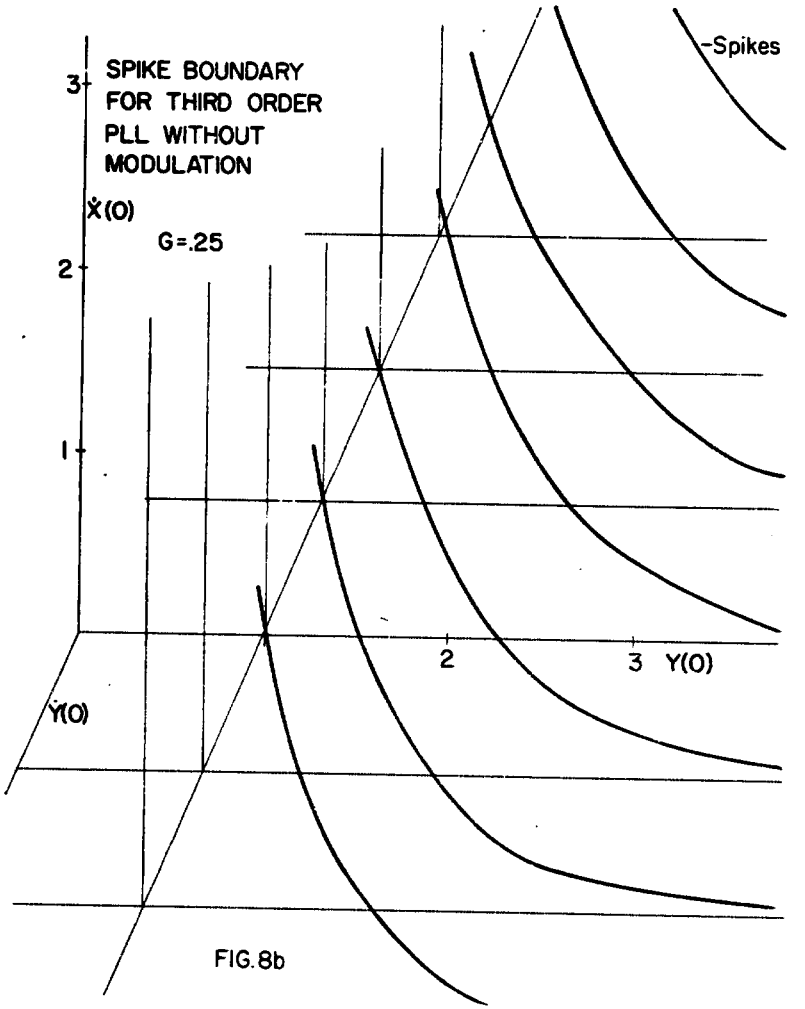

FIG. 8b

Fig. I-1.8 Spike Boundary for the Third Order PLL - No Modulation

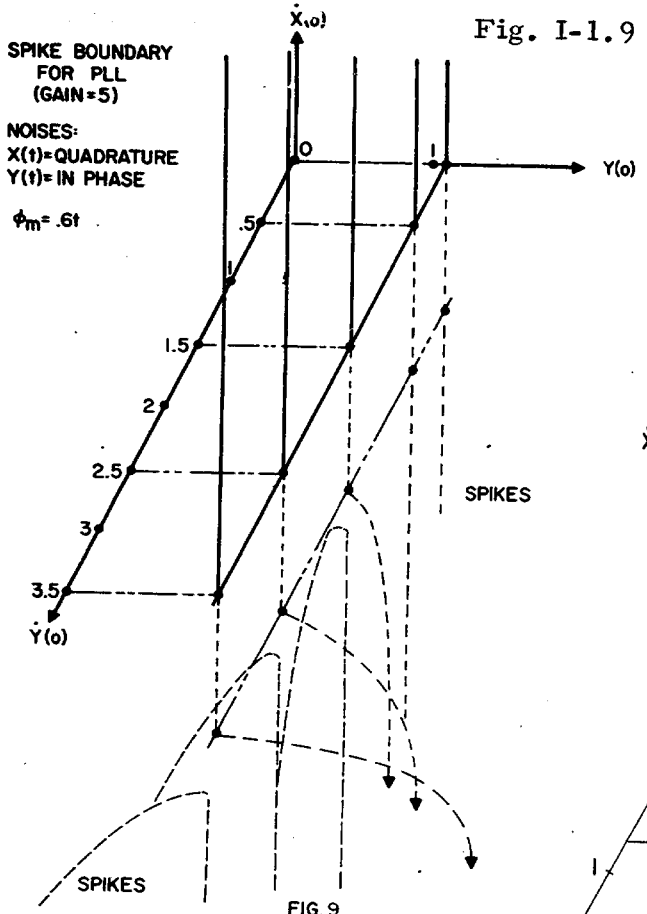

FIG. 9

Fig. I-1.9 Spike Boundary for the First Order PLL- Modulation

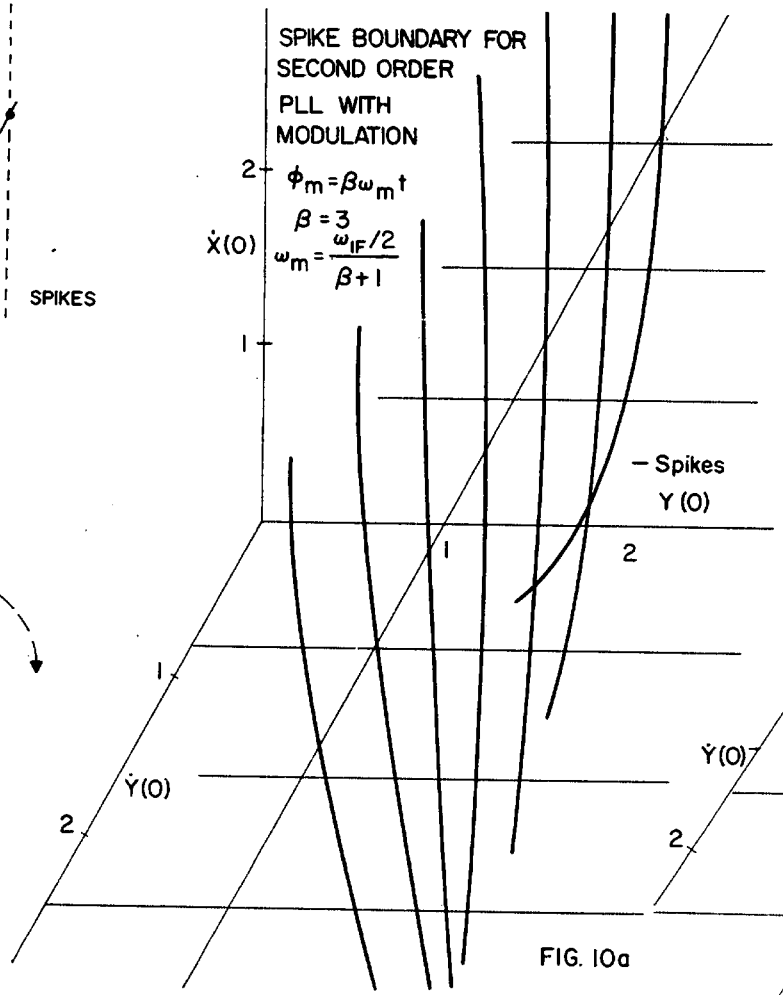

FIG. 10a

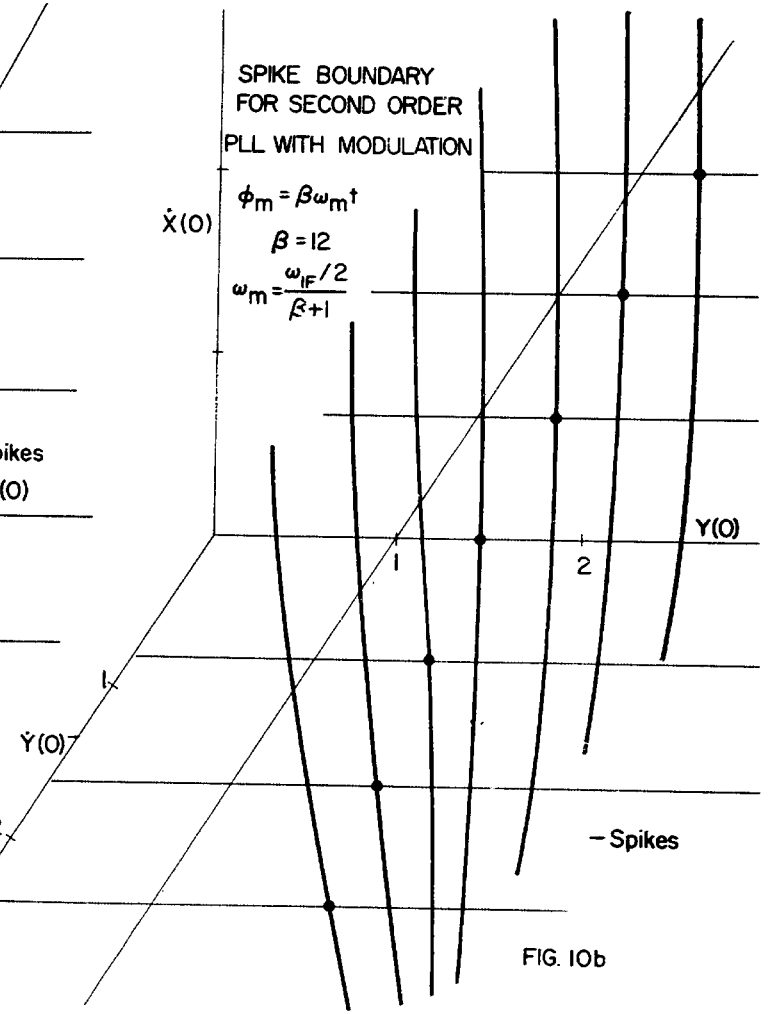

FIG. 10b

Fig. I-1.10 Spike Boundary for the Second Order PLL - Modulation

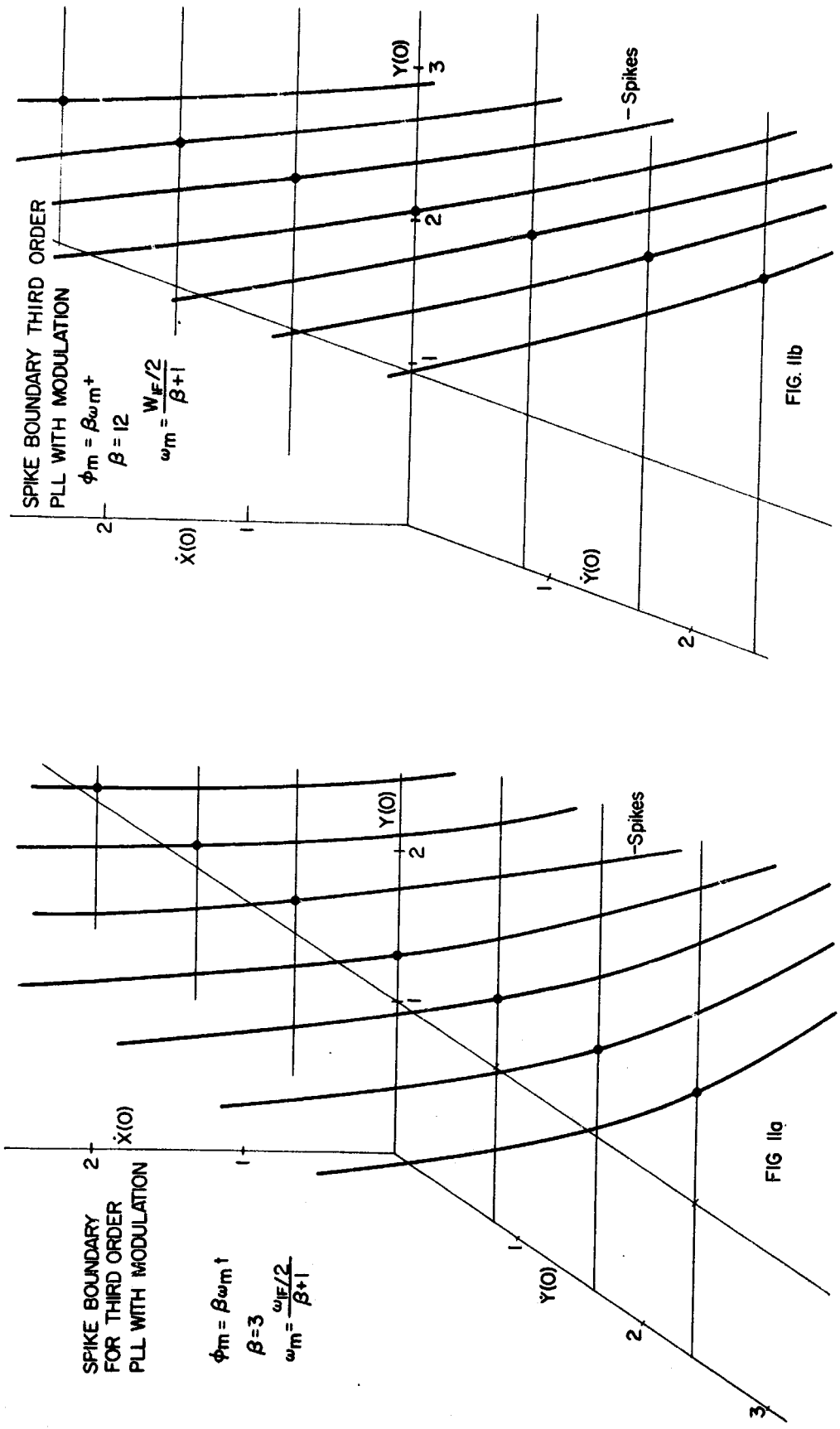

Fig. I-1.11 Spike Boundary for the Third Order PLL - Modulation

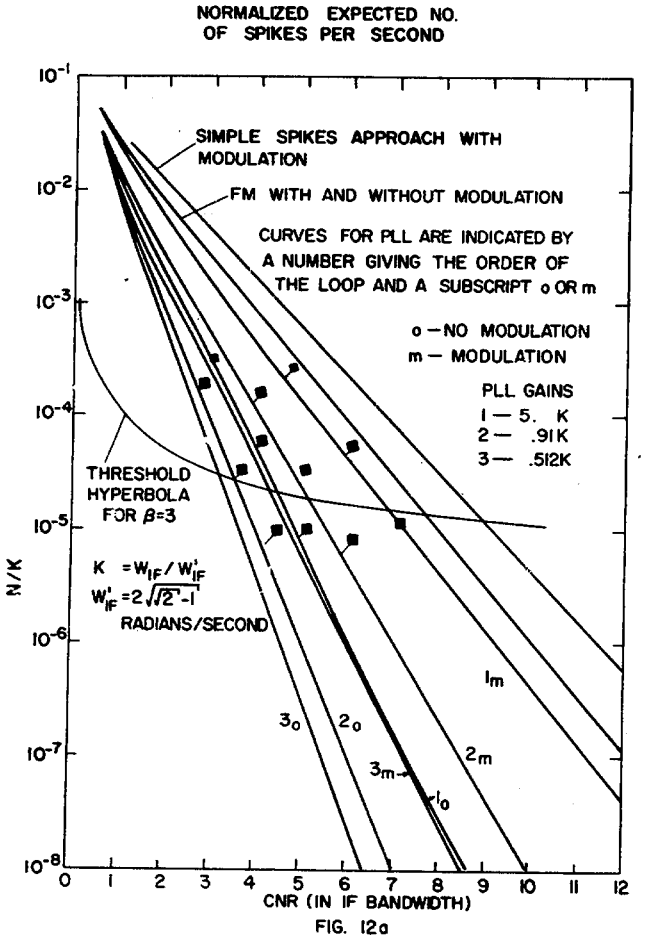

FIG. 12a

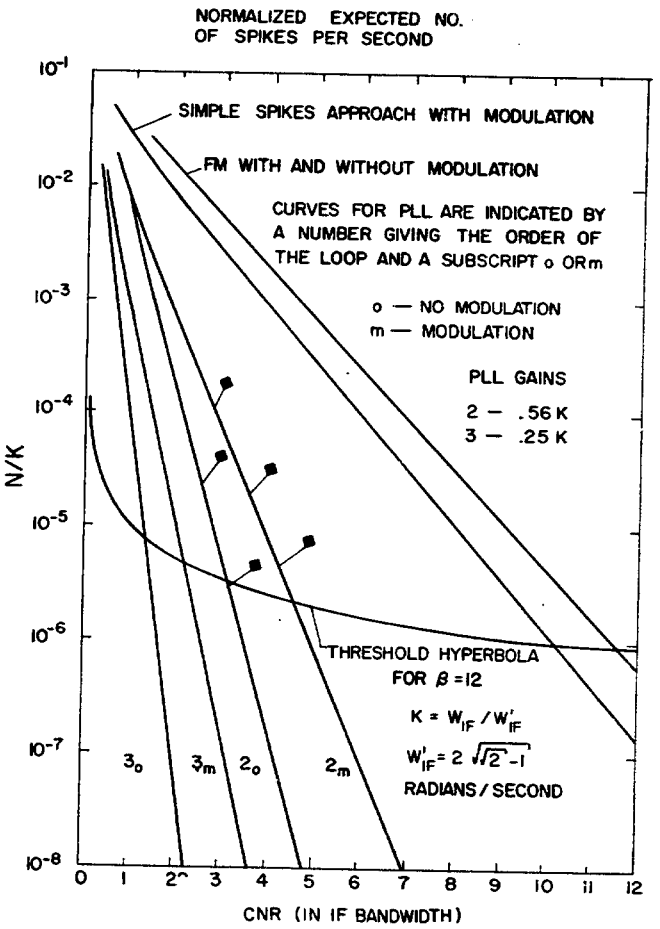

Fig. I-1.12 Comparison of the Expected Number of Spikes/Second and the Threshold of the FM discriminator and the PLL

1.2 Cycle Slipping in a Second Order Phase Locked Loop

Introduction. - The purpose of this section is to present the experimental studies made on the cycle slipping performance of a second order PLL.

Input signals to the loop are restricted to a carrier plus narrow-band noise centered at the center frequency of the loop. The case of modulation is not considered. The loop filter has a single pole and zero with its transfer function given by

$$H(s) = \frac{s + \beta}{s + \alpha} \tag{1}$$

First Order PLL "Click" Theory. - The input signal of interest consists of a carrier of frequency ω_o plus white Gaussian noise which has been passed through a symmetric narrow-band filter centered at ω_o. The filter output may be represented as

$$e_o(t) = A\cos\omega_o + n(t) = a(t)\cos[\omega_o t + \psi(t)] \tag{2}$$

From the work of Rice,[1] it is known that $\psi(t)$ contains steps of $\pm 2\pi$. The output "clicks" of a limiter-discriminator are the result of these steps. To determine the number of output "clicks" per second when $e_o(t)$ is applied to a PLL, Hess[2], takes the view that an output "click" occurs when the loop tracks the steps of $\pm 2\pi$ and no click occurs when the loop slips by a step. Thus the expected number of output clicks can be determined by calculating how many of the steps of $\pm 2\pi$ the PLL tracks.

Hess makes a model for the steps of $\pm 2\pi$ in the input carrier plus noise and derives the following result for the expected number of PLL output clicks for a first order PLL.

$$N_{\pm} = \frac{\gamma}{\pi}\ \mathrm{erfc}\left[\frac{A}{\sqrt{N}}\left(1 + \frac{1.04\gamma}{\omega_L}\right)\right.$$

where $A/\sqrt{2}N$ = carrier to noise ratio at input to PLL, γ = radius of gyration of the narrow-band noise at the loop input, ω_L = PLL hold in range, $\text{erfc } Y = \frac{1}{\sqrt{2\pi}} \int_Y^\infty e^{-1/2} dx$, and $N\pm$ = expected number of positive and negative output clicks/second. This expression is plotted in Fig. I-1.2.1 for several carrier to noise ratios. For the rectangular narrow band filter assumed, $\gamma = BW/\sqrt{3}$, where BW is the filter bandwidth.

Experimental Results and Conclusions. - Hess's model was extended to a second order loop and the expected number of output clicks was calculated for a particular loop filter. Fig. I-1.2.2 shows the filter used and the experimental and theoretical results. Agreement was not good and initial attempts to explain the discrepancies did not succeed.

An experimental approach was then taken employing a loop filter of the form $H(s) = (s + \beta)(s + \alpha)$. With β/α fixed, as α tends to infinity the filter has little effect on the loop. Consequently, the loop behaves as a first order loop with the same closed loop bandwidth as the second order loop. As α tends to zero, the loop reduces to a first order loop but with a closed loop bandwidth of $(\alpha/\beta)\omega_L$, where ω_L is the "hold in" range of the second order loop.

The expected number of "clicks" per second at these two extremes can be calculated from Hess's model for first order loops. For values of α in between, the number of clicks per second should vary in some manner which should give a clue as to how the loop operates. Fig. I-1.2.3 is the result of such an experiment for a "hold in" range of 31 kilohertz and a rectangular input filter with BW = 14kHz. Note that all the curves tend to the same value of α/ω_L increases as predicted, since in every case the loop is behaving as a first order loop of bandwidth 31 kilohertz (the "hold in" range and loop bandwidth are the same for a first order loop). As α/ω_L decreases, the

curves branch out as predicted since the loop is behaving as a first order loop with a bandwidth of 31 α/β kilohertz.

In an attempt to correlate the data, Fig. I-1.2.4 was constructed. The points were found as follows. For a given α/ω_L and β/α, the number of "clicks" per second was noted from Fig. I-1.2.3. Then using Fig. I-1.2.1, the value of $2\omega_L/BW$ to give the same number of "clicks" per second was determined. Note that this ω_{Leq} is now the bandwidth of an equivalent first order PLL which gives the same number of "clicks" per second as the second order loop. Thus the vertical axis is labled $2\omega_{Leq}/BW$. The resulting graph has several properties, as noted by the straight-line plots superimposed on the experimental curves.

First, all of the plots break at $\beta/\omega_L = 0.01$ and all have the same slope. Secondly, all are approximately equally distant from the experimental curves at the break points. This suggests that one can predict the results by simply drawing the asymptotes, making corrections and drawing a smooth curve.

To be sure the method could be used for any second order loop hold in range (Fig. I-1.2.4 is the ω_L = 31 kilohertz), curves similar to Fig. I-1.2.4 were experimentally measured for second order hold in ranges of 74 kilohertz and 190 kilohertz (Figs. I-1.2.5 and 6). In these cases the asympototes were constructed before the experimental points were taken. As can be seen, the behavior of the loop is exactly the same as for ω_L = 31 khz. The corrected curves are also given in Figs. I-1.2.5 and 6. They were constructed, as were the asymptotes, by the following rules derived from the study of the experimental points in Figs. I-1.2.4, 5 and 6:

1) Determine the desired second order loop hold in range and the zero-pole ratio of the loop filter (β/α).

2) Construct the horizontal asymptotes at $2\omega_L/BW$ and $(\alpha/\beta)\ 2\omega_L/BW$.

3) Construct the left break point at $\alpha/\omega = 0.01\alpha/\beta$.

4) Join the horizontal asymptotes from the break point with a line with slope of 0.43 decade/decade.

5) Determine the right hand break point at the intersection of the main plot and the right horizontal asymptote.

If a smooth curve is desired, the following corrections are used. The corrections are 0.08 decade at the break points and 0.04 decade an octave above and below the break points. Note the corrections are positive at the left break point and negative at the right break point. Log-log paper must be used.

In order to have further proof of the validity of these rules, a set of curves for the first case experimentally investigated was constructed using the rules above. The result is Fig. I-1.2.7 which also contains the experimental points of Fig. I-1.2.2. Note the close agreement as contrasted with Fig. I-1.2.2. It is especially significant that agreement is achieved for all the carrier to noise ratios since Fig. I-1.2.7 was constructed from the data for a carrier to noise ratio of 2 dB.

Although Hess's model cannot be directly applied to second order PLL's the use of an equivalent first order PLL bandwidth allows one to predict the performance of the second order loop. The prediction is done by means of a simple graphical construction once the loop parameters are known. Experimental verification has been obtained for several second order loop hold-in-ranges and carrier to noise ratios.

Further investigation is required to obtain the theoretical justification for the method derived in this report. Another area for future work is the

notion of an equivalent first order bandwidth to higher order PLL's.

References.

1. S. O. Rice, "Noise in FM Receivers," Proceedings Symposium of Time Series Analysis, M. Rosenblatt (ed.) (N. Y.: John Wiley and Sons, 1963) Chap. 25, pp. 395-424.

2. D. T. Hess, "Cycle Slipping in a First-Order Phase-Locked Loop," IEEE Trans. on Comm. Tech., Vol COM-16, pp. 255-260, April 1968.

3. B. Schwartz, "Cycle Slipping Events in the Second Order PLL," MSc Report, PIB, June 1968.

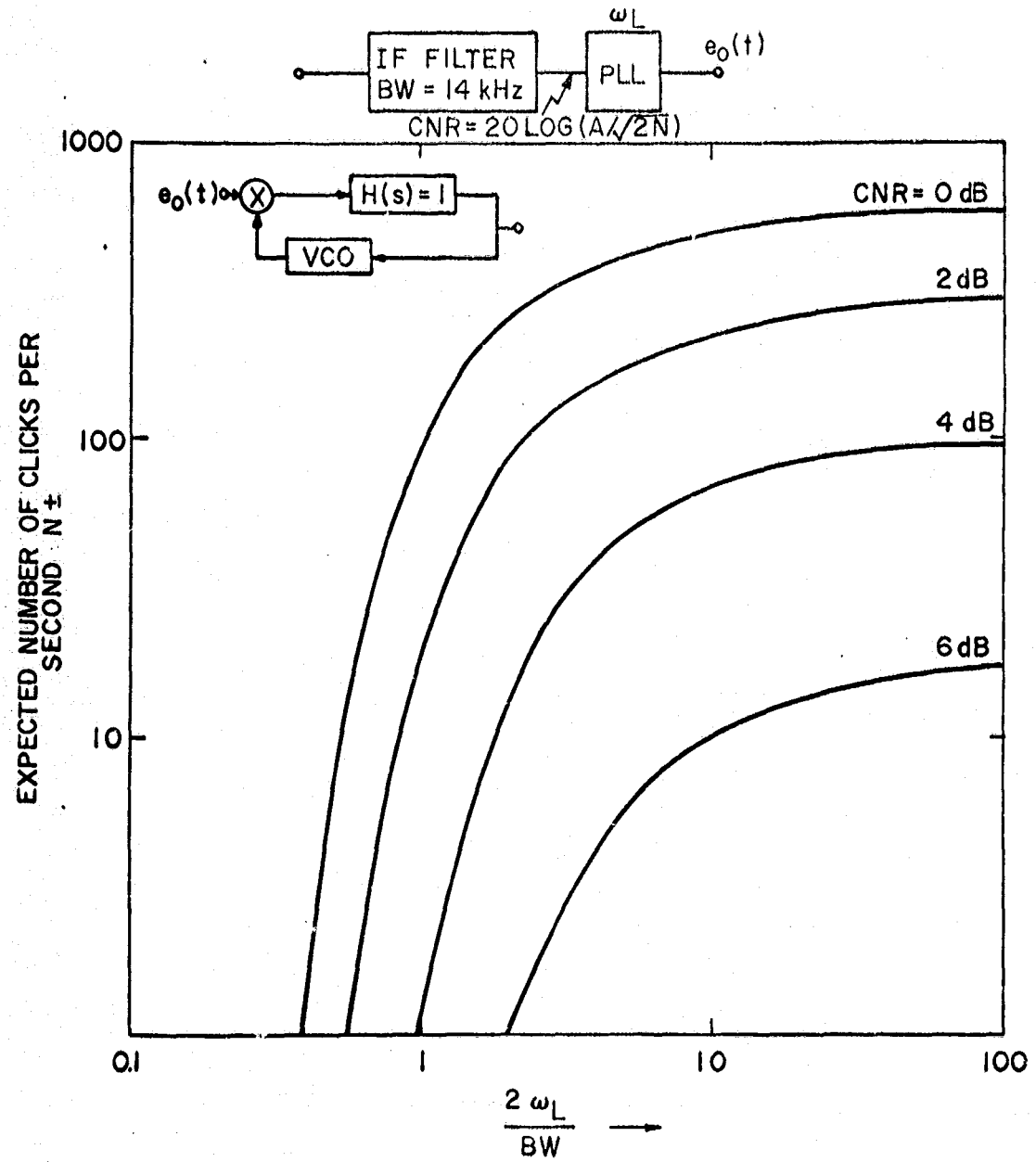

Fig. I-1.2.1 Expected Number of Output Positive and Negative Clocks per Second ($N_{\pm}$) vs. $\frac{2W_L}{BW}$ for First Order PLL.

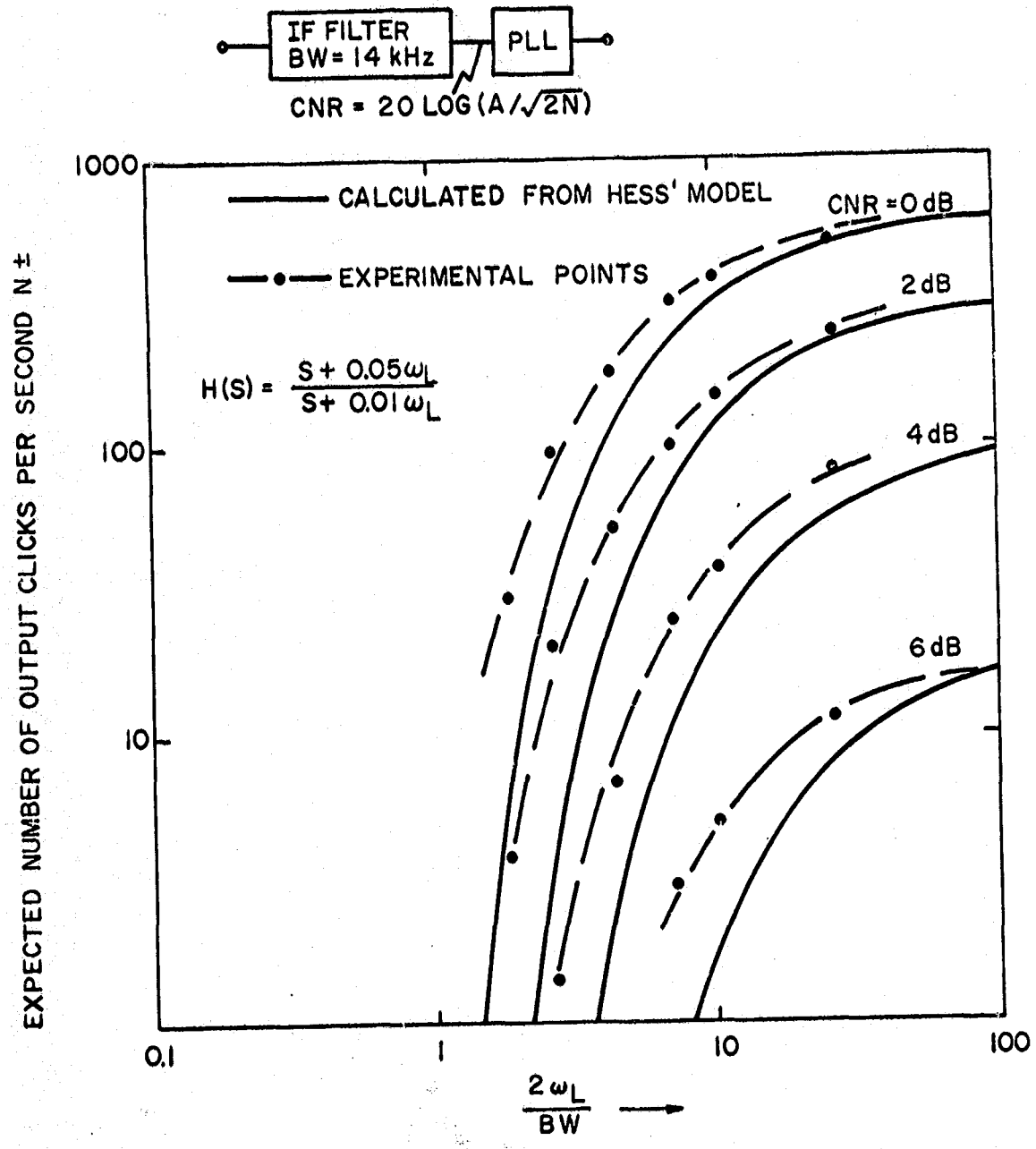

Fig. I-1.2.2 Expected Number of Second Order PLL Output Clicks per Second $(N \pm)$ vs $\frac{2W}{BW}$.

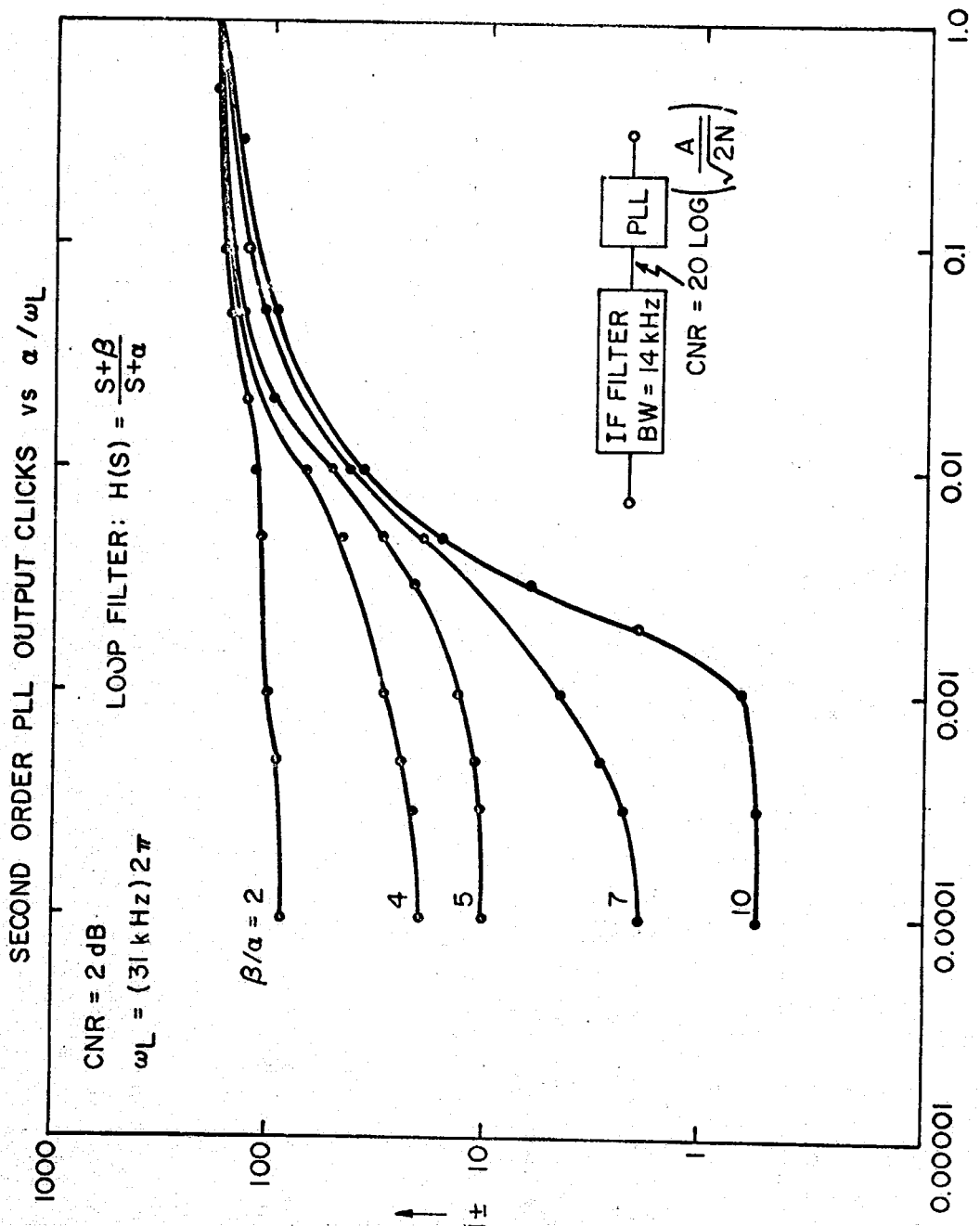
SECOND ORDER PLL OUTPUT CLICKS vs α/ωL
CNR = 2 dB
ωL = (31 kHz) 2π
LOOP FILTER: H(S) = (S+β)/(S+α)
β/α = 2
4
5
7
10
IF FILTER
BW = 14 kHz
PLL
CNR = 20 LOG (A/√2N)
N±
1000
100
10
1
0.00001
0.0001
0.001
0.01
0.1
1.0
α/ωL

Fig. I-1.2.3

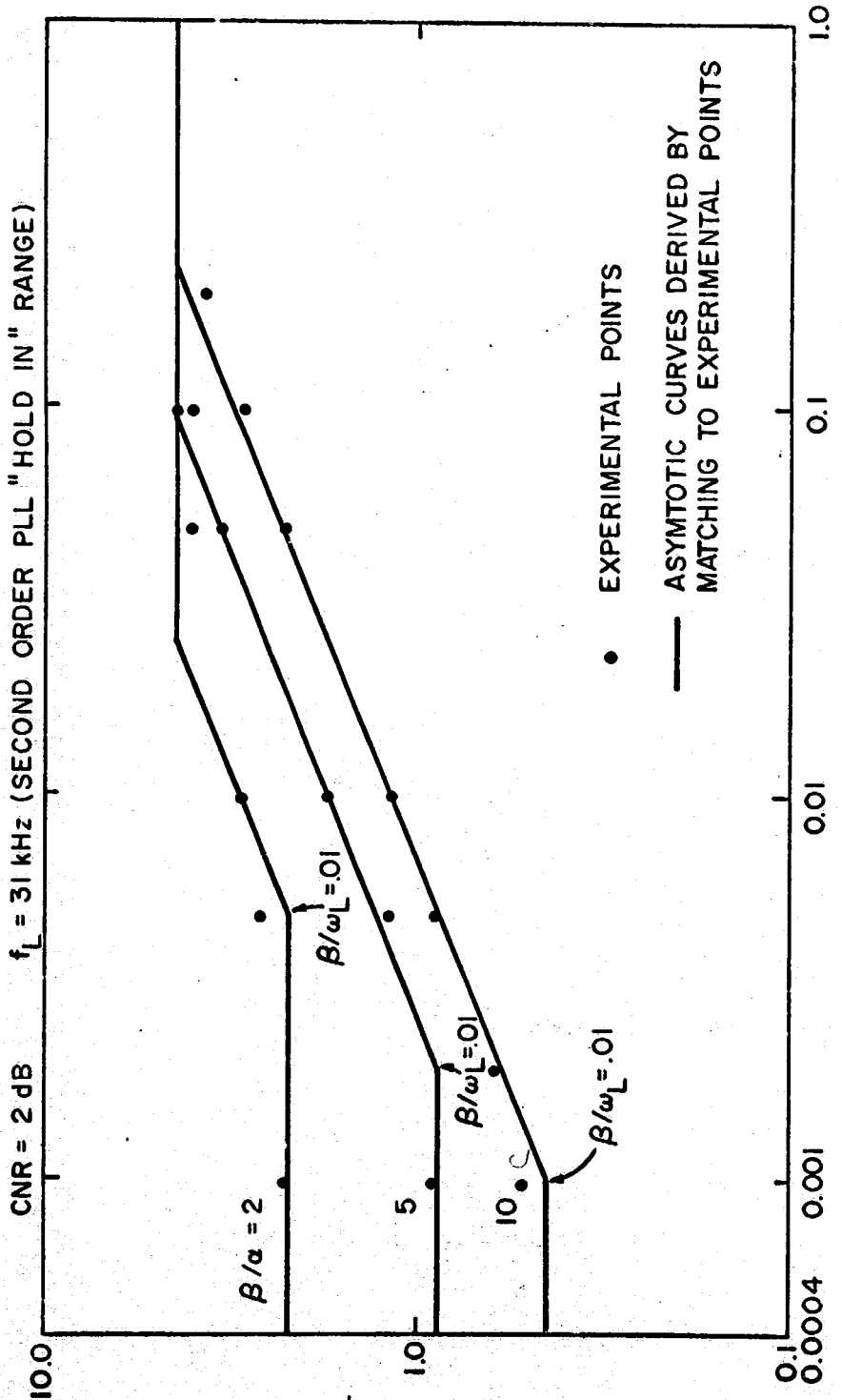

Fig. I-1.1.2.4 Data of Fig. 3 Plotted using an equivalent first order PLL closed loop bandwidth, $W_{Leq.}$ which is the bandwidth of a first order PLL which gives the same number of clicks per second as the second order loop.

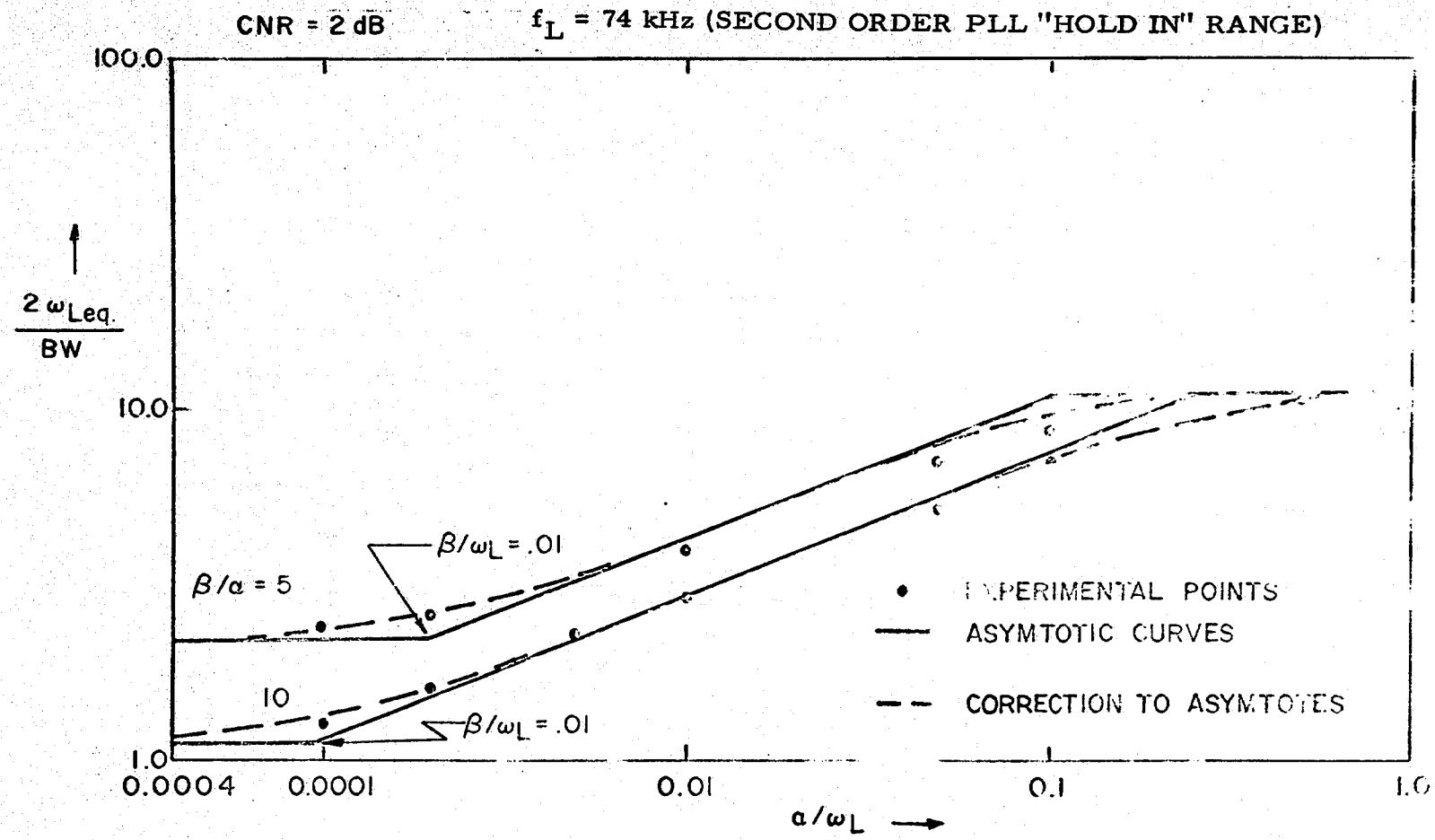

Fig. I-1.2.5 Plot of Fig. I-1.2.4 Repeated for f_L = 74 kHz

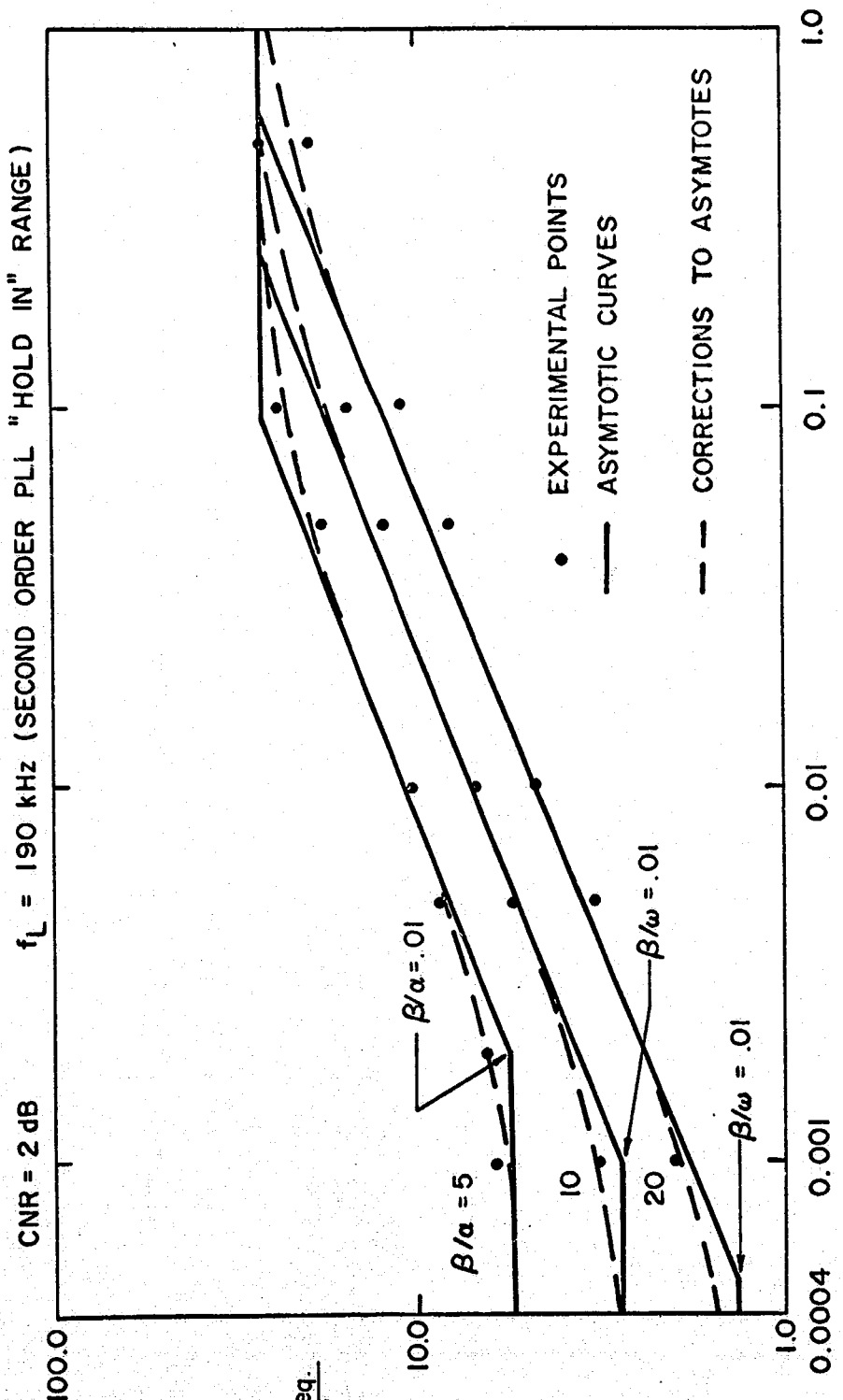

Fig. I-1.2.6 Plot of Fig. I-1.2.4 Repeated for f_L = 190 kHz.

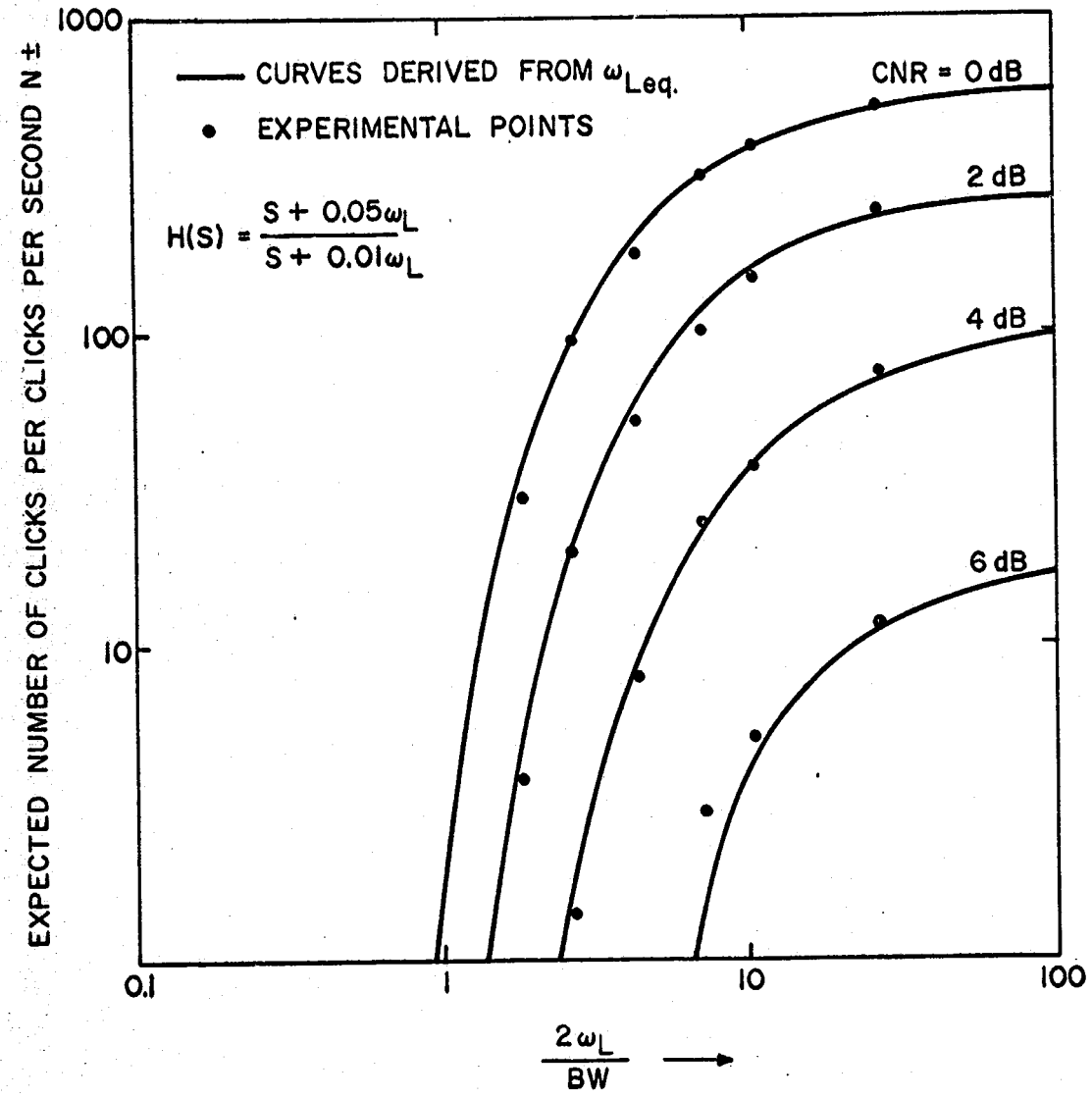

Fig. I-1.2.7 Second Order PLL Output "Clicks" per Second Calculated from an Equivalent First Order PLL Bandwidth, ω_{Leq}.

1.3 An Output Signal-to-Noise Ratio Equation for the First and Second Order Phase-Locked Loop.

Introduction. - In this report, an equation is derived which predicts the output signal-to-noise ratio (SNR) with no modulation, for the first-order phase-locked loop (PLL), and with a small modification it also holds for the second-order PLL, when the system IF filter is rectangular and the output low-pass filter frequency characteristic is known. This equation has been experimentally verified for a variety of different system conditions.

Derivation. - The initial approach to this problem is the same as that taken by M. Schwartz[1] in his derivation of a SNR equation for the discriminator. Since a no modulation analysis is being performed, a ficticious output SNR is defined as the ratio of mean-squared signal out, with the noise set equal to zero, to the mean-squared signal out, with no signal present.

The argument is employed that the spectral density of the total noise at the PLL output is the sum of the spectrum obtained in the high carrier-to noise case (Gaussian component) plus the spectrum due to noise clicks. Therefore, for a symmetric IF filter the output spectrum of the PLL is given by

$$G_{out}(\omega) = G_1(\omega) + G_2(\omega) \tag{1}$$

where $G_1(\omega)$ is the power spectrum of the Gaussian component and $G_2(\omega)$ is the power spectrum of the click component. When the input to the PLL is given by

$$e_{in}(t) = (A + x)\cos \omega_o t - y\sin \omega_o t \tag{2}$$

where x and y are independent Gaussian random variables, it has been shown[1] that

$$G_1(\omega) = \omega^2 N / 2BA^2 \qquad \begin{matrix} -B<f<B \\ A >> \sqrt{N} \end{matrix} \tag{3}$$

where N is the input noise power, and 2B is the IF filter BW; and that

$$G_2(\omega) \cong 8\pi^2 N_+ \tag{4}$$

where N_+ is the total expected number of positive clicks per second. ($N_+ = N_-$ for an unmodulated carrier.) Therefore

$$G_{out}(\omega) \cong \omega^2 N / 2BA^2 + 8\pi^2 N_+ \tag{5}$$

If there is an ideal low-pass filter (LPF) following the PLL which cuts off at f_m, the output noise power is given by

$$N_o = 2\int_o^{f_m} G_{out}(f)\, df \tag{6}$$

However, the LPF of the typical demodulation system is not ideal. To get around this situation, we define f_{mG} and f_{ms} as equivalent bandwidths of ideal filters where

$$\int_o^{f_{mG}} |F(0)|^2 f^2 df = \int_o^{\infty} |F(f)|^2 f^2 df \tag{7}$$

$$\int_o^{f_{ms}} |F(0)|^2 df = \int_o^{\infty} |F(f)|^2 df \tag{8}$$

and F(f) is the actual LPF transfer function. The noise power is therefore

$$N_o = 2\pi^2 \frac{\pi^2 f_{mG}^3}{B\gamma} + 16\pi^2 N_+ f_{ms} \tag{9}$$

where $\gamma = A^2/2N$ is the carrier-to-noise ratio the modulating signal is assumed to be of the form

$$\psi = \Delta\omega \cos\omega_m t \tag{10}$$

and it is attenuated by the output LPF by G_f, the mean-squared output signal is given by

$$S_o = 2\pi^2 (\Delta f)^2 G_f \tag{11}$$

An expression for N_+ for the PLL has been derived by Hess[2] for the

first-order PLL. His result for a rectangular IF filter is

$$N_+ = (B/2\sqrt{3})\,\mathrm{erfc}\,\sqrt{\gamma}\left[1 + \frac{(0.6)B}{f_L}\right] \tag{12}$$

where $\mathrm{erfc}\,Y = \left(2/\sqrt{\pi}\right)\int_Y^\infty e^{-x^2}\,dx$, and f_L is the closed-loop bandwidth of the PLL. It has been shown in section 1.2 that the use of an equivalent first-order PLL bandwidth f_{Leq}, in Hess' equation, allows one to predict N_+ for the second-order loop, where the loop filter for the second-order loop is shown in Fig. I-1.3.1. The determination of f_{Leq} is done by means of a simple graphical construction using the second-order parameters. Therefore, the output SNR for the first and second-order PLL with a rectangular IF filter, using the appropriate value of f_L, is given by

$$S_o/N_o = \frac{3\left(\frac{\Delta f}{f_{mG}}\right)^2 \gamma \left(\frac{B}{f_{mG}}\right) G_f}{\left(1 + 24/\sqrt{3}\right)\left(\frac{f_{ms}}{f_{mG}}\right)\left(\frac{B}{f_{mG}}\right)^2 \gamma\,\mathrm{erfc}\,\sqrt{\gamma}\left[1 + \frac{(0.6)B}{f_L}\right]} \tag{13}$$

where Δf = signal deviation, γ = input CNR, B= half the IF filter BW, f_{mG} = equivalent BW of output LPF for Gaussian noise, f_{ms} = equivalent BW of output LPF bandwidth as shown in Figs. I-1.3.2 and 3. It can be seen from these curves that agreement between theory and experimental results is good in all cases.

To test the equation for the second-order PLL, an equivalent closed-loop bandwidth had to be determined for each setting of f_L and for each loop filter, using the rules given in section 1.2 of this report. The theoretical and experimental data is shown in Figs. I-1.3.4 and 5. Again, agreement is good, which indicates the validity of the derived equation.

Conclusion. - An equation that predicts the output SNR for the first and second-order PLL without modulation, has been derived. Its validity has been examined for various system conditions and it has been shown to hold for all cases tested.

References.

1. M. Schwartz, W. R. Bennett, and S. Stein, Communication Systems and Techniques. New York: McGraw-Hill, 1966, Chap. 3

2. D. T. Hess, "Cycle slipping in a First-Order Phase-Locked Loop," IEEE Transactions on Communication Technology, vol. COM-16, pp. 255-260, April 1968.

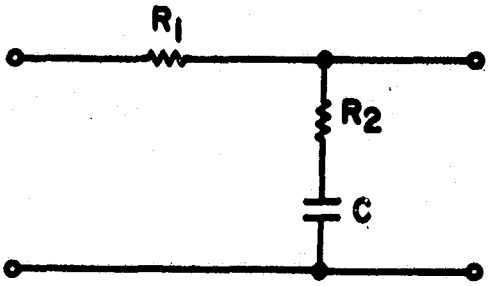

$$H(s) = (a/\mu)\frac{s+\mu}{s+a}$$

$$a = \frac{1}{(R_1+R_2)C}, \quad \mu = \frac{1}{R_1C}$$

Fig. I-1.3.1 Loop Filter for Second-Order PLL

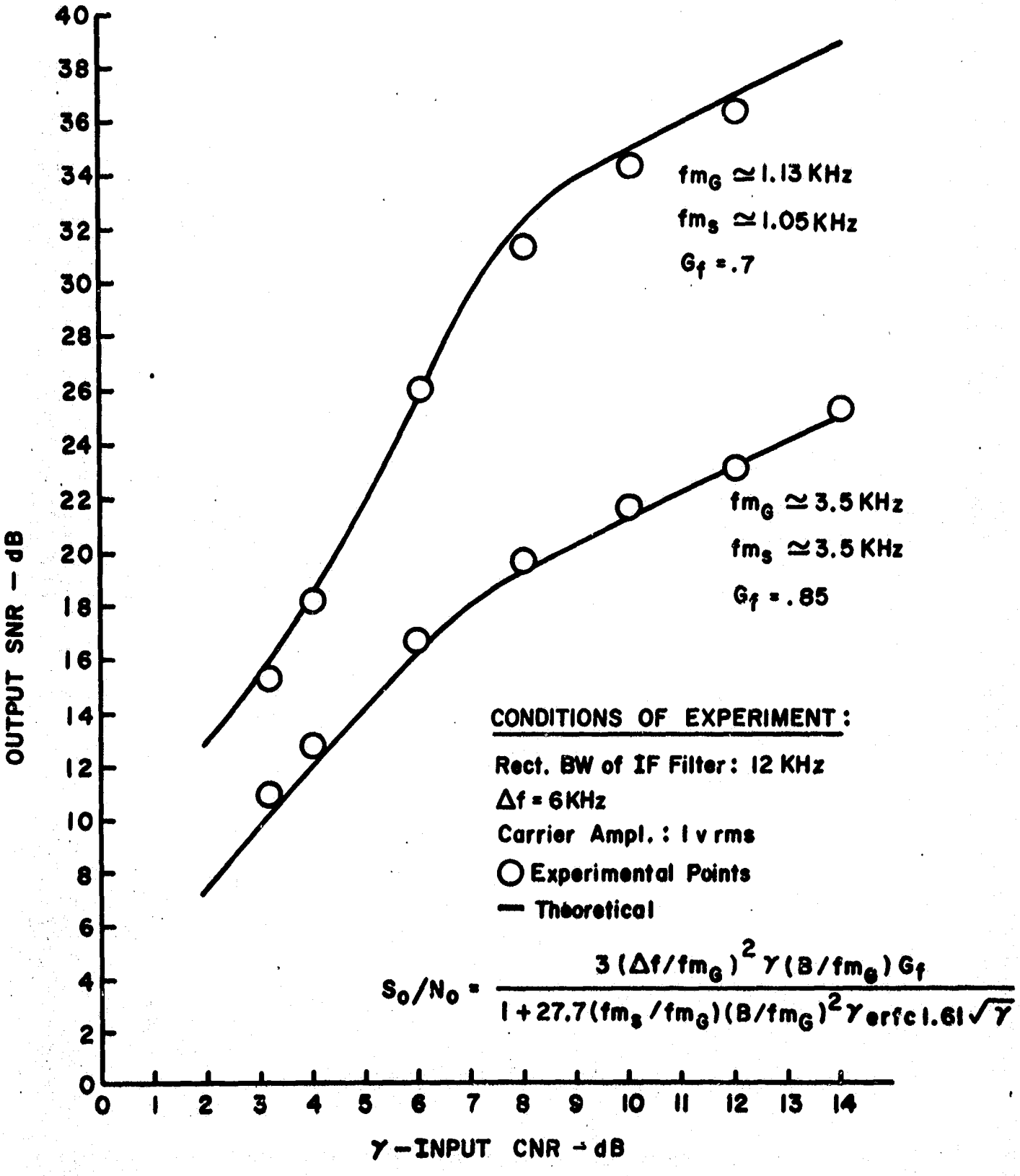

Fig. I-1.3.2 Output SNR vs Input CNR for a First Order Phase-Locked Loop

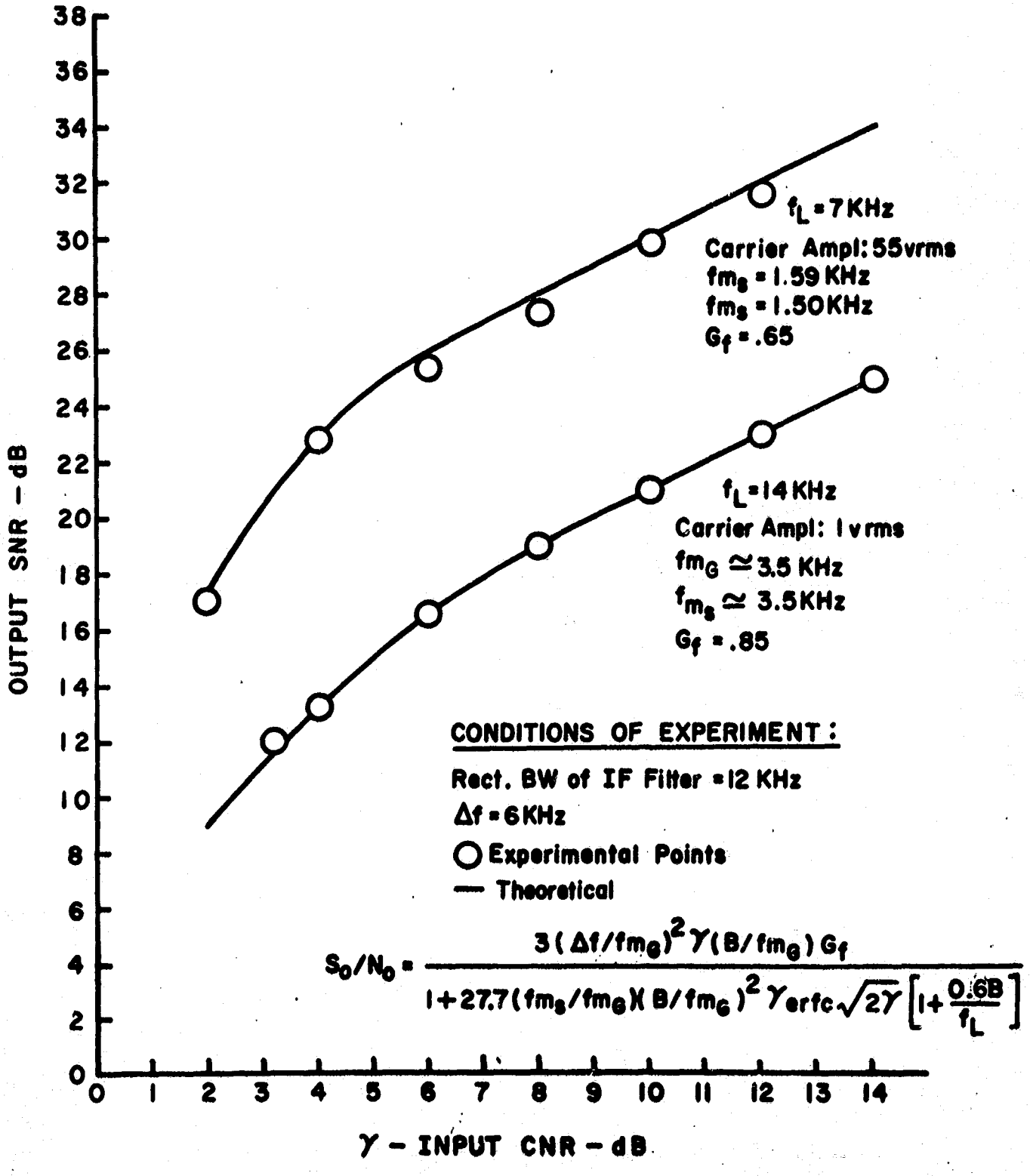

Fig. I-1.3.3 Output SNR vs Input CNR for a First Order Phase-Locked Loop

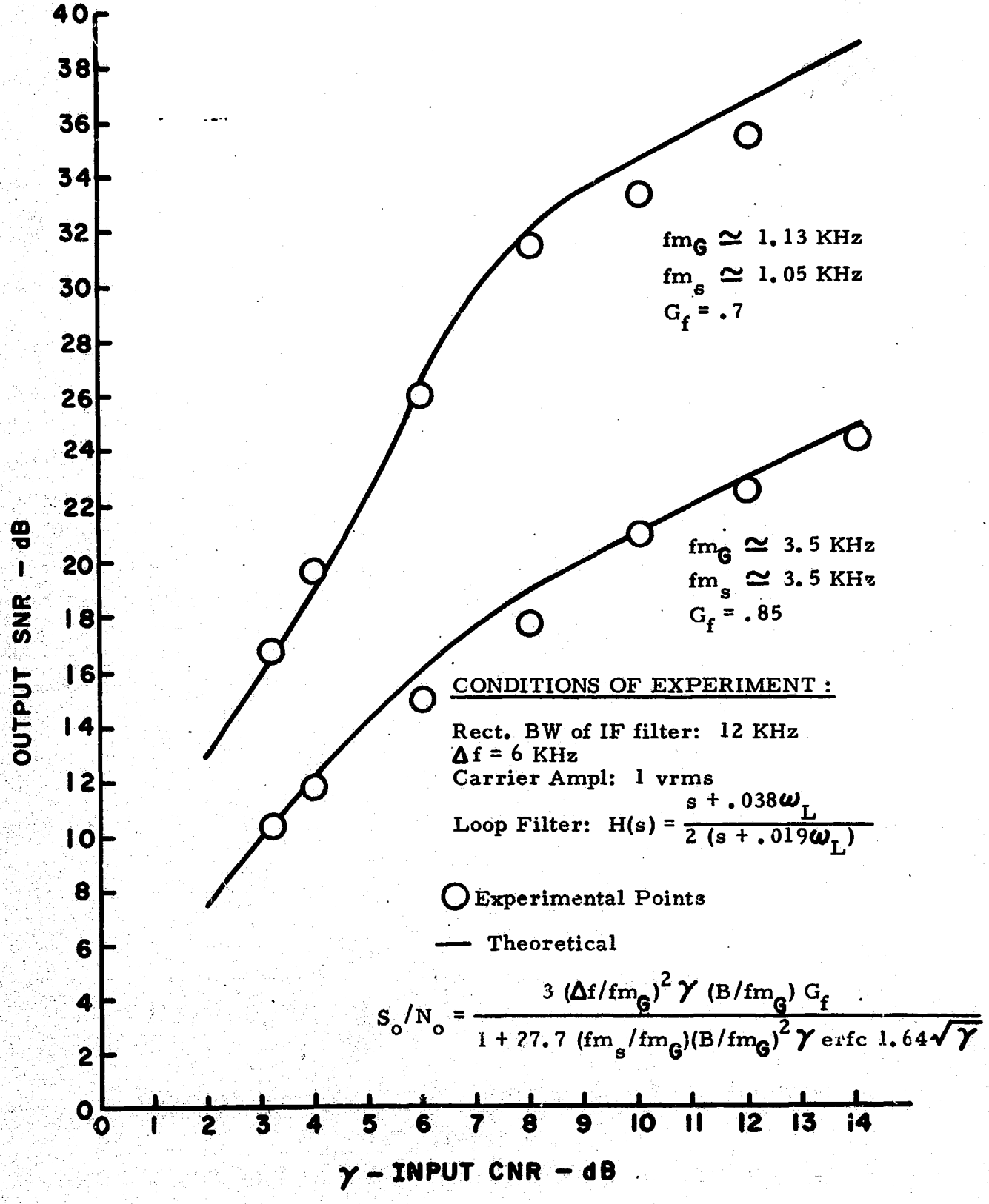

Fig. I-1.3.4 Output SNR vs Input CNR for a Second-Order Phase-Locked Loop

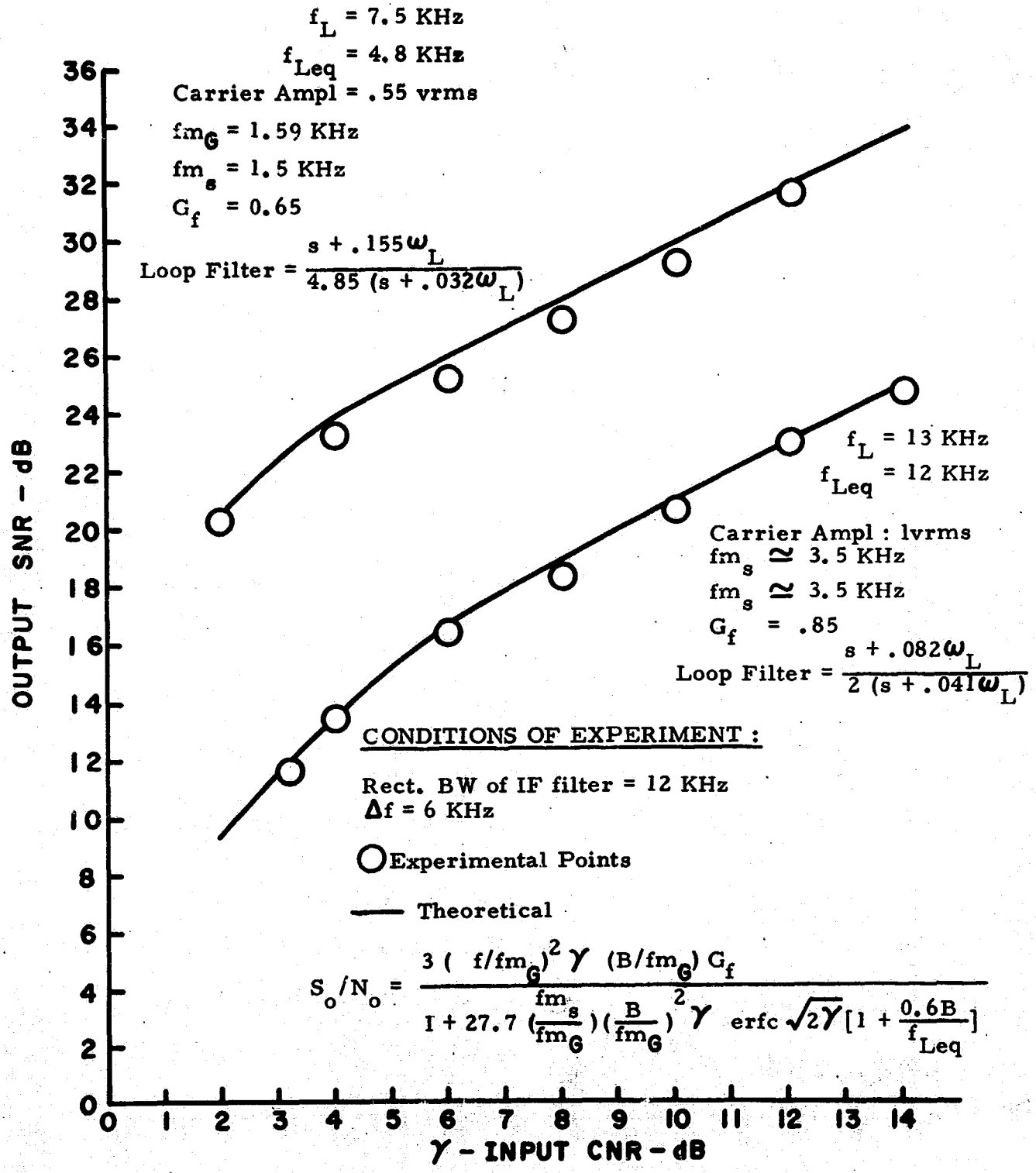

Fig. I-1.3.5 Output SNR vs Input CNR for a Second-Order Phase-Locked Loop

1.4 Optimizing Second-Order Phase-Locked Loop (PLL) Performance with Modulation.

Introduction. - In this section a purely experimental investigation into the behavior of the first and second-order PLL with modulation is described: Curves of output signal-to-noise ratio (SNR) vs. input carrier-to-noise ratio (CNR) for the PLL and limiter-discriminator were obtained by varying the numerous parameters of the system. This study culminates in the determination of a "rule of thumb" for choosing an optimum loop filter $H(s) = \frac{a}{\mu}\left(\frac{s+\mu}{s+a}\right)$ and hold-in range (the maximum static frequency deviation of the input signal from the carrier frequency before the loop loses lock) for the second-order PLL when the modulating signal fills the entire IF filter bandwidth of the system (full-deviation signal).

General Study. - To make the SNR measurements with modulation, the system of Fig. I-1.4.1 was used. The signal and noise were kept on simultaneously, while measuring the output value of either parameter. For the data taken for this report, a full-deviation signal was used, i.e., a signal with deviation Δf given by $\Delta f = \beta B/(1+\beta)$ where 2B is the IF bandwidth and β is the modulation index. Besides the many curves obtained for the PLL, some data were taken for the limiter-discriminator to use for comparison. These data were taken by replacing the PLL by a 455kHz limiter and GR discriminator (model 1142-A) in the system of Fig. I-1.4.1.

Specifically the output SNR was measured, with the input CNR fixed at 6dB and β fixed at 2, as the hold in range f_L, the pole of the loop filter a, and the zero of the loop filter if μ were independently varied. It was observed empirically that the output SNR passed through a maximum as each of the parameters, f_L, a, and μ were varied. Consequently by sequentially adjusting the parameters the optimum output SNR was obtained

for $\beta = 2$. With the signal deviation $\Delta f = 2$kHz, with the modulating signal frequency $f_m = 1$ kHz, and a rectangular IF filter with bandwidth = 6 kHz the empirically determined optimum values were found to be

$$a \sim 1.5 \text{ kHz}$$

$$f_L \simeq 12.5 \text{ kHz}$$

$$\mu/a \simeq 6$$

Fig. I-1.4.2 compares the optimum second order PLL with the optimum loop filter over the discriminator. It should be noted that with full deviation, little improvement in threshold is obtained with the PLL.

Using the above set of optimum parameters and the knowledge acquired from taking data presented in this section, one may set forth a "rule of thumb" for choosing an optimum hold-in range and second-order PLL for a full-deviation signal. The "rule of thumb" is as follows:

$$f_{L\,opt} \simeq 2 \times (\text{IF rectangular filter bandwidth})$$

$$a_{opt} = 1.5 \times f_m$$

$$(\mu/a)_{opt} = \simeq 6$$

To test this rule, experimental data were taken for two other cases ($\beta = 5$ and $\beta = 6$). The systems were set up using the above rule, and then SNR's were measured for variations of the parameters, to show the PLL was indeed optimally adjusted. In both cases the rule proved to be correct.

Conclusion

A study has been made of the first and second-order PLL behavior, with modulation, as a function of various system parameters. A "rule of thumb" has been proposed for choosing the hold-in range, pole position, and zero-to-pole ratio, which would result in optimum performance of the second-order PLL when used with a full-deviation signal. This rule has

been tested and shown to give satisfactory results; however even with the PLL optimized little SNR improvement over the discriminator was obtained.

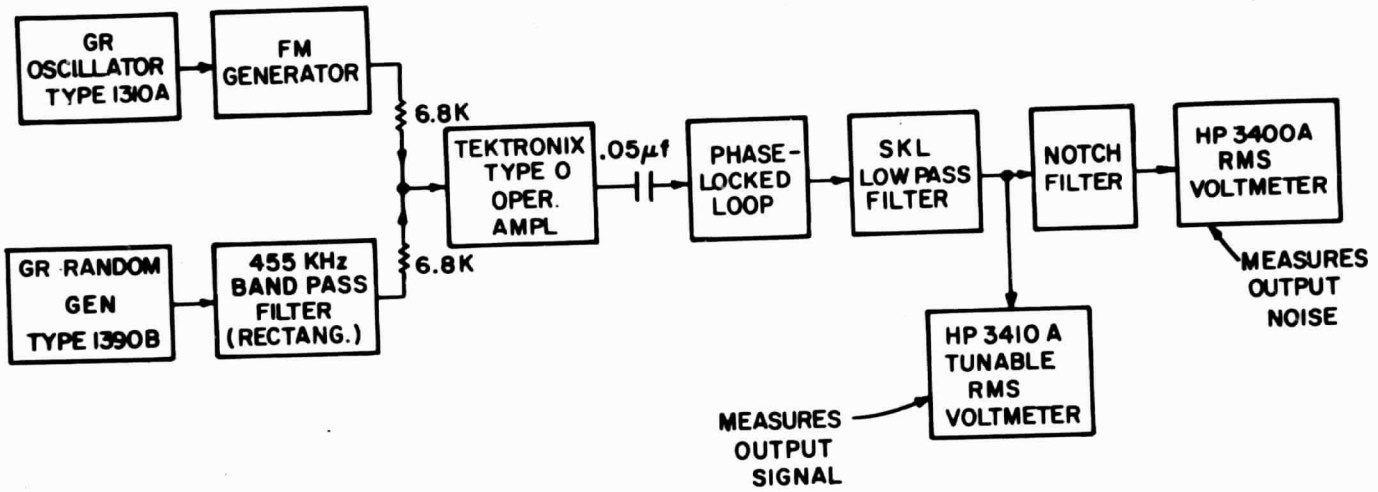

Fig. I-1.4.1 System For Taking SNR Measurements (with modulation)

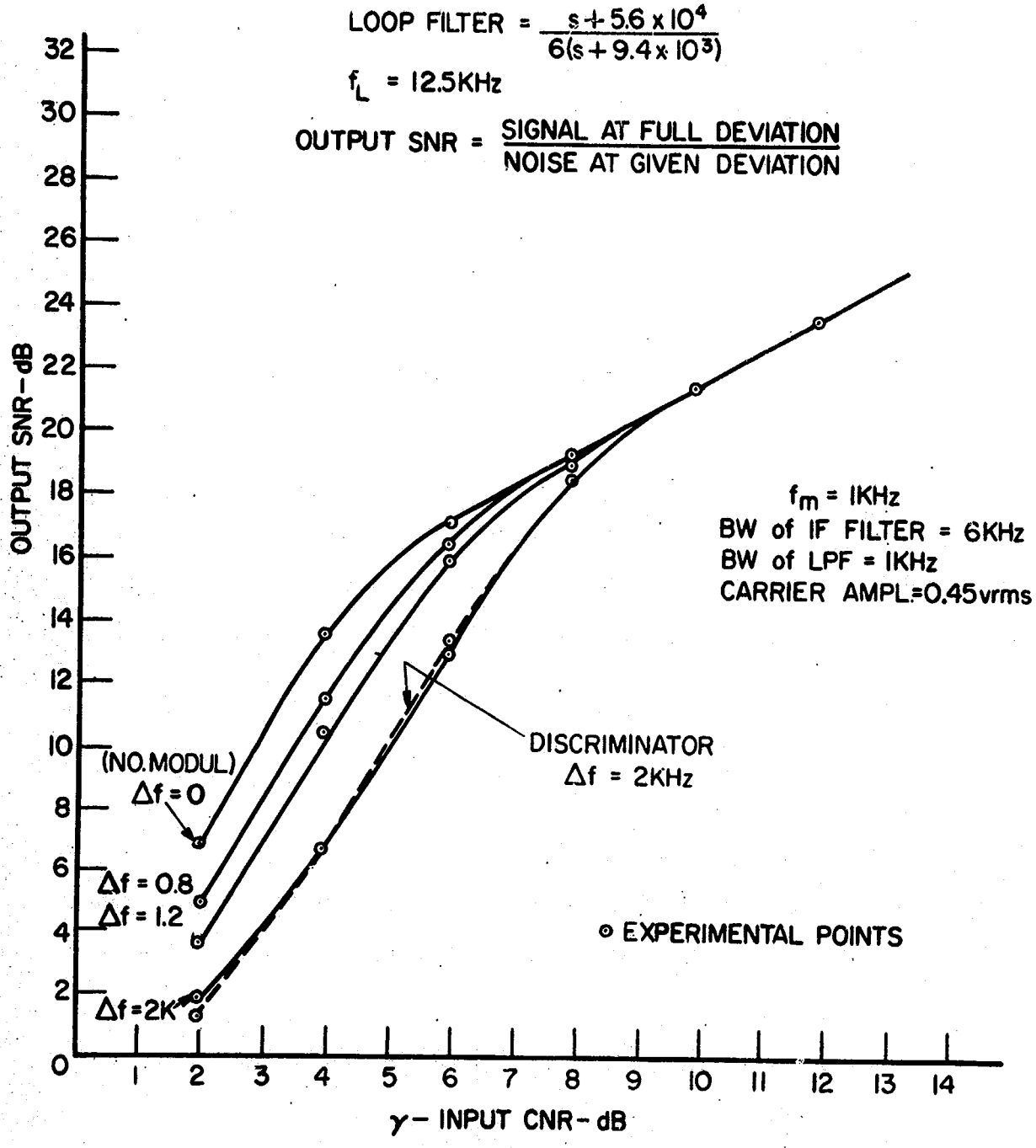

Fig. I-1.4.2 Output SNR vs. Input ONR for a Second-Order Phase-Locked Loop

2. The Frequency Demodulator with Feedback

Introduction. - The response of an FMFB system to an FM signal in the presence of additive gaussian noise has been studied. Results are compared to the FMD, PLL, and other threshold extension devices. Criteria of comparison include the expected number of output clicks as a function of SNR at the input, and modulation index, overall system bandwidth and signal distortion.

Differential Equation of FMFB. - The block diagram of the system is shown in Fig. I-2.1. This system is usually preceded by an IF filter which attenuates the noise outside the signal bandwidth. The input to the FMFB thus consists of a modulated carrier and additive colored gaussian noise. The IF filter is omitted in this section because the differential equations governing the FMFB are independent of it. The discriminator within the loop is assumed to be preceded by an ideal limiter. The input to the FMFB is expressed as:

$$e_{in} = (Y)\sin \omega_0 t - (X)\cos \omega_0 t \qquad (1)$$

where

$$X = x + \sin \phi_m \text{ and } Y = y - \cos \phi_m \qquad (1a)$$

where x and y represent independent orthogonal components of the input gaussian noise, ϕ_m represents the signal modulation and ω_0 is the transmitted carrier frequency.

The output of the VCO within the loop is expressed as:

$$e_{vco} = 2(\sin(\omega_0 + \omega_1)t + \phi) \qquad (2)$$

where ω_1 is the center frequency of the loop filter, G represents the gain of the loop amplifier (the VCO is assumed to have a gain of unity) and where ϕ is the FMFB output phase.

The output of the multiplier, e_m is expressed as:

$$e_m = e_{in}\, e_{VCO} = \big((-X)\sin(\omega_1 t + \phi) + (Y)\cos(\omega_1 t + \phi)\big) + (-X)\sin\big((2\omega_0 + \omega_1)\, t + \phi\big) + (Y)\cos\big((2\omega_0 + \omega_1)\, t + \phi\big) \tag{3}$$

The loop filter is centered at ω_1. In practice, one chooses ω_0 sufficiently large such that the terms at $2\omega_0 + \omega_1$ are attenuated to the point of being negligible.

Thus, one specifies that $H(2\omega_0 + \omega_1) << H(\omega_1)$ (4)

where $H(\omega)$ is the loop filter transfer function.

When a simple RLC circuit is chosen, the transfer function is

$$H(s) = \frac{a\omega_1 s}{s^2 + a\omega_1 s + \omega_1^2} \tag{5}$$

whose low pass equivalent using the $\frac{s}{\omega_1} + \frac{\omega_1}{s}$ transformation is

$$H(s) = \frac{a}{s + a} \tag{6}$$

or

$$ae_f + \frac{d}{dt}\, e_f = a\, e_m \tag{7}$$

If $\omega_1 >> a$, the low pass equivalent may be used with arbitrarily small error. The filter input at low pass, when sum frequency terms are neglected, according to (4), is obtained from (3):

$$e_m = -X \sin\phi + Y \cos\phi \tag{8}$$

The filter output e_f is expressed as:

$$e_f = A \cos\frac{\phi}{G} \tag{9}$$

substituting (8) and (9) into Eq. (7) one obtains:

$$(\dot{A} + a\, A)\cos\frac{\phi}{G} - \frac{\dot{\phi} A}{G}\sin\frac{\phi}{G} = a(-X \sin\phi + Y \cos\phi) \tag{10}$$

which is equivalent to

$$(\dot{A} + a\, A)\cos\frac{\phi}{G} - \frac{\dot{\phi} A}{G}\sin\frac{\phi}{G} = a\left[-X \sin\left(\frac{G-1}{G}\,\phi + \frac{1}{G}\,\phi\right) + Y \cos\left(\frac{G-1}{G}\,\phi + \frac{1}{G}\,\phi\right)\right] \tag{11}$$

letting $\gamma = \frac{G-1}{G}$ (12)

$$(\dot{A} + \alpha A)\cos\frac{\phi}{G} - \frac{\dot{\phi}}{G} A \sin\frac{\phi}{G} = -X[\sin\gamma\phi\cos\frac{\phi}{G} + \cos\gamma\phi\sin\frac{\phi}{G}]\alpha$$

$$+ Y[\cos\gamma\phi\cos\frac{\phi}{G} - \sin\gamma\phi\sin\frac{\phi}{G}]\alpha \quad (13)$$

hence one obtains the fundamental equations of the FMFB:

$$\dot{\phi} = [X\cos\gamma\phi + Y\sin\gamma\phi]\alpha\frac{G}{A} \quad (14)$$

and

$$\dot{A} = \alpha[-X\sin\gamma\phi + Y\cos\gamma\phi] - \alpha A \quad (15)$$

When the noise components x and y are not present (1a) reduces to

$$X = +\sin\phi_m \quad (16)$$

and

$$Y = -\cos\phi_m \quad (17)$$

Substituting (16) and (17) into (14) and (15) yields:

$$\dot{\phi} = -\sin(\gamma\phi - \phi_m)\frac{\alpha G}{A} \quad (18)$$

and

$$\dot{A} = -\alpha\cos(\gamma\phi - \phi_m) - \alpha A \quad (19)$$

Differentiating (18) one obtains:

$$\dot{A} = -\cos(\gamma\phi - \phi_m)\alpha G(\gamma - \frac{\dot{\phi}_m}{\dot{\phi}}) + \sin(\gamma\phi - \phi_m)\alpha G\frac{\ddot{\phi}}{\dot{\phi}^2} \quad (20)$$

Substituting (18) and (20) into (19) yields:

$$\tan(\gamma\phi - \phi_m) = -\left[\frac{\dot{\phi} - \dot{\phi}_m}{\alpha - \frac{\ddot{\phi}}{\dot{\phi}}}\right] \quad (21)$$

Linearization of FMFB. - Equation (21) may be "linearized" to determine the closed loop bandwidth of the FMFB. As the modulation is decreased with respect to the filter bandwidth α, $\tan(\gamma\phi - \phi_m)$ approaches $\gamma\phi - \phi_m$. The denominator is also expanded and only linear terms are kept.

$$\gamma\phi - \phi_m = -\frac{1}{a}\left[\dot{\phi} - \dot{\phi}_m\right]\left[1 + \frac{1}{a\phi}\right] \tag{22}$$

from the left hand side of (22) it follows that when it is small enough,

$$\dot{\phi}_m = \gamma\dot{\phi} \tag{23}$$

Combining (22) and (23), the closed loop transfer function of the FMFB is found to be:

$$\frac{\phi}{\phi_m} = G\,\frac{-\quad 1}{\left(\frac{s}{a} + G - 1\right)} \tag{24}$$

The location of the pole and a sketch of the transfer function of Eq. (24) are shown in Fig. I-2.2. The location of the pole is at:

$$s = (G - 1)\,a$$

Harmonic Distortion. - When a sinusoidal modulating signal is applied to the FMFB some of the output power will be lost to harmonics of the fundamental frequency due to the nonlinearity of the FMFB differential Eq. (21). For an input signal of modulation indix β

$$\phi m = \beta \sin\omega_m t \tag{25}$$

the output signal is assumed to have phase lag terms and odd harmonics. When β is small, the third harmonic is presumed to dominate and an output solution is assumed to have the form:

$$\phi = A\sin\omega_m t + B\cos\omega_m t + C\sin 3\omega_m t + D\cos 3\omega_m t \tag{26}$$

The harmonic distortion is then

$$\%\,\text{distortion} = \left(\frac{C^2 + D^2}{A^2 + B^2}\right)^{1/2} \tag{27}$$

A computer program has been developed whereby the coefficients of (26) are determined so as to make the difference between the right and left hand side

of (21) arbitrarily small. From (23), (25) and (26) A is assumed, to have a value

$$A = \frac{\beta}{\gamma} \tag{28}$$

Next, with B and D set to zero the value of C best fitting (21) with a solution of the form of (26) is determined. Now, with A and C as determined in the first two steps, B is calculated and then D. With the values of B, C, D obtained in the first iteration, A is recalculated. The iteration continues until convergence within an arbitrarily small error is obtained for each value.

Expected number of clicks. - Under operating conditions, the FMFB is usually preceded by an IF filter selected in accordance with Carson's rule. A double pole synchronuously tuned filter was used, each stage having a 3db bandwidth of two radians/sec.

The quadrature noise components each have the spectrum:

$$S(\omega) = Sx \pm Sy = \frac{4\sigma^2}{\omega^2 + 1} \tag{29}$$

where σ^2 is the variance of x and y. The "most-likely" noise trajectory, given the values of the noise at the axis crossing is:

$$E[x(t)/x(0) = 0,\ \dot{x}(0)] = \dot{x}(0)\, t\, e^{-|t|} \tag{30}$$

and

$$E[y(t)/y(0), \dot{y}(0)] = \{y(0)(1 + |t|) + \dot{y}(0)\, t\}e^{-|t|} \tag{31}$$

Equations (30) and (31) were used as inputs to equations (14) and (15), and the solutions obtained, using a computer, yield the click boundaries in terms of x(0), y(0) and $\dot{y}(0)$.

Results. - Spike boundaries have been obtained at $\beta = 5$ and $\beta = 12$ with no modulation, and $\beta = 5$ with modulation. (Refer to Figs. I-2.3, 4 and 5). The modulation applied was a constant offset frequency of $2/\pi$, to represent the

maximum sine wave deviation. The results shown indicate an improvement over similar boundaries for the first and second order PLL.

An experimental FMFB system was built and is observed clicks/sec. will be compared to the number predicted by the computer program.

The harmonic distortion problem in the FMFB is expected to be more severe than in the PLL since several non-linearities rather than just one occur in the FMFB differential equations. Computer results are presently being obtained.

The gain and bandwidth of the FMFB in the spike boundary calculation were selected to result in a loop modulation index of unity and a loop filter obeying Carson's rule. The output clicks obtained using this scheme is calculated. Considerations of distortion may require extension of the FMFB bandwidth to obtain a fair comparison with the PLL.

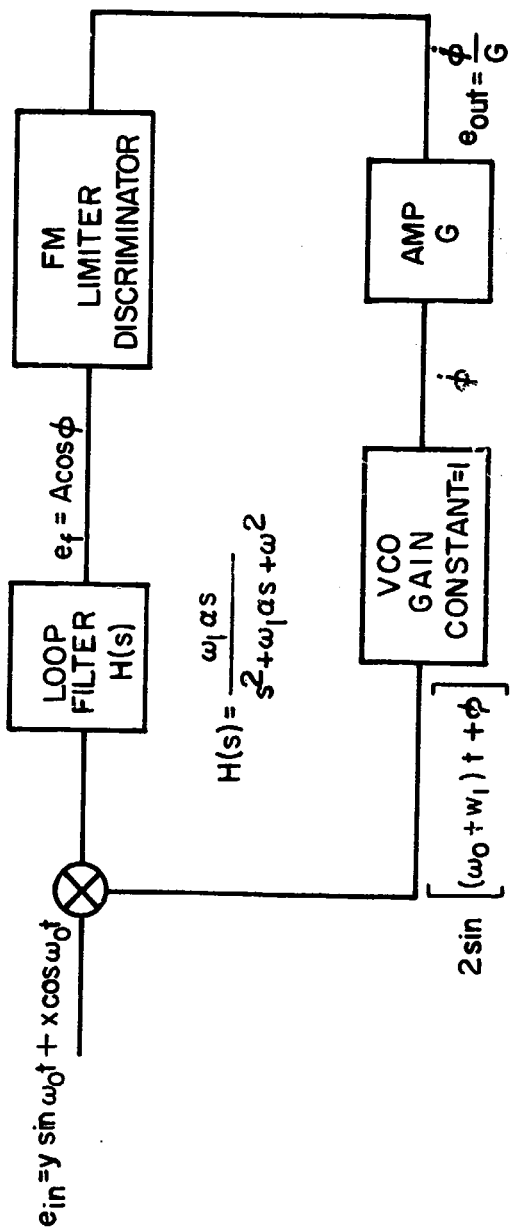

Fig. I-2.1 FMFB block diagram

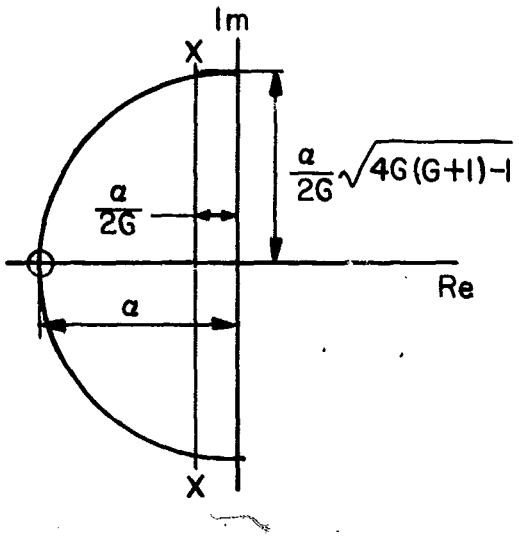

Location of poles and zeros.
FMFB closed loop transfer function.

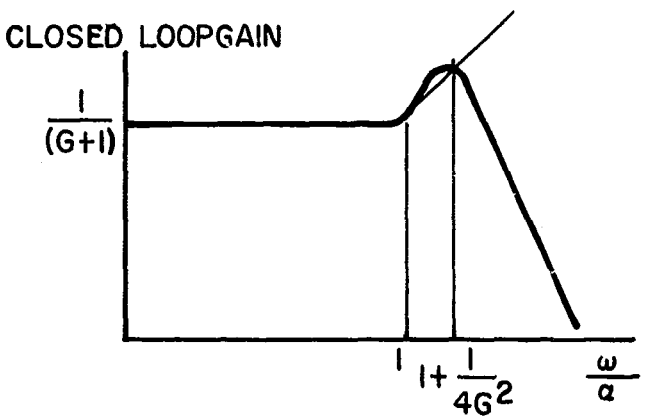

Closed loop gain - FMFB

Fig. I-2.2

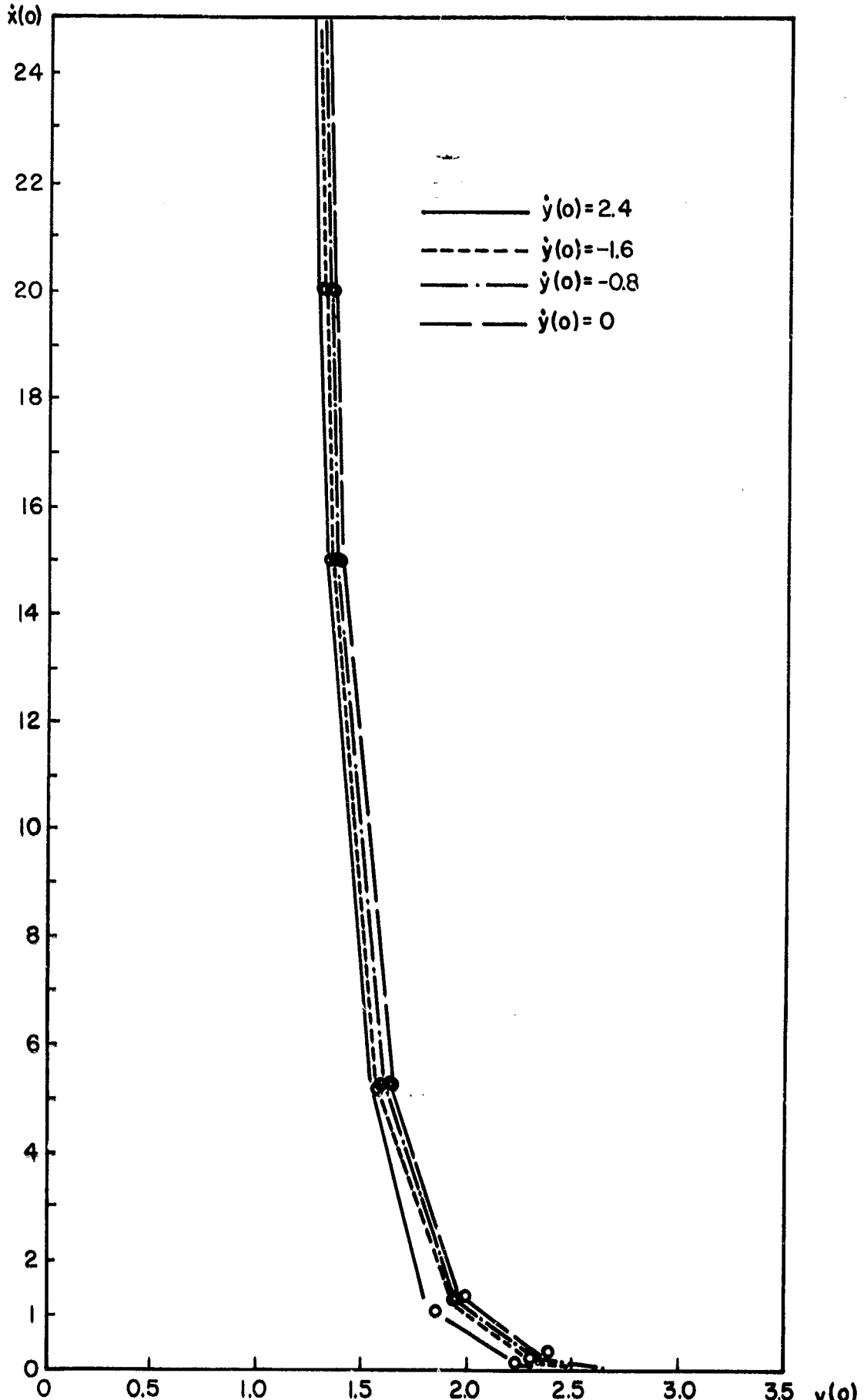

Fig. I. 2-3 FMFB no modulation. $\beta = 5$, $G = 4$, $\beta' = 1$, $a = \frac{2}{6}$ BIF, BIF $= \sqrt{2^{\frac{1}{3}} - 1}$.

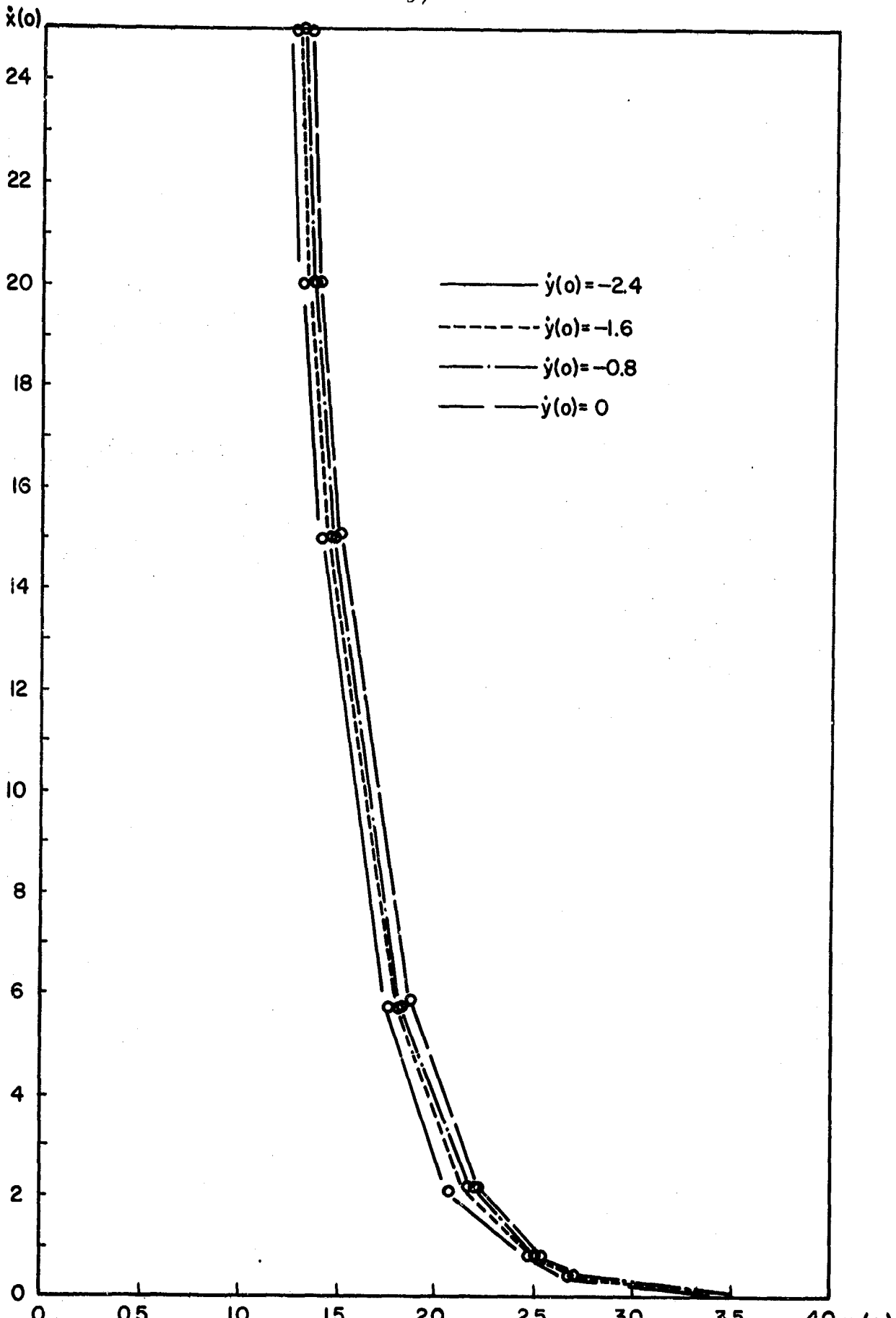

Fig. I. 2-4 FMFB no modulation. $\beta = 12$, $G = 11$, $\beta' = 1$,

$\alpha = \frac{2}{13}$ BIF, BIF $= \sqrt{2^{\frac{1}{2}} - 1}$.

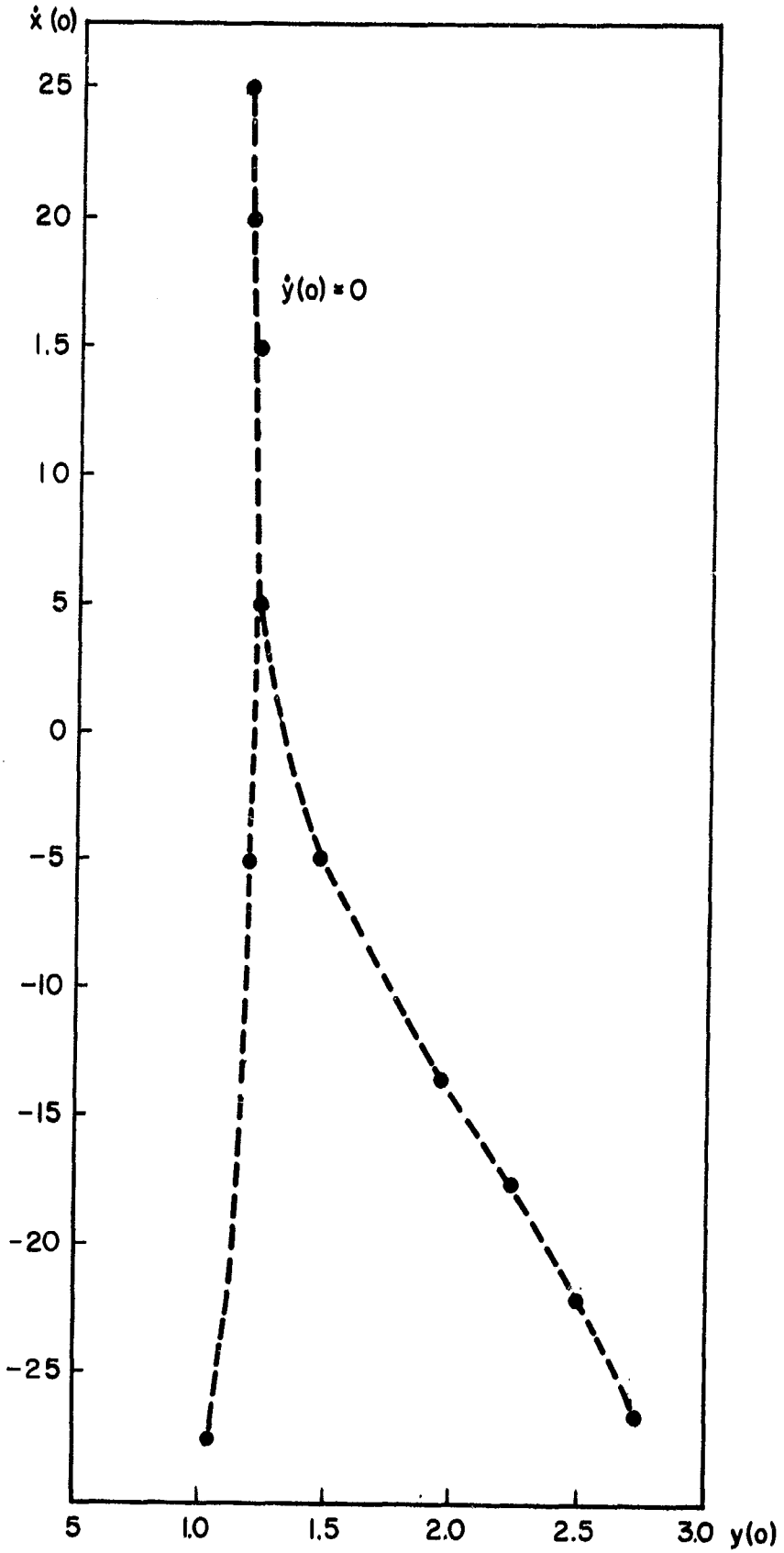

Fig. I. 2-5 Modulation $\Delta f = 0.62\,\Delta f_{max}$ • $\beta = 5$, $G = 4$.

3. The Frequency Locked Loop.

3.1 Quantized Second Order Frequency Locked Loop.

Abstract. - Several previous papers have presented the basic concepts of the threshold extending FM receiver known as the Frequency Locked Loop (FLL). In this section several significant modifications to the basic FLL are reported. Specifically the modifications entail the optimization of the loop filter and the quantization of the amplitude channel. The paper presents intuitive arguments explaining the improvements expected with these modifications.

Finally, and most important, experimental data are presented. These data indicate that even with full deviation sinusoidal modulation, the FLL extends the FM noise threshold significantly over the discriminator. In addition, when used to demodulate binary signals transmitted by Frequency Shift Keying the FLL yields an output probability of error that is within 1.4dB of that achieved with a matched filter having the same input noise spectral density. The comparison with the matched filter was made with modulation indices in the vicinity of 2 and for error rates between 10^{-5} and 10^{-2}.

A. Introduction. - In a previous paper the Frequency Locked Loop (FLL) FM Demodulator[1] is introduced and is shown to be capable of extending the FM noise threshold. This extension is achieved by using the envelope information of the incoming noise corrupted FM carrier to directly control the loop gain and in turn the bandwidth of a feedback loop through which the demodulated FM information is passed; thus if the envelope takes on a small value (relative to its average value) the information is passed through a very narrow bandwidth and effectively "held". Since the FM noise threshold is characterized by the occurrence of gross frequency disturbances of clicks[2], and since, near threshold , these clicks are almost always accompanied by low envelope levels[3] on the incoming noise corrupted FM signal, the holding

property of the FLL eliminates the majority of the clicks from its output and thus extends the noise threshold.

The first order analog FLL previously described has several shortomings. First, the "holding" operation, which occurs far more frequently than the frequency clicks occur, introduces an additional output noise component plus a signal suppression effect, both of which detract from the possible threshold improvement. Secondly, envelope variations for input carrier to noise ratios above threshold cause the FLL to have an above threshold output signal to noise ratio slightly lower than the discriminator.

In this paper intuitive arguments are presented to show that these shortcomings may be partially overcome by quantizing the envelope information before applying it to the feedback loop and by utilizing a properly designed second order filter within the feedback loop. In addition, experimental data are presented which indicate that the intuitive approach to optimization is indeed valid.

Here the input signal is assumed to be in the completely general form of a carrier centered at ω_0 modulated by an envelope a(t) and a phase $\psi(t)$. The envelope a(t) arises when the FM carrier is corrupted by additive narrowband noise centered at ω_0, whereas $\psi(t)$ consists of the desired phase modulation plus pertubations from the narrowband noise. The quantizer consists of a monostable multivibrator which reduces its output q(t) to zero for a fixed duration t_0 every time the envelope a(t) drops below the level ϵA, where A is the FM carrier amplitude. (With no noise present a(t) = A.) Fig. I-3.1.2 indicates the relationship between the quantizer output q(t) and a(t).

If the output of the FLL is designated as $\dot{\Phi}(t)$ and the impluse response of the loop filter is given by $h_0(t)$, the the defining equation for the loop takes the form

$$\dot{\Phi}(t) = q(t)\left[\dot{\psi}(t) - \dot{\Phi}(t)\right] * h_0(t) \qquad (1)$$

The advantage of quantization in the FLL is now apparent. If the input carrier to noise ratio is high, a(t) almost always remains above ϵA and $q(t) = A_0$ (a constant). Thus $\dot{\Phi}(t)$ is just a filtered form $\dot{\psi}(t)$. If in addition, an equalizing filter is incorporated after the loop, as shown in Fig. I-3.1.1, the filtering effect of the loop may be exactly compensated, and thus the equalized loop output $\dot{\Phi}(t)$ and the discriminator output $\dot{\psi}(t)$ are identical (within a scale factor) above threshold. Below threshold a(t) does indeed drop below ϵA during the occurrence of many clicks in $\dot{\psi}(t)$, thereby opening the loop and completely decoupling $\dot{\psi}(t)$ from the output.

The quantizer depends strongly on two parameters, ϵ (the quantization level) and t_0 (the holding time), for its correct operation. Both of these parameters have an optimum value which yields the best threshold improvement. Intuitively we observe that if ϵ is very small, very few holds in the loop occur and thus very few clicks are removed at the loop output. On the other hand, if ϵ is large the number of holds becomes large which permits almost all of the clicks to be removed; however, since the number of holds far exceeds the number of clicks (a(t) drops below ϵA many times when a click does not occur) noise induced by holding $\dot{\psi}(t)$ exceeds the RMS value of the click noise removed. For some intermediate value of ϵ a sufficient number of clicks are removed while the noise due to holding still remains sufficiently small such that an optimum is achieved. This optimum is found experimentally to correspond to $\epsilon \approx 0.2$ and is reasonably broad.

It is interesting to observe the structure of the output noise as ϵ is increased empirically from zero. Initially if operation of the FLL is below threshold, the output contains the same impulsive click noise as the discriminator. As ϵ is increased a number of the clicks are removed or greatly

reduced in area without much additional noise appearing. Finally, as ϵ is increased still further, almost all of the clicks disappear and the "Gaussian like" holding noise begins to greatly increase. In effect, varying ϵ provides a means of not only reducing the total RMS noise below threshold but also converting a click noise into "Gaussian like" noise. This conversion is highly desirable when video or digital information is transmitted via FM. Fig. I-3.1.3 shows the variation in the noise structure for several different values of ϵ.

It is also apparent that if the holding time t_0 is too small, the holding is not accomplished for the entire duration of the click in $\dot{\psi}(t)$ and only a small portion of the click area is removed from the FLL output. On the other hand, if t_0 is too large, the holding noise again begins to more than compensate for the click noise removed. Experimentally it has been found that the optimum t_0 is approximatley $1/2\,(BW_{RMS})$ where BW_{RMS} is the RMS noise bandwidth (in Hertz) of the input narrowband noise. Again this optimum appears experimentally to be rather broad such that a very precise setting of t_0 is not required.

If one observes the FLL output for a fixed value of ϵ as t_0 is increased from zero, one notices first that many of the output clicks become reduced in area as a portion of the input click is removed. As t_0 is increased further many of the input clicks disappear completely, and finally as t_0 is increased still further a large amount of "Gaussian like" holdings noise appears in the output. Since in general ϵ and t_0 are correlated, their optimum values must be obtained simultaneoulsy. This is indeed how they were obtained empirically.

B. Loop Filter Optimization. - The choice of an optimum loop filter is based upon three basic considerations:

1) The filter must provide a good estimate of the signal component

of $\dot{\psi}(t)$ (or $\dot{\Phi}(t)$) during a hold, i.e., when $q(t) = 0$.

2) The filter must produce a well behaved transient when $q(t)$ returns from 0 to A_0.

3) The filter must provide an absolutely stable closed loop response. Clearly requirements 1 and 2 insure that the holding noise is minimized while requirement 3 is essential for any feedback system.

From requirement 1 it is apparent that the loop filter (whose impulse is given by $h_0(t)$) should have as many poles at the origin as possible. This is the case since each additional pole permits the filter output to estimate the desired output signal with one more degree of precision when the input is reduced to zero by $q(t)$ dropping to zero. Specifically if $q(t)$ drops to zero at $t = t_1$ and $h_0(t)$ contains n poles at the origin, for $t_1 < t < t_1 + t_0$ $\dot{\Phi}(t)$ is given by

$$\dot{\Phi}(t) = \dot{\Phi}(t_1) + \ddot{\Phi}(t_1)(t - t_1) + \frac{\dddot{\Phi}(t_1)(t - t_1)^2}{2!}$$

$$+ \ldots + \frac{\Phi^n(t_1)(t - t_1)^{n-1}}{(n-1)!}; \quad t_1 < t < t_1 + t_0$$

As $n \to \infty$, $\dot{\Phi}(t)$ would be approximated exactly during a hold Eq. (2) would become the Taylor series for $\dot{\Phi}(t)$, and no holding noise would exist. Requirement 3, however, limits the number of poles to 2, since 3 poles at the origin in a feedback loop would produce at best conditional instability. With two poles at the origin for $h_0(t)$, $\dot{\Phi}(t)$ is approximated by its value and slope at $t = t_0$ during a hold as shown in Fig. I-3.1.4. Clearly a much poorer approximiation to $\dot{\Phi}(t)$ during a hold would result if $h_0(t)$ contained a single pole at the origin; specifically $\dot{\Phi}(t)$ would remain constant during the hold thereby increasing the holding noise.

Requirement 3 also specifies the zeros of $h_0(t)$. In order to keep the closed loop poles from approaching too close to the imaginary axis, $h_0(t)$

must take a form similar to that shown in Fig. I-3.1.5. The figure also indicates the locus of the poles of the closed loop FLL, with no holding, as the loop gain (or equivalently A_0) is increased. In order to meet requirement 2, a sufficiently large value of A_0 must be chosen to keep the imaginary part of the closed loop poles above the passband of the final baseband filter. At the end of each hold a transient results which has a strong frequency component at a value equal to the distance of the poles from the real axis. If this frequency component is not passed by the baseband filter, the basic holding noise is due to the inexact estimate of $\dot{\Phi}(t)$ during a hold.

On the other, A_0 should not be chosen any larger than that value which just keeps the imaginary part of the closed loop poles above the baseband bandwidth. A larger value of A_0 would increase the closed loop bandwidth of the FLL and thereby permit a larger noise component in $\dot{\Phi}(t)$. Such an additional noise component is highly undersirable since when a hold occurs, the additional noise plus the desired signal component of $\dot{\Phi}(t)$ is estimated, and the output noise is greatly enhanced. This is particularly true of the high frequency noise, which when held generates low frequency noise components which reach the output of the baseband filter. Consequently, the closed loop poles should be placed just slightly above the passband at the baseband filter and the equalization filter should be designed to exactly compensate for the closed loop poles over the entire baseband.

In the FLL which has been constructed, the imaginary part of the closed loop poles is 1.55 kHz, whereas the baseband filter has a -3dB bandwidth of 1kHz and falls off at 24dB per octave in the stop band. In addition, the zero of $h_0(t)$ is at 6.7 kHz. The equalization filter has a pair of complex conjugate zeros which lie at the same position as the closed loop poles.

A subsequent section of this report presents a theoretical derivation of SNR vs. CNR curves with ϵ as a parameter. Yet another section presents a comparison of a theoretically derived expression for probability of error in digital FSK transmission with measured results. At this point we present a quick summary of experimental data to provide a frame work for these subsequent sections.

C. Experimental Results. - Experimental results are shown for both the case of binary frequency shift keying (FSK) and for the case of sinusoidal analog modulation.

Figs. I-3.1.6 and 7 show comparative results for the detection of errors in a $\beta = 2$, noisy binary FSK signal detected both by a discriminator and by a discriminator plus a base band frequency locked loop.

Fig. I-3.1.7 plots curves of probability of error vs. the input carrier-to-noise ratio (CNR) in dB. These curves are for a discriminator, for a FLL circuit and for the theoretical matched filter. The theoretical curve for the discriminator was derived by Schilling, et al.[4] At a CNR of 8 dB the error rate from the FLL is down by a factor of more than 100 from the discriminator case. From another viewpoint, if the error rate is held constant at $1/10^5$ bits then the input CNR required by the FLL is 2.2 dB less than that required by the matched filter.

Fig. I-3.1.8 plots comparative curves of the output signal-to-noise ratio (SNR) in dN vs. the input CNR for the $\beta = 14.5$ case. These curves are actual measured curves with full sinusoidal deviation; that is, with a peak deviation of 14.5 kHz in a square IF of peak-to-peak bandwidth of 33 kHz. One should note that for an input CNR of 6 dB the FLL has an output SNR that is 7.3 dB above the discriminator. Since Fig. I-3.1.3 is for a CNR of 6 dB through the same IF filter (Δf in Fig. I-3.1.3 is 15.5 kH while Δf is 14.5 kHz

in Fig. I-3.1.8) one can see from Fig. I-3.1.3 that not only is the noise 7.3 dB less at the FLL output but the noise structure is both somewhat different and, through the control of ϵ is adjustable to best suit a particular system.

D. Conclusion. - The quantized, second order frequency locked loop has been shown to offer substantial advantages over an ordinary discriminator both in the detection of FSK and in obtaining higher SNR's in the analog modulation case.

References.

1. K.K. Clarke and D.T. Hess, "Frequency Locked Loop FM Demodulator", IEEE Trans. on Comm. Tech., Vol. Com-15, August 1967, pp. 518-524.
2. S.O. Rice, "Noise in FM Receivers", Time Series Analysis, M. Rosenblatt, E. New York: Wiley, 1963, Chapter 25.
3. L. Calandrino and G. Immovilli, "Coincidence of Pulses in Amplitude and Frequency Deviations", Alta Frequenza, English Issue No. 3, Vol. 36, August 1967.
4. D.L. Schilling and E. Hoffman, "Demodulation of Digital Signals Using an FM Discriminator", Proc. of the National Electronics Conference, Vol. XXII, 1966, pp. 369-374.

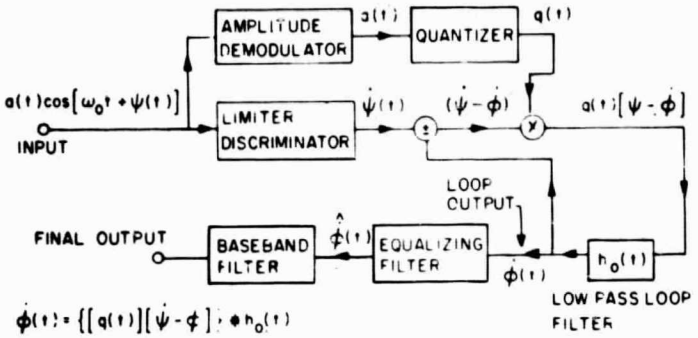

Fig. I-3.1.1 Block Diagram of the Baseband Frequency Locked Loop

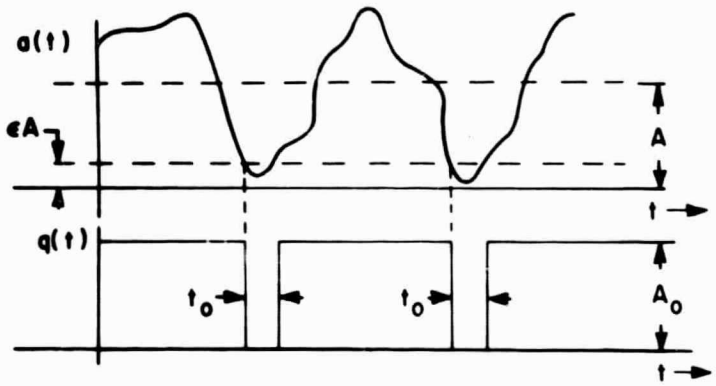

Fig. I-3.1.2 Relationship Between the Input Amplitude, a(t) and the Quantizer Output, q(t)

ε	SNR in 1kHz band
0.0	24.5dB
0.1	28.0dB
0.2	31.0dB
0.3	31.8dB
0.4	30.5dB

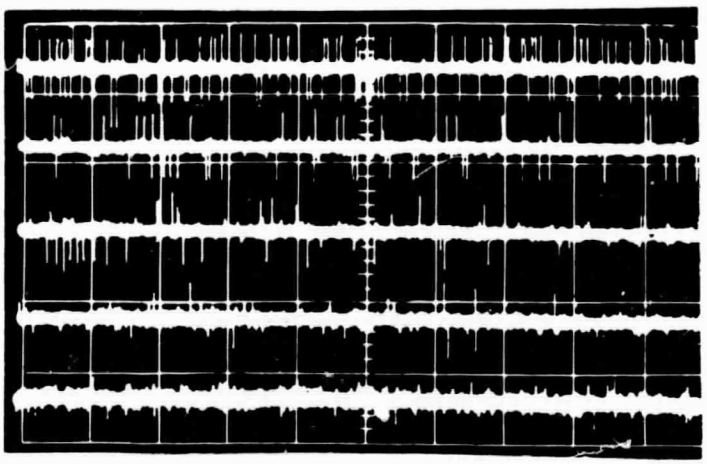

Fig. I-3.1.3 Variation of Noise Structure with ε and a Baseband FLL Input Carrier-to-Noise 6dB. Peak-to-Peak "Square" IF Bandwidth 33kHz. Δf = 15.5kHz, f_m = 1kHz t_o = 25 μsec, Modulation Notched Out by More than 50 db. Baseband Filter Widened to 3kHz to Show Individual clicks. 100mV/cm Vertical, 50ms/cm Horizontal.

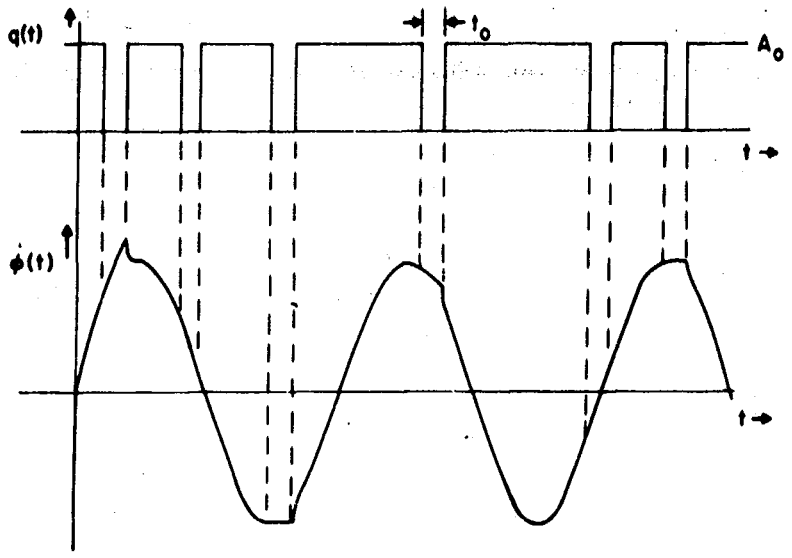

Fig. I-3.1.4 Second Order Holding

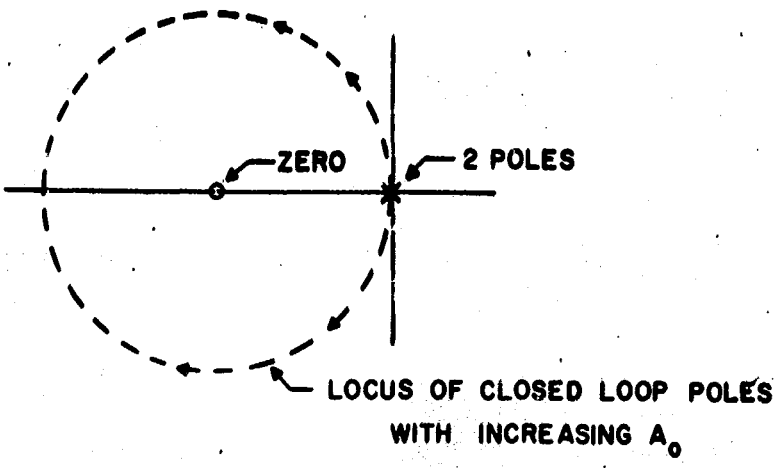

Fig. I-3.1.5 Pole-Zero Pattern for $h_o(t)$

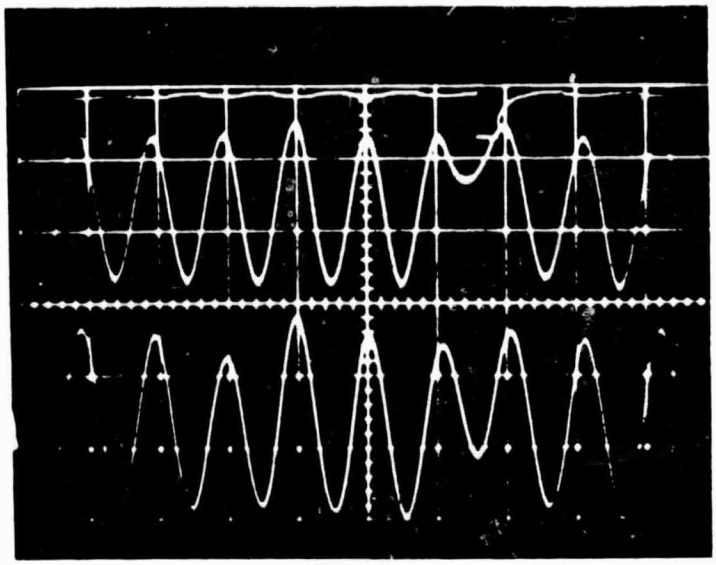

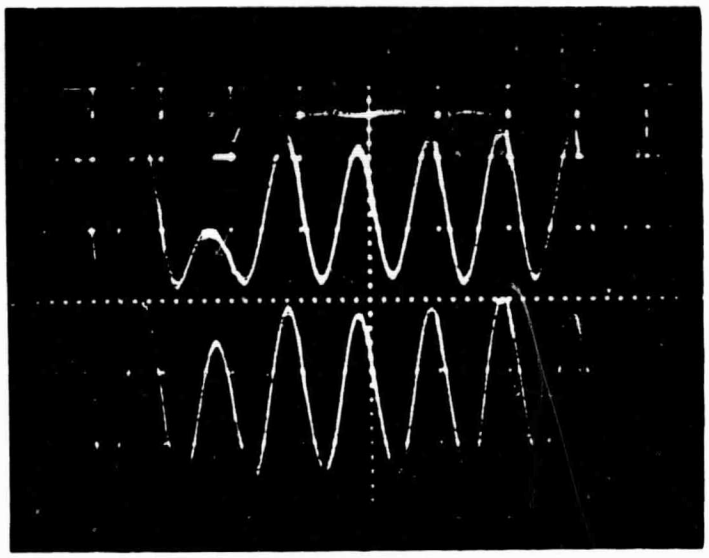

IF = 6kHz TOTAL - "SQUARE"
Δf = 2kHz PEAK
fm= 1 kHz
BASEBAND LOW PASS FILTER = 1.0kHz (-3db) 24db/OCTAVE
τ_{HOLD} = 85 μSEC., ϵ=0.3, RF DELAY=10μSEC.

Fig. I-3.1.6 Digital Errors in FSK for a Discriminator and a Frequency Locked Loop

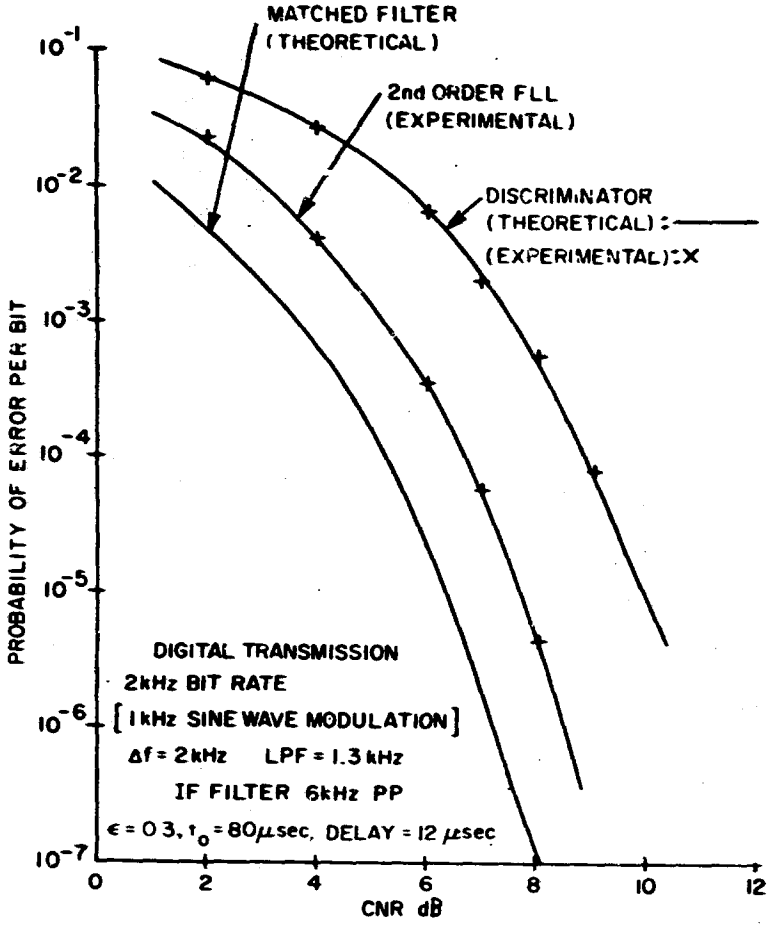

Fig. I-3.1.7 Probability of Error vs. Carrier to Noise Ratio

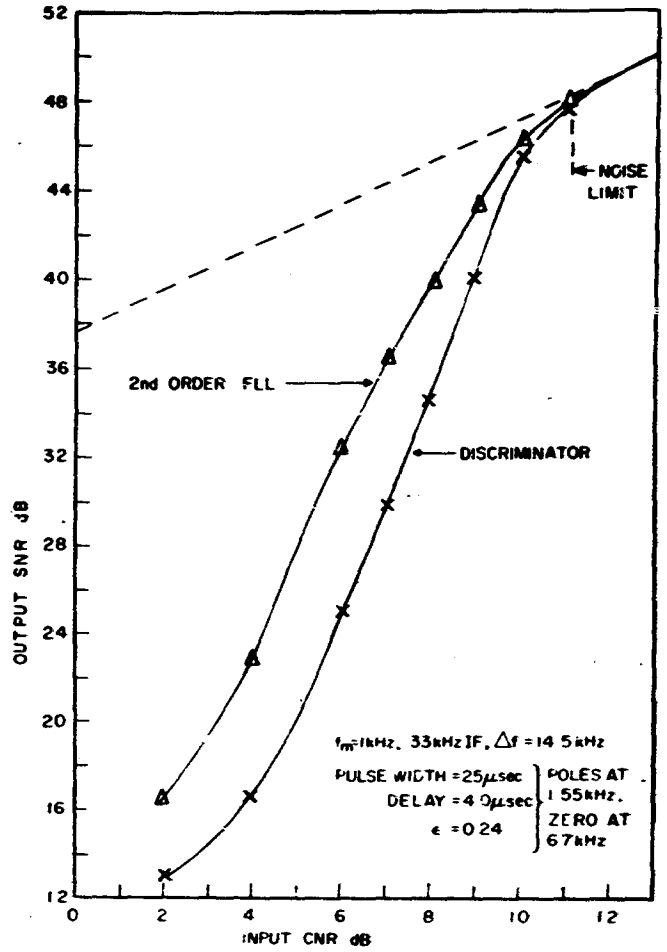

Fig. I-3.1.8 Output SNR vs. Input CNR for 2nd Order FLL and for a Discriminator with Modulation

3.2 FM Threshold Extension Performance of the Quantized Frequency Locked Loop.

1. Introduction. - The noise and signal output of the FM discriminator in the threshold region, $\dot{\psi}(t)$, may be represented as

$$\dot{\psi}(t) = e_m(t) + n_g(t) + n_c(t) \tag{1}$$

where $e_m(t)$ is the desired modulation signal, $n_g(t)$ is the gaussian noise; and $n_c(t)$ is the noise created by clicks[1]. The noise and signal output of the Quantized Frequency Locked Loop (QFLL) in the threshold region, $\dot{\psi}(t)$, is

$$\dot{\psi}(t) = e_m(t) + n_g(t) + n_c(t, e) + n_h(t, \epsilon) \tag{2}$$

where $e_m(t)$ and $n_g(t)$ are the same as for the FM discriminator; $n_c(t, \epsilon)$ is the noise due to clicks not recognized and suppressed by the QFLL; and $n_h(t, \epsilon)$ is due to the signal and gaussian noise distortion caused by holds (including the "false" holds intended for click suppression)[2]. To the extent that $n_c(t, \epsilon) + n_h(t, e)$ for the QFLL are less than $n_c(t)$ from the FM discriminator, an improvement in output signal to noise ratio will result.

To illustrate the signal to noise ratio improvement obtainable with the second order, baseband version, QFLL, the theoretical and experimental results of Unkauf[3] are presented. In this derivation it is assumed that the loop filter has the response:

$$H(s) = \frac{G(s + a)}{s^2} \tag{3}$$

and that the (pre-equalization) closed loop transfer function, T(s), is given by:

$$\frac{\omega_0^2}{a} \quad \frac{(s + A)}{s^2 + es + \omega_0^2} \tag{4}$$

2. Calculation of Signal to Noise Ratio. - Consider an FM system with rectangular IF filter of total bandwidth, B, such that $B = 2(\beta + 1)f_m$, where f_m is the highest modulating frequency, $\beta = \frac{\Delta\omega}{\omega_m} = \frac{\Delta f}{f_m}$ is the modulation index, and Δf is the peak frequency deviation of the FM carrier. Consider also maximum deviation, maximum frequency modulation of the form:

$$e_m(t) = \Delta\omega \cos \omega_m t \tag{5}$$

For the system parameters given and a rectangular output low-pass filter of cut-off frequency f_m, the QFLL output noise power has been calculated by Unkauf.

The power corresponding to $n_g(t)$, N_g, is:

$$N_g = \frac{4\pi^2 f_m{}^2 \delta}{3\rho} \tag{6}$$

where ρ is the input carrier to noise ratio and δ is the modulation induced, noise reduction factor; $\delta \cong 1$ for the system considered and large β. The power corresponding to $n_c(t, \epsilon)$, N_c, is

$$N_c = 8\pi^2 f_m n_c(\epsilon, \rho) \tag{7}$$

where $n_c(\epsilon, \rho)$ is the expected number of clicks per second at the FM discriminator output which are not recognized by the QFLL as given in the Appendix. The noise power corresponding to $n_h(t, \epsilon)$, N_h, is:

$$N_h = \mu^2 8\pi^2 f_m [n_c(0, \rho) - n_c(\epsilon, \rho)] + 2\sigma_D{}^2 f_m. \tag{8}$$

where $(1 - \mu)$ is the average percentage of click area suppressed by a hold; $\sigma_D{}^2$ is the mean-square disturbance created by the holding mechanism on the discriminator gaussian noise and signal components; and $n_h(\epsilon, \rho)$ is the expected number of holding events per second. These constants are given in the Appendix.

N_h is plotted in figure 1 for small μ, $\beta = 5$, and $Bt_0 = 1$ (where t_0 is the length of the holding interval). N_n displays a pronounced minimum in the region $1.5 < \frac{\omega_0}{\omega_m} < 3$ and hence specifies the second order QFLL loop filter design, Eqs. (3) and (4). Since the other QFLL noise terms are independent of ω_0, the QFLL also displays a maximum output signal to noise ratio in the region $\frac{\omega_0}{\omega_m} \cong 2$. The position of the loop zero is not critical so long as it is sufficiently large.

The signal power at the QFLL output, S_0, is:

$$S_0 = \frac{\Delta\omega^2}{2} = \frac{\beta^2 \omega_m^2}{2} \tag{9}$$

and the total QFLL output signal to noise ratio, S_0/N_0, is:

$$\frac{S_0}{N_0} = \frac{S_0}{N_g + N_c + N_h} \tag{10}$$

This expression for output signal to noise ratio is plotted in Fig. I-3.2.2 for a modulation index of 5 with ϵ (the click detection parameter) as a parameter. Note that the theoretical results are really only valid for $\rho \gtrsim 4$ dB due to the neglect of discriminator signal suppression and the initial conditions for validity of the noise model, Eq. (1). Similar curves for modulation idices of 2 and 15.5 are contained in Reference 3.

The operation of the second order QFLL is clear from Fig. I-3.2.2 and Fig. I-3.2.3 of the previous section. As ϵ increases from zero, the average number of clicks suppressed by the QFLL rapidly increases and the QFLL click noise decreases. Also, the number of holding events (attempted click suppression events) increases rapidly with ϵ and the noise due to holding increases. Thus, the QFLL output signal to noise ratio first increases with click noise reduction and later decreases again due to holding noise production as ϵ is increased. The optimum value of ϵ for best overall signal to noise ratio improvement is approximately 0.2 which is experimentally

verified. In a future paper, this trade-off in the nature of the QFLL output noise will be shown to be of great value in the demodulation of digital FM signals.

The overall threshold extension obtainable (for all modulating frequencies) with the QFLL is on the order of 1.5 dB as indicated by the results of Fig. I-3.2.2. This results agrees well with the work of Malone[4] who simulated the case of a linear interpolation during a click detection and erasure events on the digital computer. It also agrees in the limit with the work of Calandrino and Immovilli[5] who considered the open-loop problem of detecting and processing the discriminator clicks to achieve threshold extension.

Unkauf showed that the threshold extension of the QFLL improves with increased carrier frequency deviation and modulating frequency. Hence, the spectrum of the modulation employed with the QFLL system may be heavily pre-emphasized to yield still further signal to noise ratio improvement on final de-emphasis filtering of the QFLL output.

As a further comparison of the second order QFLL, Fig. I-3.2.3 compares this circuit with a second order Phase Locked Loop (PLL) that was optimized for the condition of maximum system carrier frequency deviation. This comparison was made for the $\beta=5$ case under identical experimental conditions. The PLL results are dotted curves. For no modulation the PLL shows an improvement of 1.5dB in output SNR at an input CNR of 7-8dB at the peak sinewave deviation the PLL is not experimentally distinguishable from the ordinary discriminator. From 2-7dB input CNR the FLL shows an improvement of 4dB or more in output CNR over the discriminator. Similar results have been obtained for betas of 2 and 15.5.

References.

1. S.O. Rice, "Noise in FM Receivers", Time Series Analysis, M. Rosenblatt, E. New York: Wiley, 1963, Chapter 25.

2. K. K. Clarke and D.T. Hess, "Quantized Second Order Frequency Locked

Loop", IEEE Proc. Group on Aerospace and Electronic Systems, Eascon 1968 Convention Record, pp. 193-198.

3. M.G. Unkauf, "Quantized Frequency Locked Loop", Ph. D. Dissertation, Polytechnic Institute of Brooklyn, June 1969.

4. M. J. Malone, "FM Threshold Extension without Feedback", IEEE Proc., Vol, 56, No. 2, pp. 200-201.

5. L. Calandrino and G. Immovilli, "On the Performance of Amplitude-Phase Correlation FM Demodulators", Alta Frequenza, English Issue No. 2, Vol. 7.

6. R. Schulman, "A Study of the Behavior of the Phase Locked Loop", M.S. Report Project, P.I.B., June 1968.

Appendix.

The following constants and functions have been computed by Unkauf[3] for the conditions indicated in this paper.

The expected number of clicks per second at the QFLL output, $n_c(\epsilon, \rho)$, is:

$$n_c(\epsilon,\rho) \cong \frac{2\sqrt{2a}}{\pi} e^{-\rho(1+e)^{\frac{1}{2}}} + \frac{2\gamma e^{-\rho(1+\epsilon)^2}}{2\pi(1+\epsilon)\sqrt{4\pi\rho}} e^{-a\rho(1+\epsilon)} I_0(a\rho(1+\epsilon)) \qquad A-1$$

where γ is the radius of gyration of the IF filter and

$$a = \frac{e_m^{\,2}(t)}{\gamma^2} = \frac{\Delta\omega^2}{2\gamma^2} \quad .$$

The expected number of holds per second, $n_h(\epsilon, \rho)$, is:

$$n_h(\epsilon,\rho) = \int_0^{\frac{\Delta^2\omega}{\gamma^2}} H(a^2)\, P_{a^2}(a^2)\, da^2 \qquad A-2$$

where $P_{a^2}(a^2)$ is the probability density of a^2 and

$$H(a^2) = \frac{\epsilon\gamma}{\sqrt{\pi}}\, e^{-\rho(1-\epsilon^2)}\left[e^{-x}I_0(x)\right]\left\{e^{-y}I_0(y) + 2\sum_{n=1}^{\infty}\frac{I_{an}(x)}{I_0(x)}I_n(y)\,e^{-y}\right.$$

$$\left. + \frac{a^2}{e}\sum_{n=1}^{\infty}\frac{I_{2n-1}(x)}{I_0(x)}\left[I_n(y) + I_n(y)\right]e^{-y}\right\} \qquad \text{A-3}$$

where $a^2 = \dfrac{e_m^{\,2}(t)}{\gamma^2}$ and $x = 2\epsilon\rho$ and $y = \dfrac{a^2\rho}{2}$. These results are plotted in Fig. I-3.2.4 for the full deviation since wave modulation assumed. The expected value of μ is determined experimentally:

$$\mu = \operatorname{erfc}\left(0.51\left[1 + \frac{|e_m(t)|}{\sqrt{3}\,\gamma}\right]\right) \qquad \text{A-4}$$

And the mean-square holding disturbance, $\sigma_D^{\,2}$, is approximated by:

$$\sigma_D^{\,2} \cong \frac{\delta}{2\pi}\int_{-\infty}^{\infty}\frac{d\omega S\varphi\omega}{\omega^2}\left\{1 - 4\omega^2/\omega_0^{\,2} + \frac{t_0^{\,4}\omega^4}{4} + \frac{2\omega^4}{\omega_0^{\,2}} + \frac{t_0^{\,2}\omega^4}{\omega_0^{\,2}} + 2\omega^2 t_0^{\,2}\right.$$

$$+ \left[\cos\omega t_0\right]\left(-\frac{2\omega^4}{\omega_0^{\,4}} - \frac{\omega^4 t_0^{\,2}}{\omega_0^{\,2}} - \omega^2 t_0^{\,2} + \frac{4\omega^2}{\omega_0^{\,1}} - 1\right)$$

$$\left. - \left[\sin\omega t_0\right]\left(\omega t_0 - \frac{2\omega^3 t_0^{\,2}}{\omega_0^{\,2}}\right)\right\} \qquad \text{A-5}$$

where

$$S\varphi(\omega) \cong \frac{\omega_0^{\,4}}{2\rho B}\,\frac{\omega^2}{\omega^4 + (4e^2 - 2\omega_0^{\,2})\omega^2 + \omega_0^{\,4}}$$

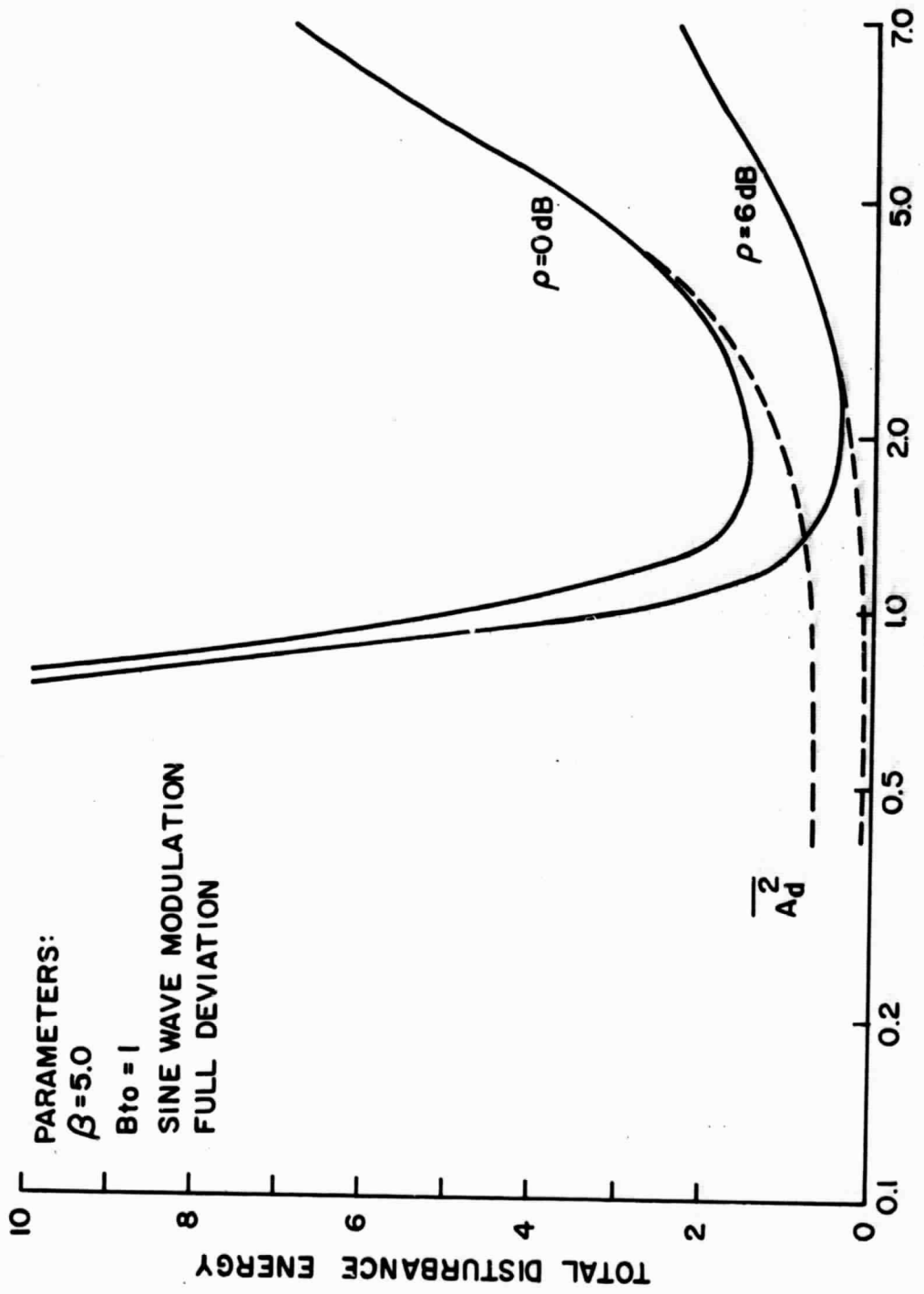

Fig. I-3.2.1 Second Order FLL Disturbance Energy Versus ω_o/ω_m with ζ as a parameter

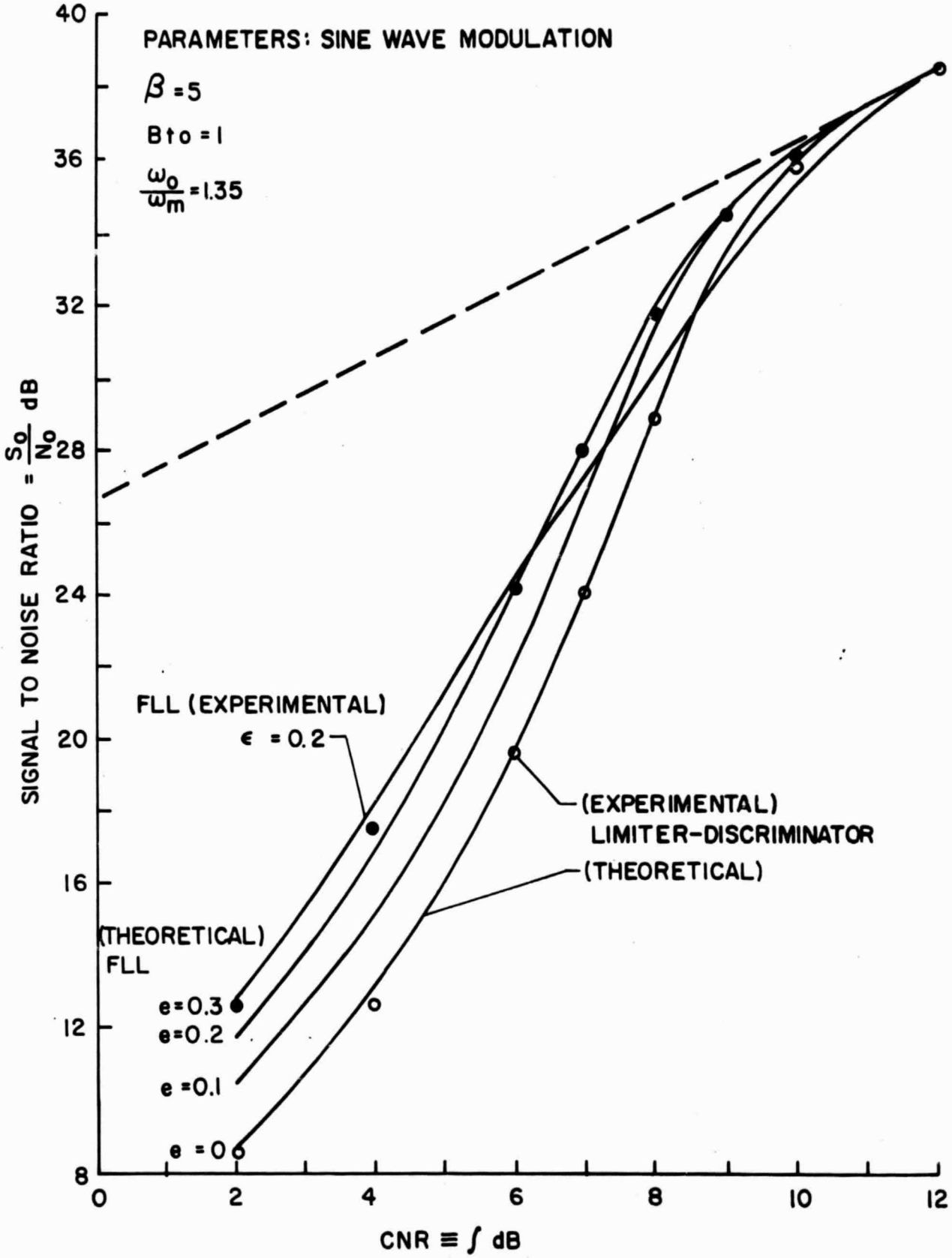

Fig. I-3.2.2 Threshold Extension Performance of Second Order Frequency Locked Loop

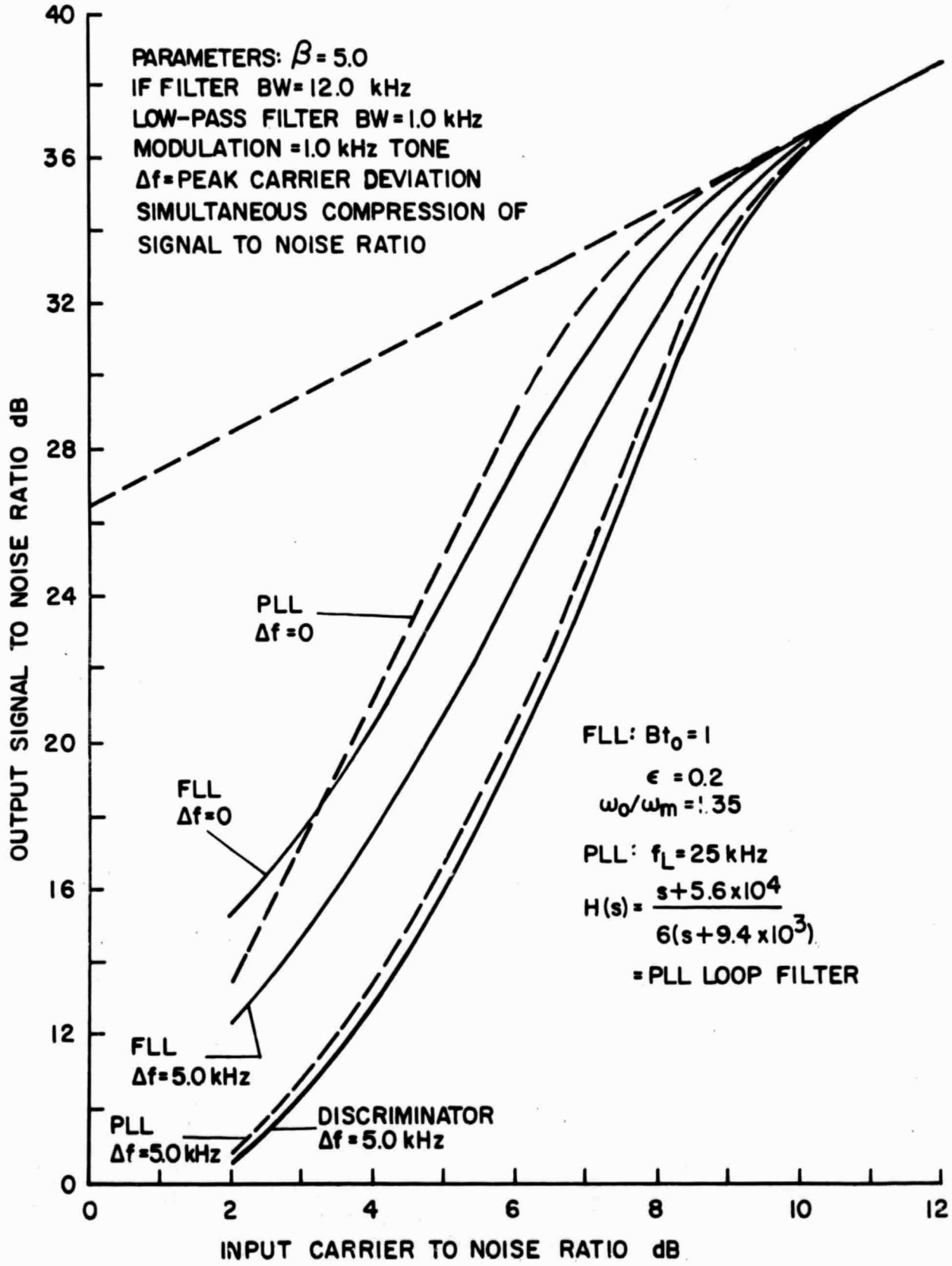

Fig. I-3.2.3 Signal to Noise Ratio Comparison of Second Order Quantized FLL and Second Order PLL

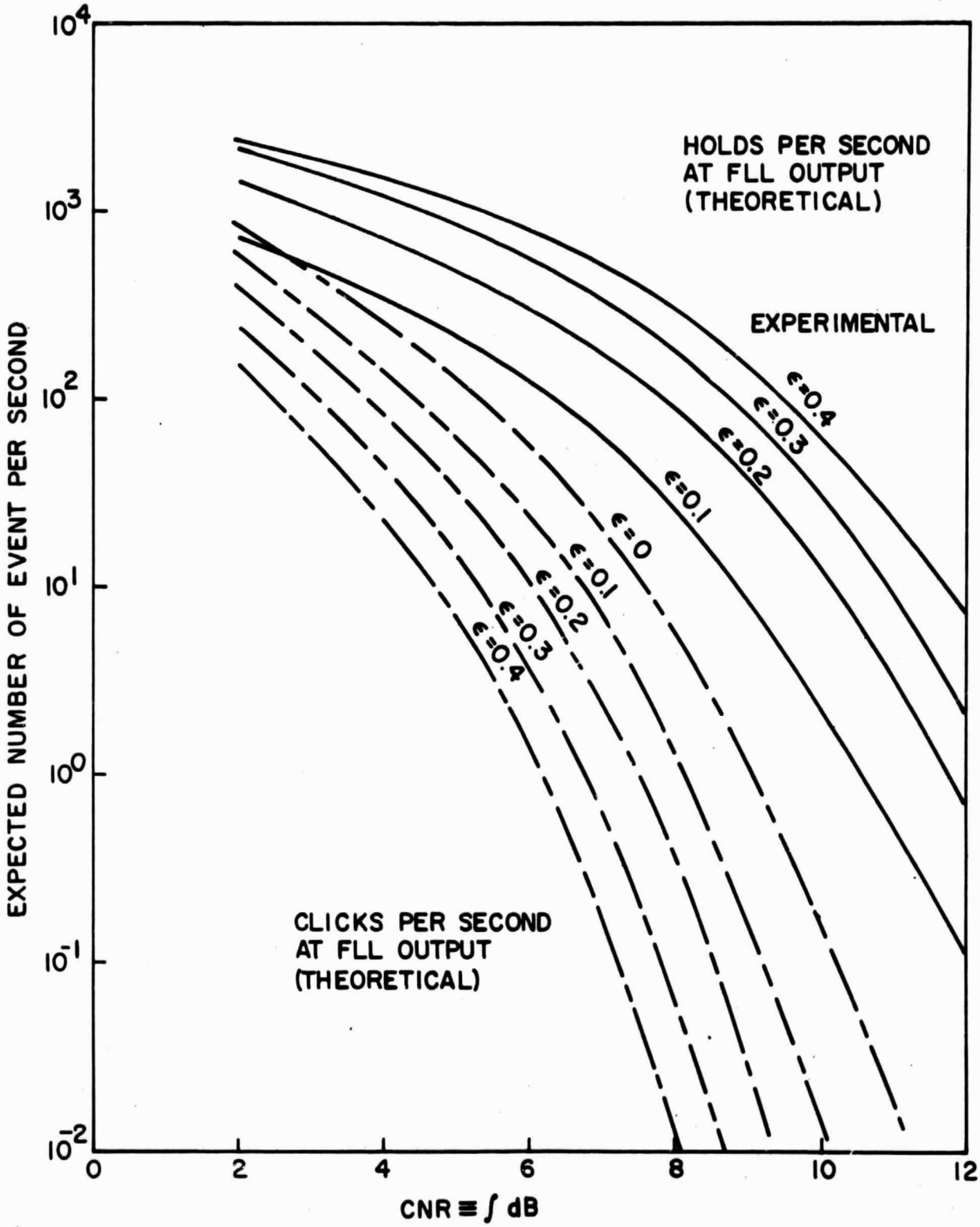

Fig. I-3.2.4 Expected Number of Clicks and Holds at Quantized FLL Output Versus ζ and ε

3.3 Probability of Error for the Frequency Locked Loop (FLL) Digital Demodulator.

Schilling and Hoffman[1] showed that the errors incurred in the discriminator demodulation of binary FM signals corrupted by noise could be treated as errors due to clicks and errors due to gaussian noise. Thus, the probability of error in demodulation, P_e, is:

$$P_e = P_{eg} + P_{ec} \tag{1}$$

where P_{eg} is the probability of error due to the gaussian noise and P_{ec} is the probability of error due to click noise. Since the FLL suppresses clicks, it can reduce the errors due to clicks. However, as seen in the previous section, the FLL introduces an extra holding noise which may introduce errors. Thus the probability of error for the FLL is:

$$P_e = P_{eg} + P_{ec}(\epsilon) + P_{eh}(\epsilon) \tag{2}$$

where $P_{ec}(\epsilon)$ is the probability of error caused by clicks which were not recognized by the FLL and $P_{eh}(\epsilon)$ is the probability of error caused by the holding noise due to "false" holds.

Consider a binary FM system as shown in the block diagram of Fig. I-3.3.1. The binary information is pre-modulation filtered such that for a maximum information rate, 1010 test sequence, only the first harmonic of the information is FM modulated and transmitted. The IF filter is rectangular of total bandwidth $B = 2(\beta + 1)f_m$, where $f_m = 1/T$ and T is the period of a bit. The resultant modulation has the form:

$$e_m(t) = \Delta\omega \cos \omega_m t \tag{3}$$

The output low-pass filter is approximately gaussian with 3 dB cut-off frequency f_m.

For the above system parameters, Schilling and Hoffman showed that the probability of error due to gaussian noise, P_{eg} is:

2.2 dB improvement (a decrease in error probability by more than 100 for $\rho = 9$ dB) over the discriminator and comes to within 1.8 dB of the matched filter result. The experimental results for $\epsilon = 0.3$ agree well with the theoretical results. It should be noted that a further improvement in system performance can be gained by optimizing the low-pass filter bandwidth. This adjustment results in a further 0.4 dB improvement in the FLL performance.

Caution must be exercised when employing the above theoretical results for ϵ greater than 0.3 due to the effect of interference between adjacent holds. The value of ϵ employed for the FLL in Fig. I-3.3.2 was the experimentally determined optimum. The errors due to clicks decrease with increasing ϵ while those due to holds increase. When the expected number of clicks and holding errors are equal, the overall error rate is lowest and this occurs for $\epsilon \cong 0.3$ in the experimental system.

The FLL as indicated in Fig. I-3.3.2 would require 3.3 dB more signal to noise ratio to perform as well as the matched filter for coherent PSK (assuming constant energy per bit). By way of comparison, a differential detection scheme for binary FM using a product demodulator was shown by Anderson, Benett, Davey, and Salz[3] to require 4.8 dB more signal to noise ratio for this same performance. Thus the FLL FM demodulator should prove to be of significant advantage in the demodulation of digital FM signals due to its excellent error rate characteristics and its inherent simplicity of construction.

References.

1. D. L. Schilling and E. Hoffman, "Demodulation of Digital Signals Using an FM Discriminator", Proc. of National Electronics Conference, Vol. 22, 1966, pp. 369-374.

2.2 dB improvement (a decrease in error probability by more than 100 for $\rho = 9$ dB) over the discriminator and comes to within 1.8 dB of the matched filter result. The experimental results for $\epsilon = 0.3$ agree well with the theoretical results. It should be noted that a further improvement in system performance can be gained by optimizing the low-pass filter bandwidth. This adjustment results in a further 0.4 dB improvement in the FLL performance.

Caution must be exercised when employing the above theoretical results for ϵ greater than 0.3 due to the effect of interference between adjacent holds. The value of ϵ employed for the FLL in Fig. I-3.3.2 was the experimentally determined optimum. The errors due to clicks decrease with increasing ϵ while those due to holds increase. When the expected number of clicks and holding errors are equal, the overall error rate is lowest and this occurs for $\epsilon \cong 0.3$ in the experimental system.

The FLL as indicated in Fig. I-3.3.2 would require 3.3 dB more signal to noise ratio to perform as well as the matched filter for coherent PSK (assuming constant energy per bit). By way of comparison, a differential detection scheme for binary FM using a product demodulator was shown by Anderson, Benett, Davey, and Salz[3] to require 4.8 dB more signal to noise ratio for this same performance. Thus the FLL FM demodulator should prove to be of significant advantage in the demodulation of digital FM signals due to its excellent error rate characteristics and its inherent simplicity of construction.

References.

1. D. L. Schilling and E. Hoffman, "Demodulation of Digital Signals Using an FM Discriminator", Proc. of National Electronics Conference, Vol. 22, 1966, pp. 369-374.

2. MG. Unkauf, "Quantized Second Order Frequency Locked Loop", Ph. D. Dissertation, Polytechnic Institute of Brooklyn, June, 1969.

3. R.R. Anderson, W.R. Bennett, J.R. Davey and J. Salz, "Differential Detection of Binary FM", Bell System Technical Journal, Vol. 64, No. 1, January, 1965.

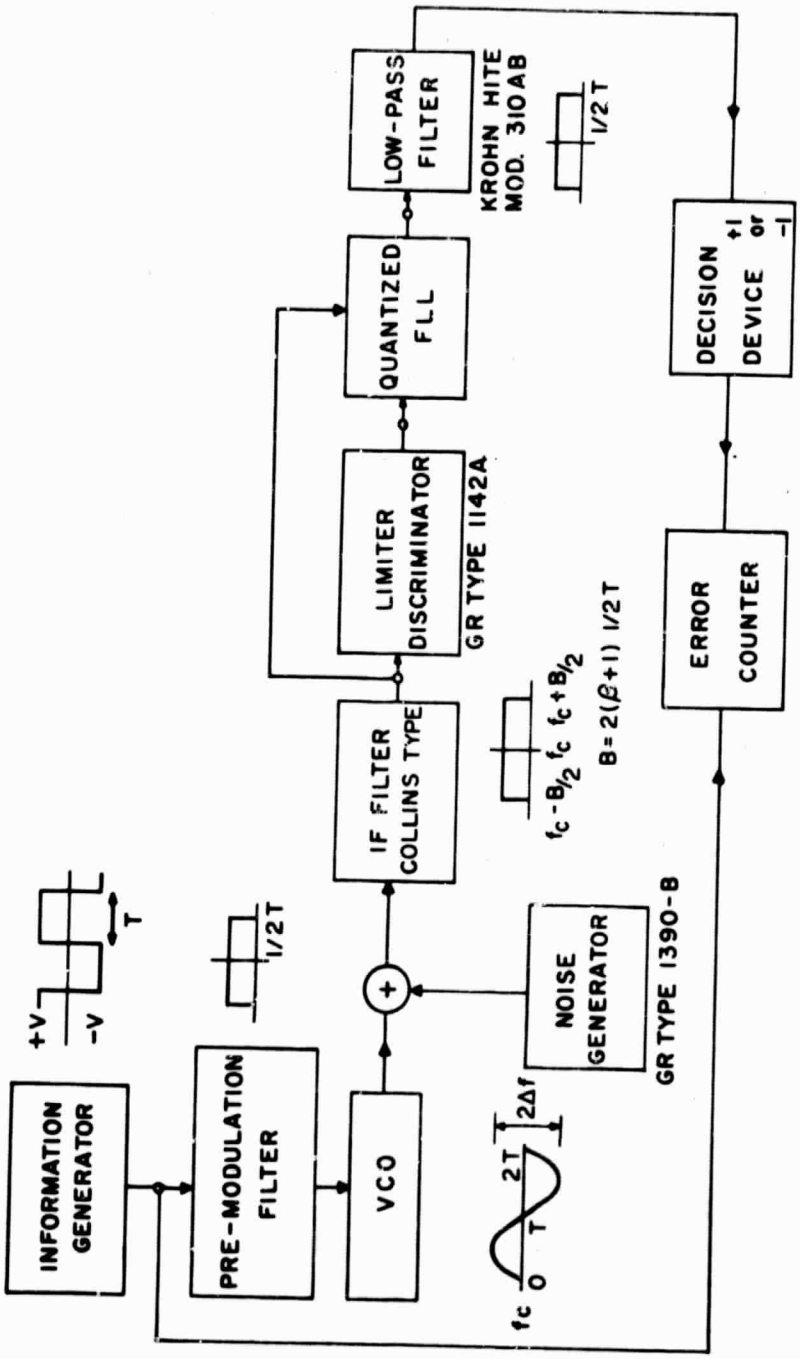

Fig. I-3.3.1 Digital FM System Block Diagram

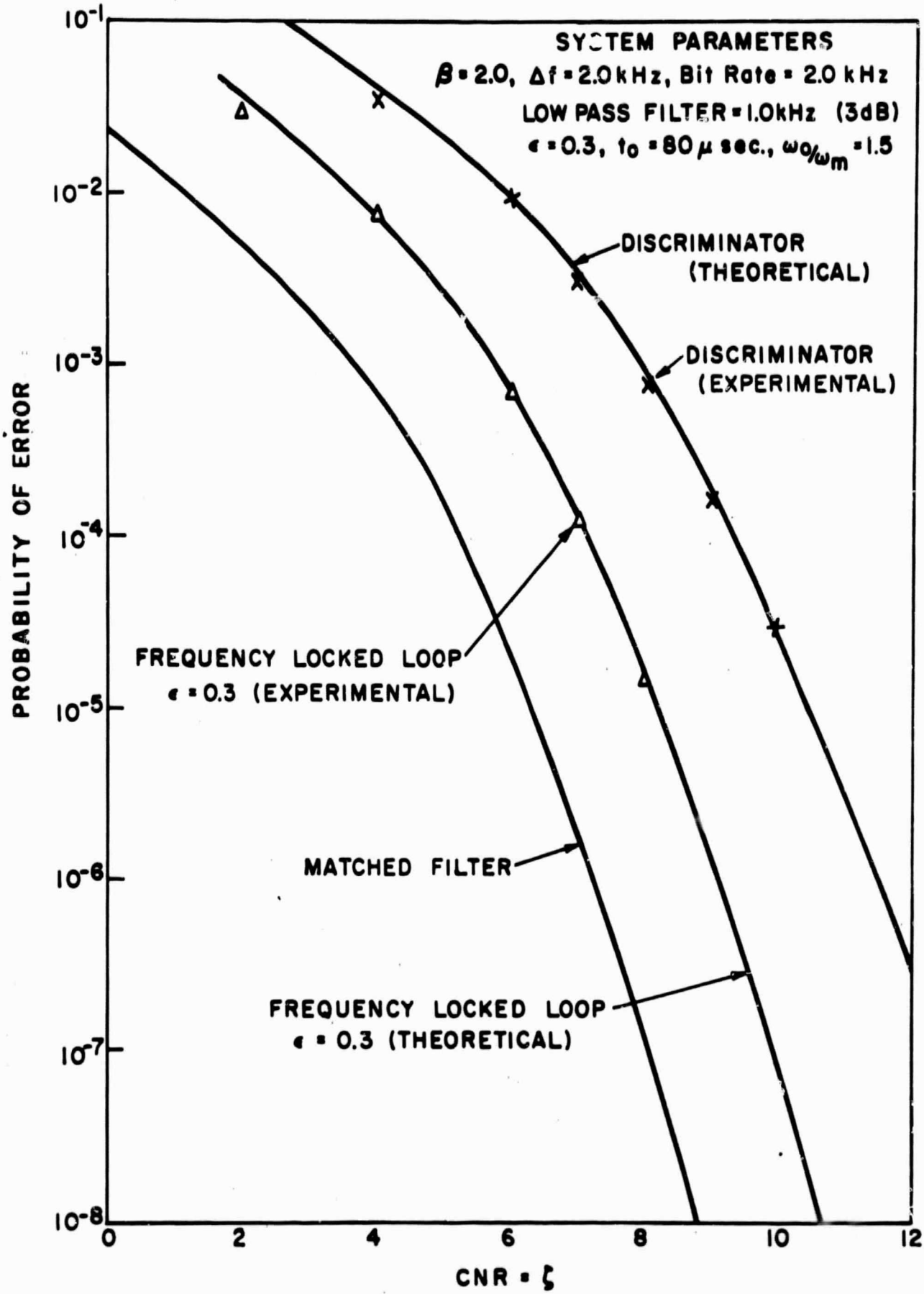

Fig. I-3.3.2 Digital Error Rates

II. TELEVISION RECEPTION USING FM

1. Slow Scan TV System Results.

The video portion of PIB experimental television system consists of a versatile flying spot scanner and receiver. These units are coupled with other laboratory designed RF transmitters and receivers to provide a wide range of video transmission facilities.

The raster generator horizontal sweep operates at 110 times the frequency of the vertical sweep, however 10% of the time is consumed by retrace periods hence the basic raster is 100 lines. The frame rate is easily adjustable from 0.1 to 10 frames per second. Output video bandwidths of approximately 1kHz to 50kHz result from these frame rates.

The raster generator contains facilities for single frame or single line operation. (line on or line deleted) It also has the capabilities of producing a raster delayed or advanced by any desired portion of a line. This capability allows one to compensate for channel delays of up to 10 milliseconds.

Fig. II-1.1 indicates the basic video spectrum produced by the blanking pulses alone.

The addition of picture material broadens and blurs the high frequency terms but has little effect upon the first several peaks in the horizontal frequency spectrum. Fig. II-1.2 indicates the changes caused in the spectrum by the slide of Fig. II-1.3. Fig. II-1.3 also shows an overall video spectrum as measured with a NR1310-A spectrum analyzer and the probability density of the video output as measured with a PIB probability density analyzer. The relatively flat probability density would be expected to lead to a relatively flat FM spectrum if the video is used to frequency modulate an FM generator with a beta of 5 or more. Fig. II-1.4 indicates such a spectrum, using a 4. MHz PIB FM generator with more than 1MHz deviation and modu-

II.

2. The Effect of a first order, open loop holding circuit upon FM "spikes" in a video signal.

The PIB experimental TV system was used with a PIB FM system to study single frame video transmission via a noisy FM channel operating at or below threshold. A simple first order, open loop holding circuit was then added to the receiver output in an attempt to improve reception by suppressing some of the below threshold FM "spikes".

The details of basic equipment set-up are videc signal was used to modulate a wide band, essentially distortionless FM generator. This FM signal at 4MHz was added to wideband noise centered at 4MHz and applied to a PIB FM receiver. The receiver selectivity was determined primarily by a single high Q adjustable bandwidth tuned circuit.

The receiver output was then filtered amplified and reproduced upon a suitable synchronized viedo receiver. Single frame operation was utilized to show distortion per frame rather than distortion integrated over several frames as is normally observed by the human eye. Fig. II.2.1 indicates that effects of below threshold FM transmission upon video material initial distortion is largely of a "spike" or "click" type leading to the characteristic white spots in black material and black spots in white material. An approach to the reduction of this distortion is indicated below. (In sections of the report dealing with the Frequency Locked Loop it is demonstrated that feedback loop operators are always superior in theory to open loop operators for distortion reduction of the type studied here. This section illustrates what can be accomplished with open loop systems as well as indicating some of the variables in such systems.)

Assume that video signal is sampled regularly at times t_i and represented

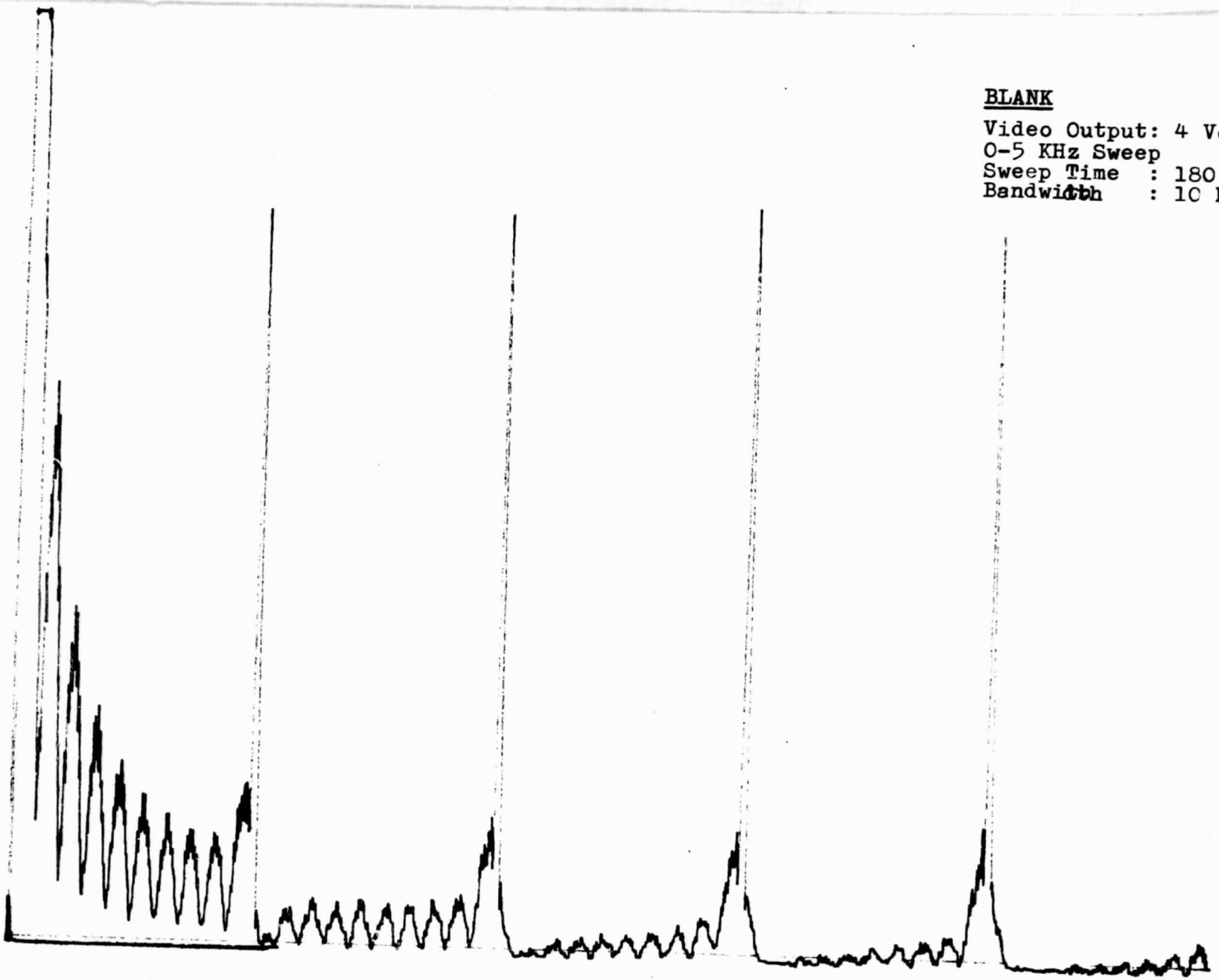

Fig. II.1.1 Spectrum of Blanking Pulses Alone. Frame Rate 7.5 Frames/sec. Measured with Quantech 304 with 0-5kHz Sweep, 180 Second Sweep Time, 16 Hz Bandwidth, 0.1 sec. time Constant, 300 mV Scale. Video Output 4V Peak-Peak.

SLIDE 2

Vidoe Output: 4 Volts p-p.
0-5 KHz Sweep
Sweep Time : 180 Second.
Bandwidth : 10 Hz.

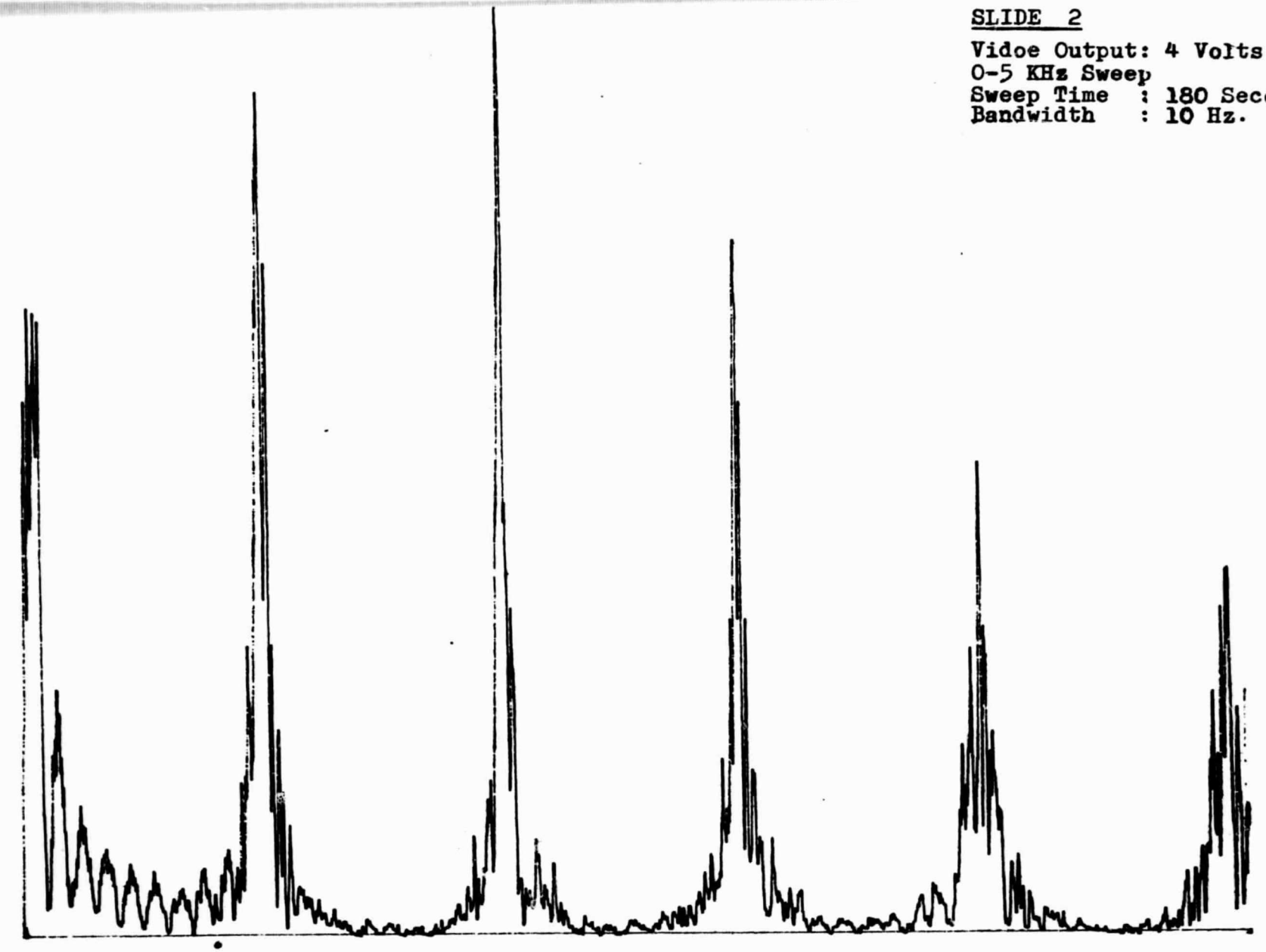

Fig. II.1.2 Spectrum of Blanking Plus Slide of Fig. 3. Frame rate 7.5 Frames/sec. Measured with Quantech 304 with 0-5 kHz Sweep Sweep, 180 Second Sweep Time, 16 Hz Bandwidth, 0.1 sec. time Constant, 300 mV Scale. Video Output 4V Peak-Peak.

Slide

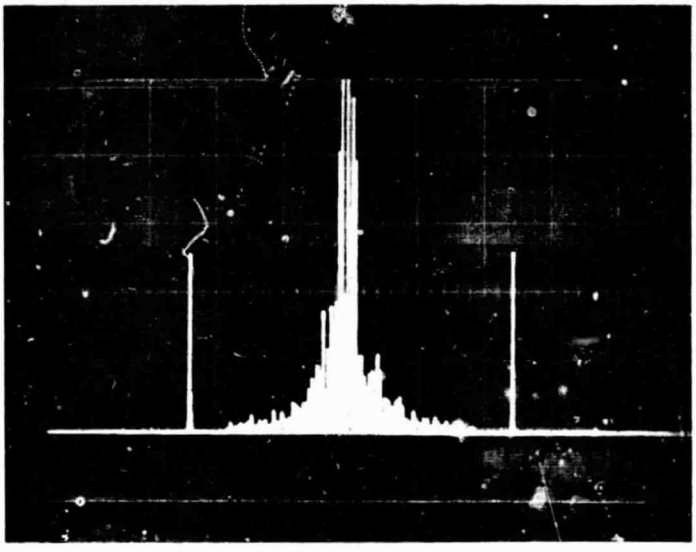

Video Spectrum

Minimum Frame Rate, 3.5 frame/sec.
Markers: 25 kHz, 2.5 Vp-p Sinewave.
Horizontal Sweep 5 sec/cm.

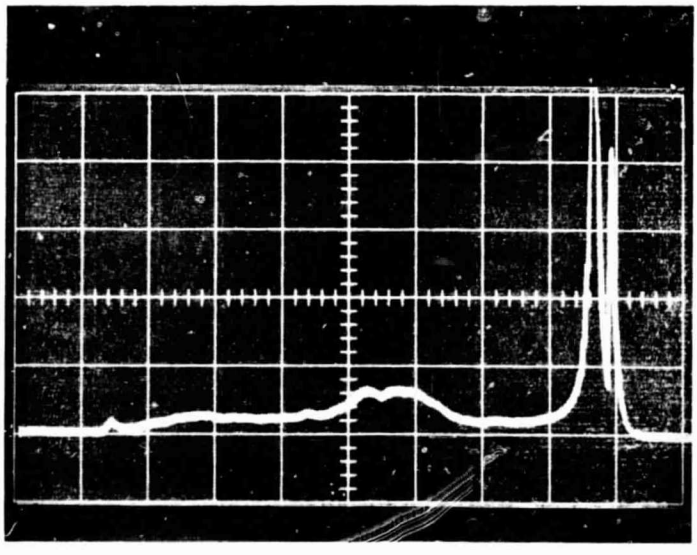

Probability density function

Vertical Scale: 0.1 V/cm.
Markers: 15 and 25 Volts
Horizontal Sweep: 5 sec./cm.

Fig. II.1.3 Three Different Viewpoints of Video Data

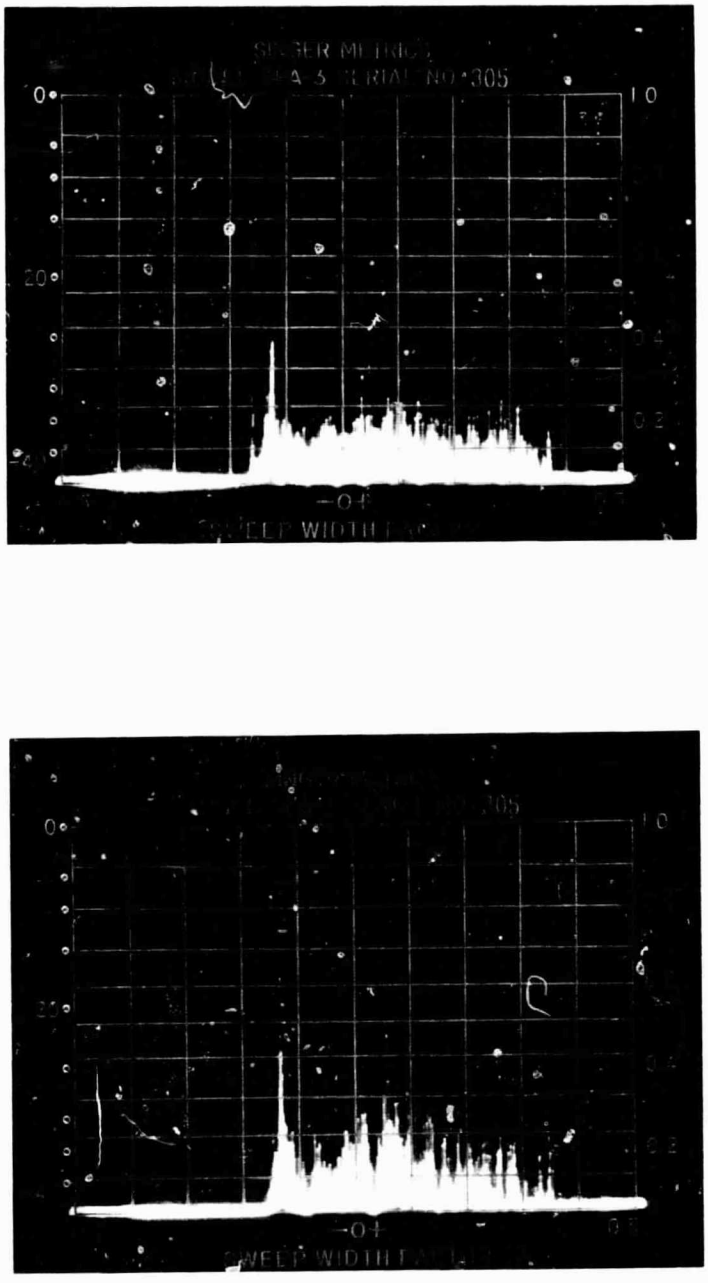

Fig. II.1.4 FM Spectrum from Picture of Slide Shown in Fig. II.1.3. 3.5 Frames/sec. Modulation Sensitivity, 30 kHZ/volt. 11 v pp video Signal. Linear Vertical. 50 kHz/cm Horizontal.

II.

2. The Effect of a first order, open loop holding circuit upon FM "spikes" in a video signal.

The PIB experimental TV system was used with a PIB FM system to study single frame video transmission via a noisy FM channel operating at or below threshold. A simple first order, open loop holding circuit was then added to the receiver output in an attempt to improve reception by suppressing some of the below threshold FM "spikes".

The details of basic equipment set-up are videc signal was used to modulate a wide band, essentially distortionless FM generator. This FM signal at 4MHz was added to wideband noise centered at 4MHz and applied to a PIB FM receiver. The receiver selectivity was determined primarily by a single high Q adjustable bandwidth tuned circuit.

The receiver output was then filtered amplified and reproduced upon a suitable synchronized viedo receiver. Single frame operation was utilized to show distortion per frame rather than distortion integrated over several frames as is normally observed by the human eye. Fig. II.2.1 indicates that effects of below threshold FM transmission upon video material initial distortion is largely of a "spike" or "click" type leading to the characteristic white spots in black material and black spots in white material. An approach to the reduction of this distortion is indicated below. (In sections of the report dealing with the Frequency Locked Loop it is demonstrated that feedback loop operators are always superior in theory to open loop operators for distortion reduction of the type studied here. This section illustrates what can be accomplished with open loop systems as well as indicating some of the variables in such systems.)

Assume that video signal is sampled regularly at times t_i and represented

by the set (x_i). If N past samples are available then the next sample $_{i+1}$ can be predicted using a suitable procedure. Then using the amplitude data provided by an envelope detector, one can perform a test and determine the probability of spike occurance during (i+1) th sampling interval. If the test reveals that a spike may have occured, the one uses the estimate x_{i+1} instead of the next sample. The procedure has the potentiality of eliminating most of the spikes. Not all spikes will be removed because of the finite uncertainity in spike detection. Actually there will be many "false alarms" between two spike occurances and therefore an additional distortion will be introduced. However, the video signal is highly correlated and the rms error due to the estimation procedure as well as due to replacing x_i by $\hat{x}_i$ may be reasonably small.

A simple sub-optimum system[1] can be obtained if the predicter is replaced by a sample and hold circuit (actually it is a zero-order predictor) and the spike detector is replaced by an amplitude comparator that causes the video signal to be held at its sampled value whenever the envelope of the RF signal drops below a certain percentage ϵA of its "normal" amplitude A. If the timing is accurate enough, then spikes that occur during a hold period will be eliminated from the video output. The upper bound of the rms error for the described scheme can be expressed as:

$$\epsilon^2_{rms} = 2R_{xx}(0)[1 - R_{xx}(a)/R_{xx}(a)]\ P\{r < \epsilon\}$$

where $R_{xx}(\tau)$ is the autocorrelation function of video signal, a is a constant delay term and $P\{r < \epsilon\}$ is the probability of the envelope of carrier being less then the threshold level ϵ.

To demonstrate the feasibility of such a system an amplitude detector feeding an amplitude comparator that fired a monostable multivibrator was added to a PIB FM receiver. The monostable multivibrator fired whenever

the envelope of the noisy FM signal fell below ϵ A where A was the normal carrier level. The output pulse of the monstable circuit operated a sample and hold circuit to maintain the FM detector video output at its initial value during the duration of the monostable pulse.

The variables of the system include the level setting ϵ, the monostable pulse width, t_0, the amplitude and frequency demodulator base band filtering and the distribution of this filtering, and any additional delays introduced between the two channels.

For optimum spike removal the monostable pulse should be as wide as the majority of the spike and centered upon it. Thus the optimum pulse width is a function of the IF bandwidth and of the modulation. Widening the pulse width beyond the minimum required value will increase the signal detail suppression caused both during spike removal and during false hold cases.

For ϵ = 0 no spike removal occurs. As ϵ increases then near threshold nearly all spikes should be removed. Below threshold a higher percentage of the spikes are accompanied by larger amplitudes and ϵ must be increased. On the other hand increasing ϵ leads to more false holds and to excessive signal suppression.

Fig. II.2.2 indicates the effect of varying ϵ with t_0 = 60 μsec and a pre sample and hold filter consisting of two poles each at 30kHz.

While some spike reduction is accomplished the picture quality reduction is unacceptable.

Following the work reported in the sections on the Frequency Locked Loop it is expected that substantial improvement could be obtained by a combination of:

a. Widening and peaking the pre-holding filter to narrow the click width without introducing excessive high frequency noise. (Such noise may

introduce new "spikes" when "held".)

b. Narrowing the post holding filter and using it to equalize the overall transmission during non-holding periods.

c. Narrowing the monostable pulse width to correspond to (a).

d. Introducing proper channel delays so that the pulse and the output spike occur simultaneously.

It remains to be seen whether the post holding transient will allow adequate equalization without excessive ringing. It also remains to be determined whether the results of such a system are sufficiently good to argue for its use instead of a more complicated, but allegedly superior system, such as a second order quantized frequency locked loop.[2]

References.

1. F. R. Ergul - Slow Scan TV Systems and the Transmission of Pictures using FM. MSc Report, PIB, June 1968

2. D. T. Hess and K. K. Clarke, "Quantized Second Order Frequency Lockec Loop". IEEE Transactions on Aerospace and Electronic Systems - Eascon '69 Convention Record pp. 193-197.

Direct Transmission

CNR = 8 db

CNR = 6 db

CNR = 3 db

Fig. II.2.1 Video Transmission via a Noisy FM Channel. 70kHz pp Single Tuned IF. 1 3 volts peak-peak video. 5kHz/V. FM Sensitivity 3.5 frames/sec. rate. Single frame operation.

CNR = 5 db
IF Bandwidth: 70 kHz.
Deviation: 5 kHz/Volt.
Video: 3.5 frame/Second.
No Spike Elimination.
ϵ = 0

CNR = 5 db
IF Bandwidth: 70 kHz.
Deviation: 5 kHz/Volt.
Video: 3.5 frame/second.
ϵ = 0.2

CNR = 5 db
IF Bandwidth: 70 kHz/Volt.
Deviation: 5 kHz/Volt.
Hold time: 60 microsec.
ϵ = 0.4

Fig. II.2.2 Spike Elimination As A Function of Quantization Level, ϵ.

II.

3. Comparative TV Transmissions: Second Order Quantized Frequency Locked Loop vs. Limiter Discriminator.

In order to investigate the effect of the "spike" reduction properties of the second order quantized frequency locked loop[1] (FLL) in video transmission a comparative test was run with a modified version of the PIB TV system as the video source. For the purposes of this test the normal slide input was replaced by a bar pattern synchronized to the raster generator. The composite video output was used to frequency modulate a FM generator. The raster generator was operated in a single frame manner at a 0.2 frame/second rate. The modulating amplitude was adjusted so that the modulated signal occupied 11kHz centered at 455kHz. This FM signal was mixed with filtered white noise and applied to the FM receiver under test. The IF noise filter was a 12kHz pp bandwidth "square" filter (nine pole) centered at 455kHz.

The FM receiver output was passed through a 1kHz base band filter and presented on a PIB video monitor. Single frame outputs were recorded on film. Figs. II-3.1 and 2 indicate comparative results for the second order, quantized frequency locked loop[1], and a well adjusted limiter discriminator combination.

The conditions for the FLL were holding pulse width t_0 = 70 μsec and normalized holding level, ϵ = 0.28. The feedback loop zero was at 6.7kHz while the closed loop poles were at 1.55kHz. (As a comparison the optimum conditions for minimizing digital error rates in a β = 2, 6kHz IF system were found in Reference No. 2 to be ϵ = 0.30 and t_0 = 80 μsec) Hence, the "optimum" pulse width for spike "suppression" in video is wider than it would be in the digital error case. (For the present example 70 μsec as compared to the extrapolated value of 40 μ sec for the digital case.)

One would expect t_0 to be larger for a given ϵ since the amount of spike reduction necessary to cause the spike to be unnoticed in a picture is larger than the amount ot reduction necessary to prevent an error in the digital situation. For a given ϵ a wider t_0 gives a better spike suppression, when a spike occurs. Of course the wider pulse also gives more signal suppression on false holds hence the wider t_0 should be couplex with a small ϵ. Fig. II-3.3 of Section 3.1 indicates the conversion of large spike noise into small spike noise and a gaussian like term as ϵ is increased. With digital transmission the small spikes are unlikely to cause errors, however in video they may be visible. (The visibility of the spikes is of course a function of oscilloscope intensities and of the gamma of the film.)

Comparison of the two figures clearly indicates a significant reduction in the number and intensity of "spikes" in the FLL case. Whether the 4dB FLL picture would be acceptable in places where the 4dB discriminator picture would not is an as yet unanswered question.

Further studies to be conducted in this area include comparative transmissions with phase locked loop and FMFB demodulators as well as the study of pre-emphasised signals upon the various circuits. The literature[2] reports that FMFB circuits can not handle pre-emphasized material properly. However the FLL operates in a completely satisfactory manner for relatively high deviation, and relatively high modulating frequency signals, hence further overall system gains may be achieved by utilizing pre and post filtering circuits of this type.

References.

D. T. Hess and K. K. Clarke, "Second Order Quantized Frequency Locked Loop" IEEE Professional Group on Aerospace and Electronic Systems, Eascon '68 Convention Record, p 193-197.

2. A.J. Giger and J.G. Chaffee, "The FM Demodulator with Negative Feedback, BSTJ, July 1963, Part I p 1109-1135. Section 4.3.3 on p 1131-1133 concerns television threshold tests.

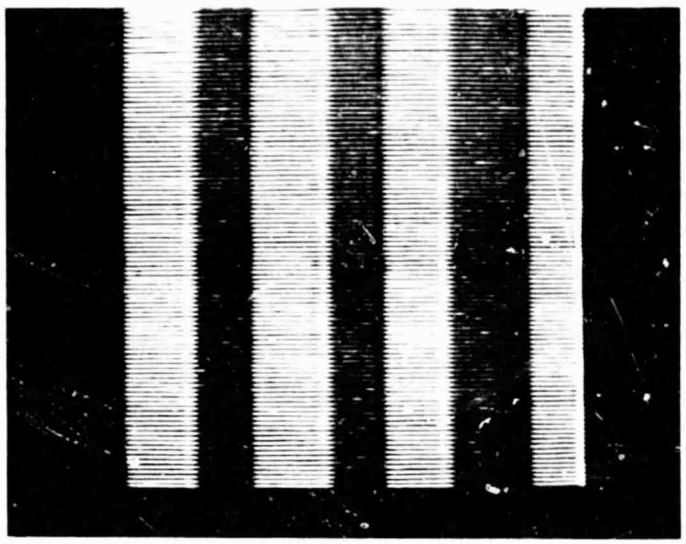

a) Frequency Locked Loop

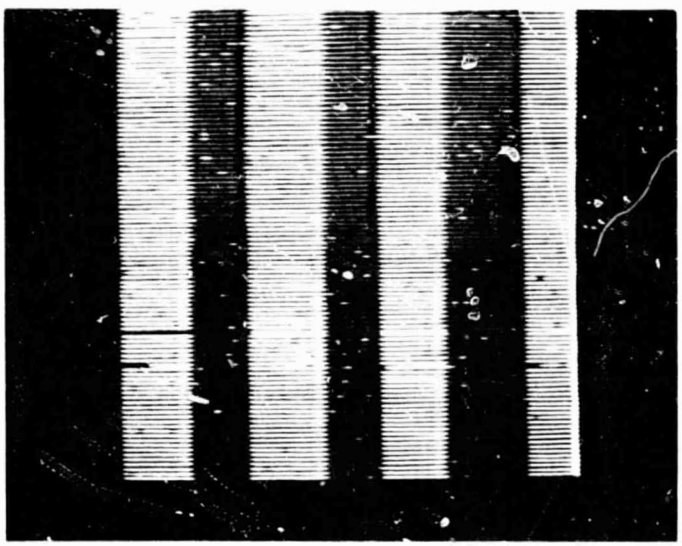

b) Discriminator

Fig. 1 Spike Noise in a Video Bar Pattern Transmitted Via a Noisy FM Channel. Comparison of Frequency Locked Loop and Discriminator for 6 dB Carrier to Noise Ratio. 12kHz pp Square IF. 1kHz Baseband Filter.

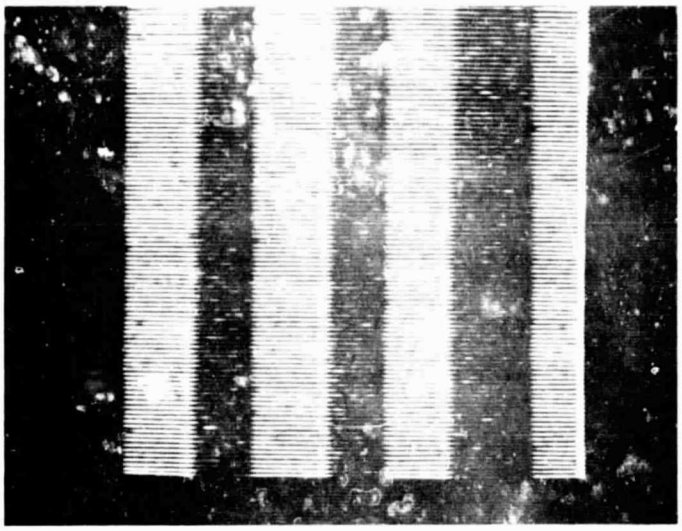

a) Frequency Locked Loop

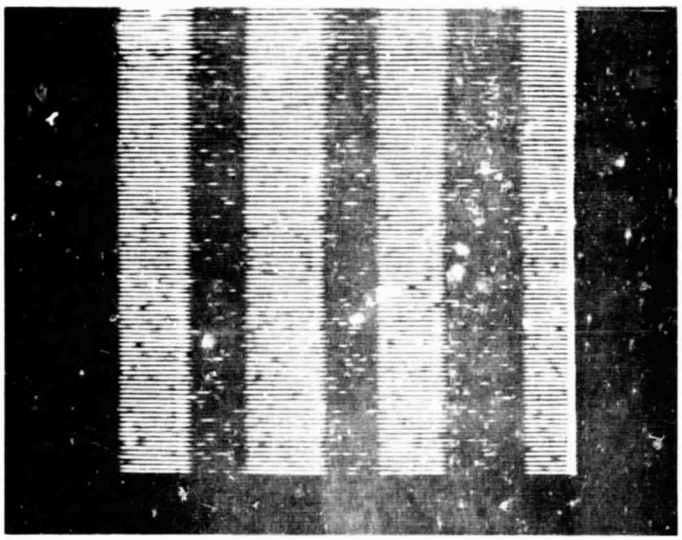

b) Discriminator

Fig. II-3.2 Spike Noise in a Video Bar Pattern Transmitted Via a Noisy FM Channel. Comparison of Frequency Locked Loop and Discriminator for 4 dB Carrier to Noise Ratio. 12kHz pp Square IF. 1kHz Baseband Filter.

III. CHARACTERISTICS OF FM

1. Single Sideband FM.

Introduction. - The attempts to find better communications systems have lead to various combinations of signal encoding at the transmitter and processing at the receiver. A new type of system called "single-sideband frequency modulation" (SSB-FM) which employes simultaneous angle and amplitude modulation has been invented by Powers[1]. It was hoped that this scheme would combine the noise immunity of FM with the bandwidth savings of single sideband operation. The concept of the analytic signal was applied[2] to explain the one sided nature of the SSB-FM Spectrum. Investigation showed that for the case of sinusoidal modulation and large values of the modulation index, β, the bandwidth required for SSB-FM was approximately 1/3 less than that of the conventional FM system. Also the structure of an posteriori most probable receiver for demoudlating SSB-FM in additive gaussian noise was derived[3]. Later the SSB-FM spectrum was calculated for the case of gaussian modulation[4]. Results show that for small modulation indices the spectrum occupies approximately 1/2 the bandwidth of conventional FM but for modulation indices of 3 or more the SSB-FM spectral width is equal to or greater than that of double sided FM. These seemingly contradictory results are not surprising since FM is a non-linear process and thus one would not expect both sinusoidal and gaussian modulation to yield a power spectrum with similar characteristics.

Experiments showed[5] that narrow-band (low β) sinusoidally modulated SSB-FM had similar threshold characteristics to conventional FM but occupied less bandwidth.

Bandwidth Properties. - Consider the wave form x(t) and its Hilbert transform $\hat{x}(t)$

$$\hat{x}(t) = \int_{-\infty}^{\infty} \frac{x(\tau)}{\pi(t-\tau)}\, d\tau \triangleq x(t) * \frac{1}{\pi t} \tag{1}$$

$\hat{x}(\omega) \longleftrightarrow -i\,\mathrm{sgn}(\omega)\, x(\omega)$ where $x(\omega)$ is the fourier transform of $x(\tau)$ and

$$\mathrm{sgn}(\omega) = \begin{cases} 1 & \omega > 0 \\ 0 & \omega = 0 \\ -1 & \omega < 0 \end{cases}$$

Now $z(t) = x(t) + i\hat{x}(t)$ transforms into

$$z(\omega) = x(\omega) + i\,(-i\,\mathrm{sgn}(\omega))x(\omega) = \begin{cases} 2x(\omega) & \omega > 0 \\ x(0) & = 0 \\ -1\,\omega & < 0 \end{cases} \tag{2}$$

thus the spectrum of $z(t)$, the analytic signal, is one sided in the frequency domain.

Now consider:

$$y(t) = e^{i\,z(t)} = e^{-\hat{x}(t)}\, e^{ix(t)} = \sum_{K=0}^{\infty} \frac{(i\,z(t))^K}{K!} \tag{3}$$

Since multiplication in the time domain corresponds to convolution in the frequency domain the spectrum of $y(t)$ will remain one-sided about $\omega = 0$. Taking the real part of $y(t)$, a linear operation, one obtains the expression for SSB-FM

$$\mathrm{Re}\, y(t) = e^{-\hat{x}(t)} \cos x(t) \tag{4}$$

All that is necessary now is to shift the carrier frequency from $\omega = 0$ to $\omega = \omega_0$. Had we started with $z(t) = x(t) - i\hat{x}(t)$ the lower sideband would have been obtained. It is to be noted that in this type of SSB-FM the zero crossings of conventional FM are unaltered. This would not have been true had the signal spectrum been made single-sided by filtering.

<u>SineWave Modulation</u>[3]. - A good measure of the bandwidth of a SSB-FM signal is the second central moment of its power spectrum Ω_μ^2. The smallest frequency band which contains approximately 90% of the average power is usually 3 or 4 times Ω_μ. Let $y(t)$ have a fourier series.

$$y(t) = \sum_{k=-\infty}^{\infty} c_k \, e^{ik\omega_m t} \tag{5}$$

and $\sum_{k=-\infty}^{\infty} |c_k|^2 < \infty$. The second moment of the $k = -\infty$ signal is defined by:

$$\Omega^2 = \frac{\sum_{k=-\infty} (k\omega_m)^2 |c_k|^2}{\sum_{k=-\infty} |c_k|^2} \tag{6}$$

whenever $\sum_k (k\omega_m)^2 |c_k|^2$ exists. Its mean μ is defined by

$$\mu = \frac{\sum_{k=-\infty} k\omega_m |c_k|^2}{\sum_{k=-\infty} |c_k|^2} \quad \text{where} \quad \sum_k k\omega_m |c_k|^2 < \infty. \tag{7}$$

The second central moment Ω_μ^2 is:

$$\Omega_\mu^2 = \frac{\sum_{k=-\infty}^{\infty} (k\omega_m - \mu)^2 |c_k|^2}{\sum_{k=-\infty} |c_k|^2} \tag{8}$$

and $\Omega_\mu^2 = \Omega^2 - \mu^2$.

Let us compare an FM and a SSB-FM signal which are both angle modulated by the sinusoid $x(t) = \beta \sin \omega_m t$. It is well known that the FM Signal may be written:

$$A \, e^{i\beta \sin \omega_m t} = A \sum_{k-\infty}^{\infty} J_k(\beta) \, e^{ik\omega_m t} \tag{9}$$

As for the SSB-FM signal, the Hilbert transform of $\sin \omega_m t$ is $-\cos \omega_m t$ thus $z(t) = \beta \sin \omega_m t - i\beta \cos \omega_m t = i\beta \, e^{i\omega_m t}$ and $y(t) = A \exp\{\beta \exp(i\omega_m t)\}$

$$A \sum_{k=0}^{\infty} \frac{\beta k}{k!} \, e^{ik\omega_m t} \tag{10}$$

Comparing the average power for the two we find for FM:

$$\langle P_{FM} \rangle = A^2 \sum_{k=-\infty}^{\infty} J_k^2(\beta) = A^2 \tag{11a}$$

and for SSB-FM:

$$\langle P_{SSB\text{-}FM} \rangle = A^2 \sum_{k=0}^{\infty} \left(\frac{\beta^{2k}}{k!} \right)^2 = A^2 I_0(2\beta) \tag{11b}$$

Since the generation of SSB-FM involves amplitude modulation which is a function of β the average power is seen also to be a function of β. (The average power in the real waveforms will be 1/2 that shown above.)

The mean, μ, of the FM wave is zero since:

$$J_k^2(\beta) = J_{-k}^2(\beta)$$

thus $$\Omega_{\mu\,FM}^2 = \Omega_{FM}^2 \tag{12}$$

therefore

$$\Omega_{\mu FM}^2 = \sum_{k=-\infty}^{\infty} (k\omega_m)^2 J_k^2(\beta) = \frac{\beta^2 \omega_m^2}{2} \tag{13}$$

and $\Omega_{\mu FM} = \frac{\omega_m}{\sqrt{2}} \beta$. Hence the FM bandwidth is a linear function of β, whose slope is equal to $\frac{\omega_m}{\sqrt{2}}$.

On the other hand the SSB-FM spectrum being considered has a mean

$$\mu_{SSB\text{-}FM} = \frac{\sum_{k=0}^{\infty} (k\omega_m) \frac{\beta^{2k}}{(k!)^2}}{I_0(2\beta)} = \omega_m \beta \frac{I_1(2\beta)}{I_0(2\beta)} \tag{14}$$

For $\beta >> 1$, due to the nature of the modified Bessel functions, μ increases almost linearly with β, (with a different slope then μ_{FM}). The second moment

$$\Omega_{SSB\text{-}FM}^2 = \frac{\sum_{k=0}^{\infty} (k\omega_m)^2 \frac{\beta^{2k}}{(k!)^2}}{I_0(2\beta)} = \omega_m^2 \beta^2 \tag{15}$$

This is precisely double that of the FM case. Since we must compare the two second central moments:

$$\Omega_{\mu\,SSB\text{-}FM} = \omega_m \beta \sqrt{1 - \frac{I_1^2(2\beta)}{I_0^2(2\beta)}} \tag{16}$$

which approaches $\omega_m \beta/2$ asymptotically for large β. The ratio of the two bandwidths is:

$$\frac{\Omega_{\mu\,\text{SSB-FM}}}{\Omega_{\mu\,\text{FM}}} = \sqrt{2}\sqrt{1 - \frac{I_1^2(2\beta)}{I_0^2(2\beta)}} \tag{17}$$

For $\beta < 1$ it is seen that the bandwidth for SSB-FM is actually greater than that for FM but as β gets larger the ratio decreases heading toward zero asymptotically. This is so because the bandwidths of the two signals become large at different rates.

Gaussian Modulation[4]. - The auto correlation function of the SSB-FM waveform is:

$$R_y(\tau) = E\left\{\frac{A^2}{2}\exp[-\hat{x}(t+\tau) - \hat{x}(t) + i\,x(t+\tau) - i\,x(t)]\right\} \tag{18}$$

The above calculation is simplified by using the fact that if a and b are both zero mean jointly gaussian random variables where $E\{a^2\} = \sigma a^2$ $E\{b^2\} = \sigma_b^2$ and $E\{ab\} = \rho$ then

$$E\{\exp(-a+ib)\} = \exp\{\sigma_{a/2}^2 - \sigma_{b/2}^2 - i\rho\}$$

In the above a may be identified with $\hat{x}(t+\tau) + \hat{x}(t)$ b with $x(t+\tau) + x(t)$, $E\{x(t+\tau)\,x(t)\} = E\{\hat{x}(t+\tau)\,\hat{x}(t)\} = R_x(\tau)$ and $E\{x(t+\tau)\,\hat{x}(t)\} = -\hat{R}_x(t)$. Thus $\sigma_a^2 = 2(R_x(0) + R_x(\tau))$ $\sigma_b^2 = 2(R_x(0) - R_x(\tau)$ and $\rho = -2\hat{R}_x(\tau)$. Therefore $R_y(\tau) = \frac{A^2}{2}\exp(2[R_x(\tau) + i\hat{R}_x(\tau)] = \frac{A^2}{2}\exp 2z(\tau)$. By using the same arguments presented earlier, it is seen that the power spectrum of y(t), $S_y(\omega)$, is also one sided about $\omega = 0$. The average power in y(t), $R_y(0) = \frac{A^2}{2}\exp 2R_x(0)$ where $R_x(0) = \sigma_x^2$.

Let us assume that both $R_x(\tau)$ and $\hat{R}_x(\tau)$ go to zero for $|\tau| \to \infty$. This will be so if the baseband signal has finite power and no specular components. Thus $\exp(2\,z(\tau))$ goes to one as $|\tau|$ goes to infinity and will have a delta

function in its fourier transform. Consider only the continuous portion of the spectrum, $G(\omega)$ where $g(\tau) = \exp(2z\tau) - 1$. The function $g(\tau)$ satisfies the following differential equation:

$$\dot{g}(\tau) = 2\dot{z}(\tau)\, g(\tau) + 2\dot{z}(\tau) \tag{19}$$

Hence its Fourier transform satisfies the integral equation:

$$\omega\ G(\omega) = \frac{1}{\pi} \int_0^{\min(\omega, \omega_c)} \lambda z(\lambda) G(\omega - \lambda)\, d\lambda + 2\omega\, z(\omega) \tag{20}$$

The limits on the convolution integral arise from the fact that $Z(\omega)$ the transform of $z(\tau)$ is nonzero only at frequencies between $\omega = 0$ and $\omega = \omega_c$ and $G(\omega - \lambda)$ is zero for $\lambda > \omega$. We will now normalize the equation so that $\omega_c = 1$ and the entire spectrum will have the same total power for all modulation signals. Let $\bar{g}(\eta) = \omega_c G(\omega_c \eta)$ and $s(\eta) = s_x(\omega_c \eta)$, since $z(\omega) = 2s_x(\omega)$ for $\omega > 0$:

$$\eta \bar{g}(\eta) = 4\omega_c \eta s(\eta) + \frac{2\omega_c}{\pi} \int_0^{\min(\eta, 1)} \lambda s(\lambda)\, \bar{g}(\eta - \lambda)\, d\lambda$$

Noting that $\sigma_x^2 = \frac{\omega_c}{\pi} \int_0^\infty s(\eta)\, d\eta$ and letting $g(\eta) \triangleq \frac{1}{2\pi} \exp(-2\sigma_x^2)\, \bar{g}(\eta)$

Let:

$$I \triangleq \int_0^\infty s(\eta) d\eta \tag{21a}$$

The final form of the integral equation is obtained.

$$\eta g(\eta) = \frac{2\sigma_x^2}{I} \exp(-2\sigma_x^2)\, \eta\, s(\eta) + \int_0^\infty \lambda s(\lambda)\, g(\eta - \lambda)\, d\lambda \tag{21b}$$

This equation has been solved numerically[4] and several spectra are shown in Fig. III-1.1 for the case where

$$s(\eta) = \begin{cases} \cos^2 \frac{\pi \eta}{2} & |\eta| \leq | \\ 0 & |\eta| > | \end{cases} \tag{21c}$$

The Circuit. - A block diagram of the SSB-FM generator is shown in Fig. III-1.2. There are two component blocks in it which are critical. The first

is the exponential function circuit which for a wideband system must have an output dynamic range of four decades, and the second is the 90° all pass phase shifting network, the "Hilbert transformer". Such a network is non-causal and thus can only be approximated. To date the exponential and modulator circuits have been built. The design finally arrived at is shown in Fig. III-1.3.

The operation of the circuit depends on the fact that the current flowing through a forward biased p-n junction is an exponential function of the voltage across it. The first operational amplifier acts as an attenuator, level shifter, and low output impedance source. The second two amplifiers provide a voltage gain of 200. The diode current is monitored by the 47Ω resistor which is much smaller than the mimimum diode impedance. For maximum symmetric input swing the diode is forward biased to the center of the linear portion of its $\log_{10}$ vs. V characteristic, which for the 1N205 diode used was about 150 mV. The bias voltage also determines the gain, V, of the exponential circuit, where $V_{out} = V \exp(-V_{in})$. It is this V-i characteristic which determines the maximum modulation index of the SSB-FM generator. A plot of $\log_{10}$ i vs. V for the diode used is shown in Fig. III-1.4. The diodes were found to have uniform characteristics so selection among them was not helpful or necessary. The overall static $\log_{10}$ Vout vs. Vin of the exponentiator is shown in Fig. III-1.5. The output showed no visible distortion for sinewave input frequencies up to 30 KC. Fig. III-1.6 shows a picture of V in and V out at 10 KC.

The output of the exponentiator is coupled, via a 10K resistor, to a transistor multiplier whose output is the desired SSB-FM signal. The 10KΩ resistor is large enough compared to the 200Ω output impedance of the operational amplifier to prevent undesirable interaction between the two

circuits. The exponentiator must be D. C. coupled to the multiplier otherwise double-sided FM will also be produced. A picture of the SSB-FM spectrum with a 1 KC sine wave input is shown in Fig. III-1.7. The SSB-FM signal was demodulated using a conventional FM discriminator. There was no visible distortion in the output.

It was noticed on the spectrum analyzer that by changing the β of the FM chopping waveform but keeping the input to the exponentiator constant, that the mean of the SSB-FM spectrum could be shifted in frequency. The following calculations show the effects of this change.

Let $\phi(t) = \alpha \sin \omega_m t - i\beta \cos \omega_m t$ $\alpha \neq \beta$ thus $\phi(t)$ is now no longer an analytic signal.

$$\phi(t) = -i\left[\beta e^{i\omega_m t} + i(\alpha-\beta) \sin\omega_m t\right]$$

$$e^{i\phi(t)} = e^{\beta e^{i\omega_m t}} e^{i(\alpha-\beta)\sin\omega_m t}$$

$$= \sum_{k=0}^{\infty} \frac{\beta^k}{k!} e^{ik\omega_m t} \sum_{n=-\infty}^{\infty} J_n(\alpha-\beta)\, e^{in\omega_m t}$$

$$= \sum_{n=-\infty}^{\infty} \sum_{k=0}^{\infty} J_n(\alpha-\beta) \frac{\beta^k}{k!} e^{I(n+k)\omega_m t} \qquad (22)$$

let $\gamma = n+$

$$= \sum_{\gamma=-\infty}^{\infty} e^{i\gamma\omega_m t} \sum_{k=0}^{\gamma} J_{(\gamma-k)}(\alpha-\beta) \frac{\beta^k}{k!}$$

For $\alpha = \beta$ this reduces to SSB-FM since $J_n(0) = \begin{cases} 1 & n = 0 \\ 0 & \text{otherwise} \end{cases}$

References.

1. K.H. Powers US Patent 3, 054, 073 (assigned to R.C.A.)

2. E. Bedrosian - "The Analytic Signal Representation of Modulated Waveforms" Proc. IRE Vol. 50 pp 2071-2076 Oct. 1962.

3. R.E. Kahn and J.B. Thomas - "Bandwidth Properties and Optimum Demodulation of Single-Sideband FM" IEEE Trams. on Com. Tech., Vol. com-14, No. 2, April 1066.

4. J.E. Mazo and J. Salz - "Spectral Properties of SSB-FM" IEEE Trans. on Com. Tech., Vol. com- Feb. 1968.

5. R.M. Gloriosso and E.H. Brazeal Jr. - "Experiments in SSB-FM Communication Systems" IEEE Trans. on Communication Technology Vol. com-13 pp 109-116 Mar. 1965.

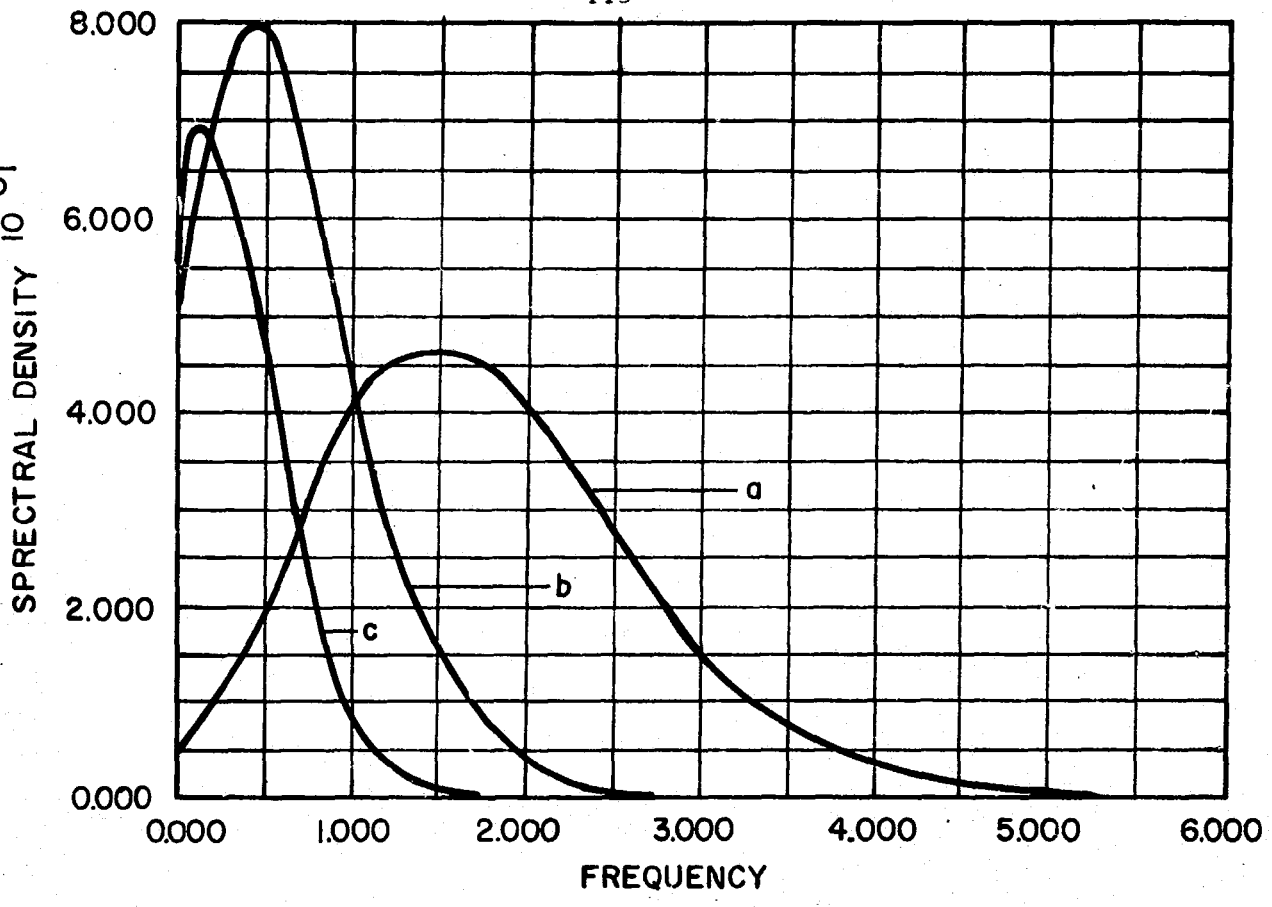

Fig. III-1.1 Spectral density of SSB-FM with Gaussian modulation

$$s(n) = \begin{cases} \cos^2 \frac{\pi n}{2} & |n|<1,\ (a)\sigma_x^2 = 3,\ (b)\sigma_x^2 = 1,\ (c)\sigma_x^2 = 0.3. \\ 0 & |n|>1 \end{cases}$$

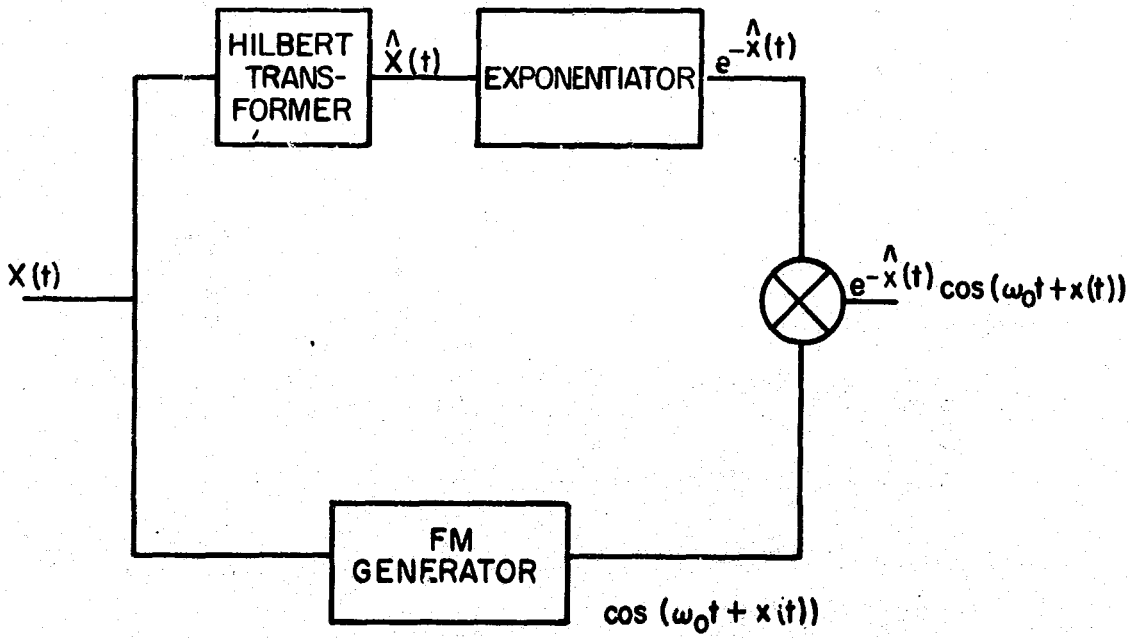

Fig. III-1.2 Block diagram of an SSB FM generator.

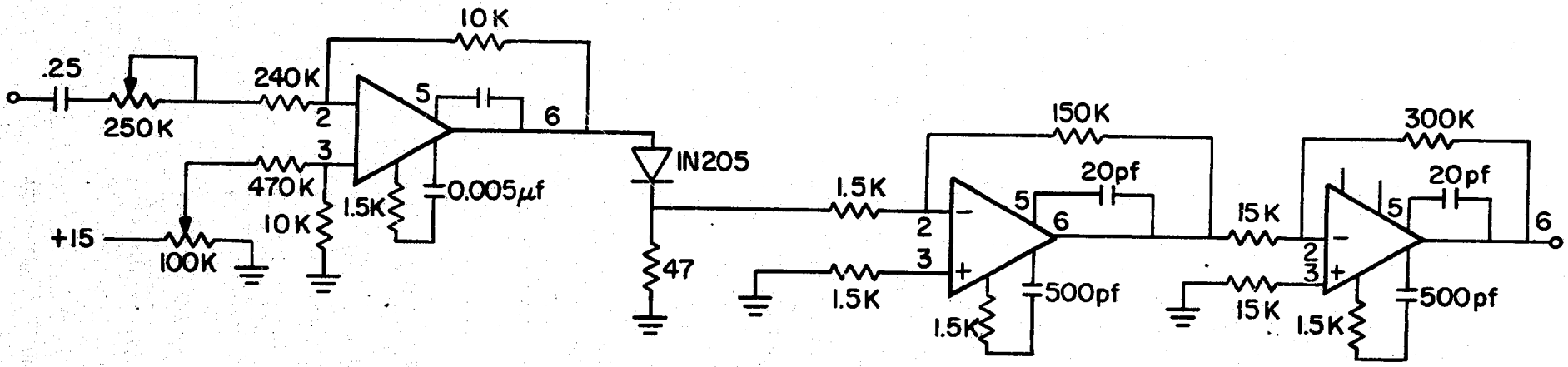

Notes: IC's Fairchild μA709, Pin 4 to -15v Pin 7 + 15v.

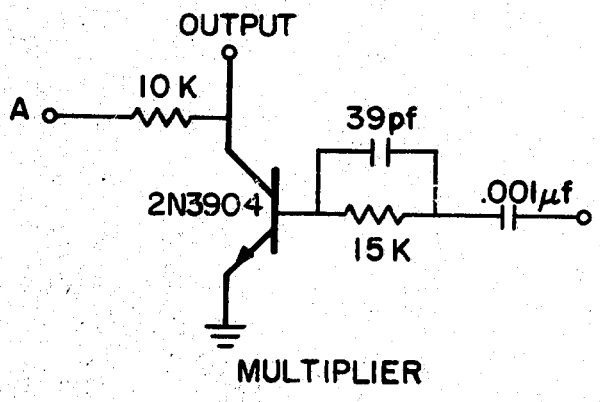

FM INPUT from Wavetek voltage controlled generator model III.

Fig. III-1.3 SSB-FM generator for sinusiodal modulation. The 90° phase shift occurs in the FM generator and filtering of unwanted harmonics is done in the IF amplifier of the receiver.

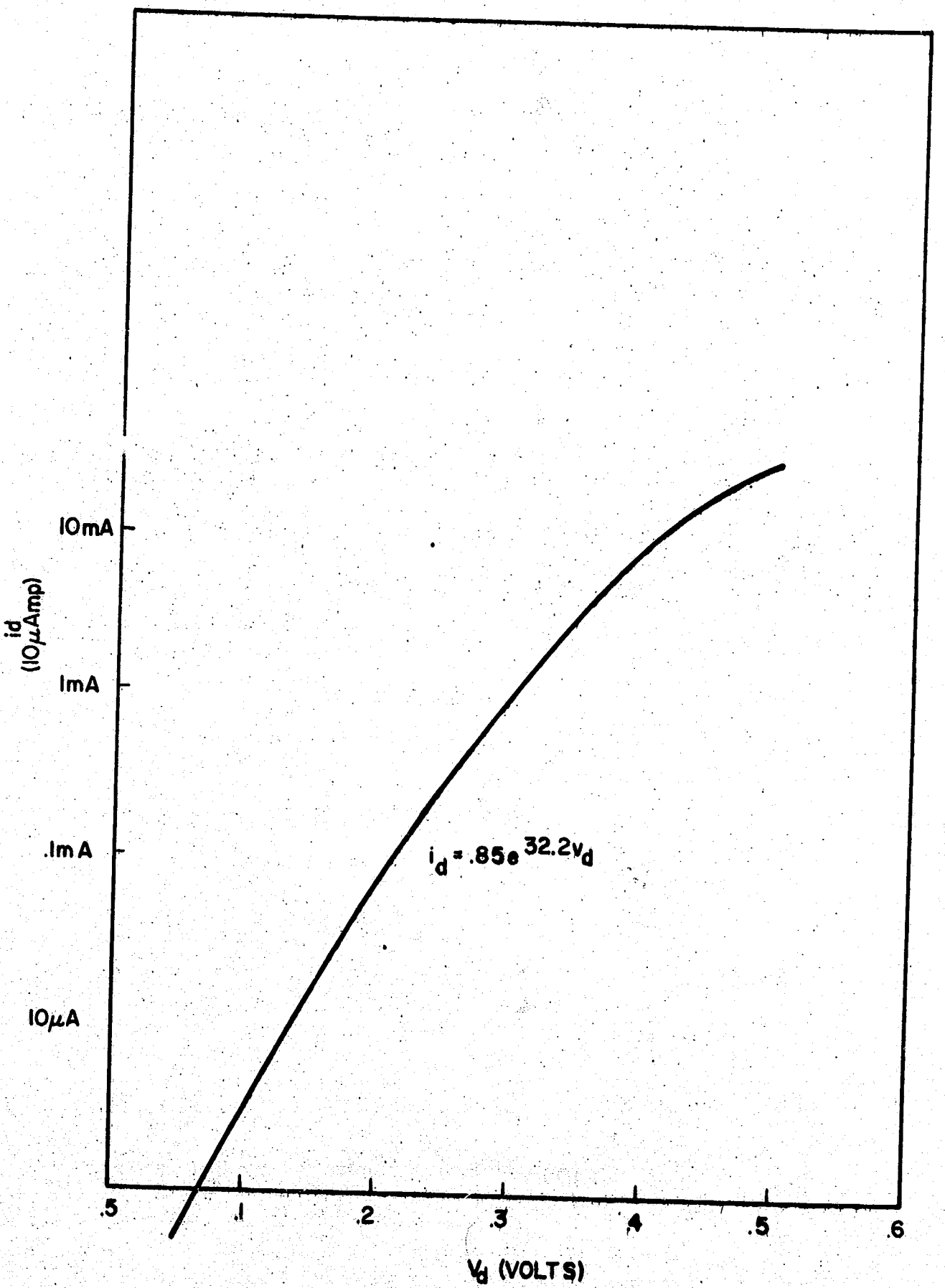

Fig. III-1.4 Diode current vs. diode voltage for the diode fused in the exponentiator.

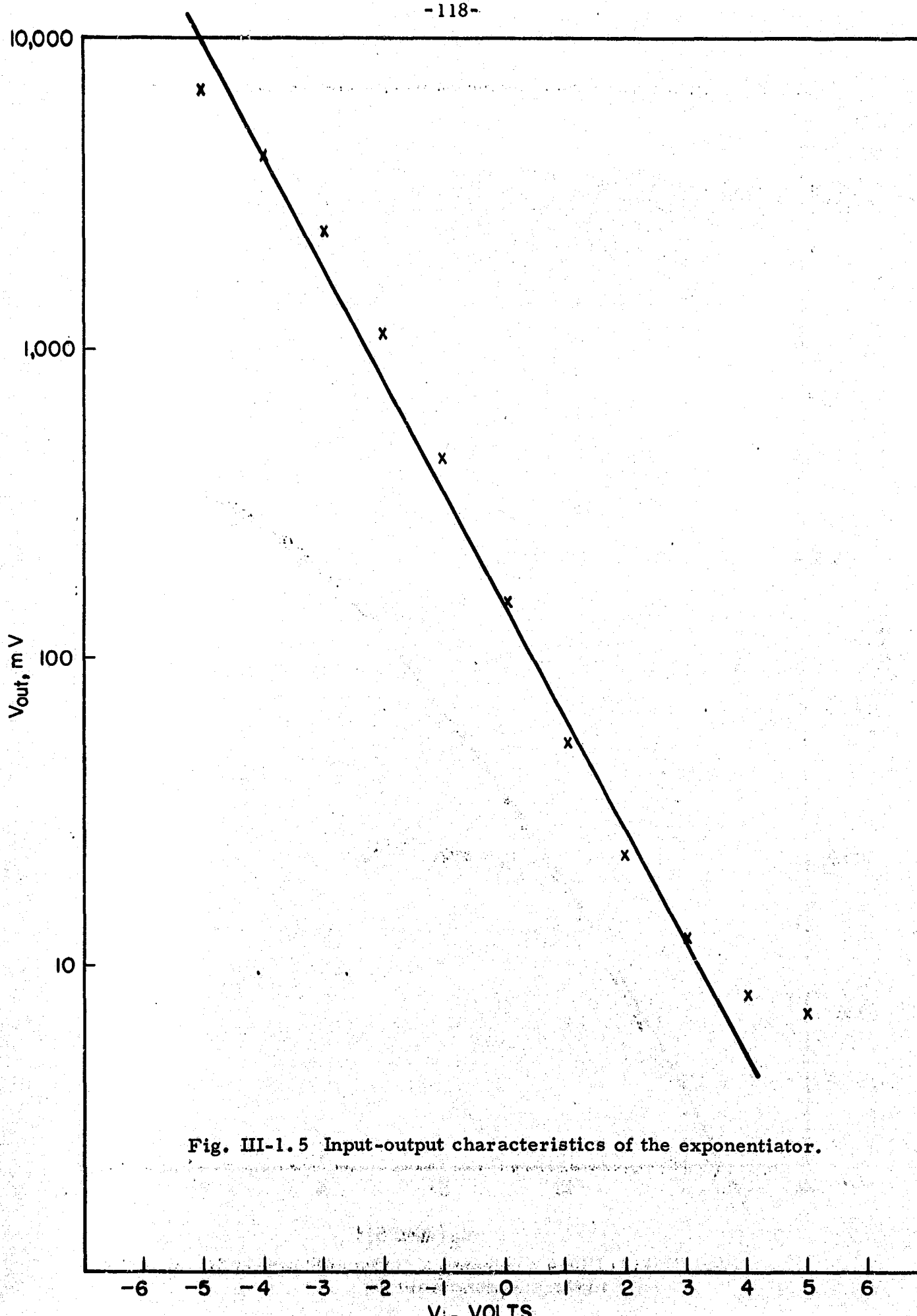

Fig. III-1.5 Input-output characteristics of the exponentiator.

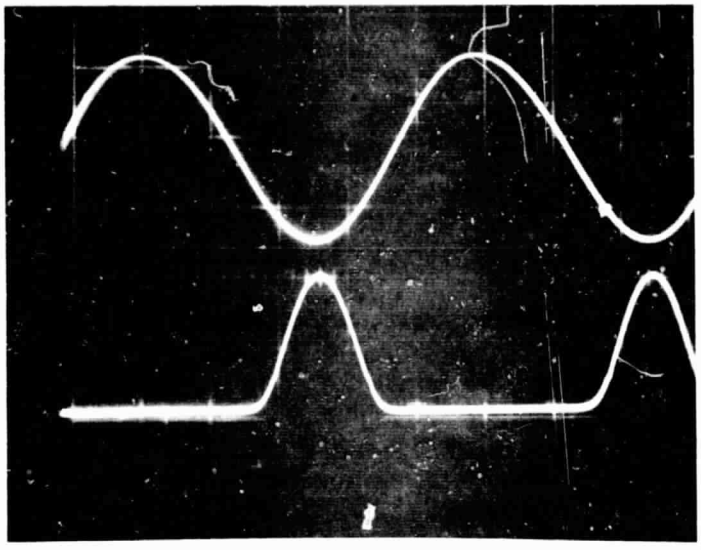

Fig. III-1.6 Top: 10kc sine wave imput to the exponentiator. Bottom: Exponentiator output. Scale, 5 volts per division.

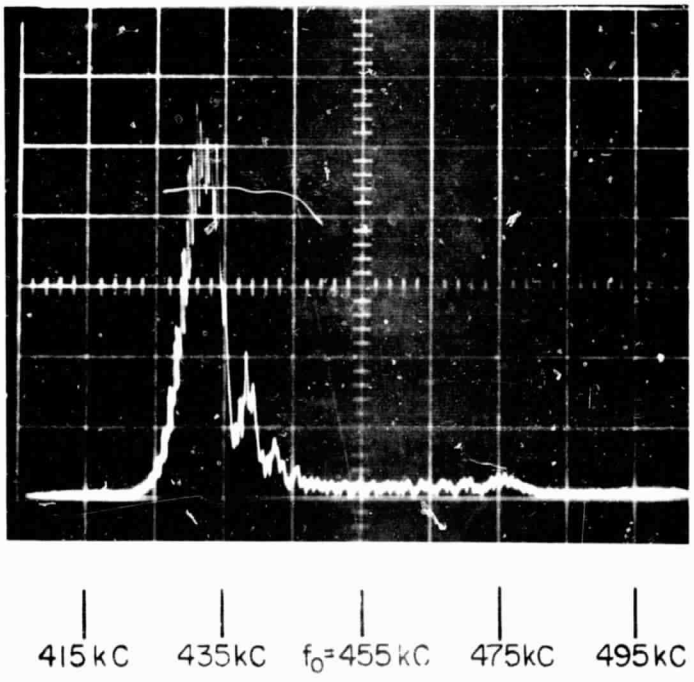

Fig. III-1.7 Output spection of SSB-FM generator with sine wave input of 7.5 volts at 1 kc to exponentiator and .12 volts to Wavetek FM generator. Center frequency of Wavetek generator is 455 kc.

2. FM Noise.

This section generalizes the work done by Rice[1] in approximating the noise output of an FM discriminator, (FMD).

Rice[1] has shown that the output noise of a FMD may be approximated by the sum of two uncorrelated noise components; a parabolic spectrum gaussian noise term and a Poisson shot noise term consisting of impulses of area 2π. In this report the noise is considered as a sum of a gaussian term plus a shot noise term that are in general correlated. The shot noise term becomes Poisson for large input carrier to noise ratios (CNR).

It is assumed that the input to the FMD is an unmodulated carrier plus symmetrical bandpass gaussian noise centered on the carrier. Thus the input may be represented as

$$A \cos \omega_0 t + n(t) =$$

$$A \cos \omega_0 t + x(t) \cos \omega_0 t - y(t) \sin \omega_0 t =$$

$$\sqrt{(A + x)^2 + y^2} \cos [\omega_0 t + \psi(t)] \tag{1}$$

$$\psi(t) = \tan^{-1} \frac{y(t)}{A + x(t)}$$

where A is the carrier amplitude, ω_0 the carrier frequency and $x(t)$ and $y(t)$ are the low pass equivalents of the noise $n(t)$. The output of the FMD is $\dot{\psi}(t)$,

$$\dot{\psi}(t) = \frac{d}{dt} \tan^{-1} \frac{y(t)}{A + x(t)} \tag{2}$$

This output is approximated by $z(t)$,

$$\dot{\psi}(t) \simeq z(t) = g(t) + p(t)$$
$$= \frac{\dot{y}(t)}{A} + p(t) \tag{3}$$

where $g(t) = \frac{\dot{y}(t)}{A}$ is the familiar output noise for large CNR and $p(t)$ is the

click process. The two terms, p(t) and g(t) are, in general, correlated.

The click process is formed in the following manner, when $x(t)$ is less than -A and y(t) approaches zero with $\dot{y}(t)$ negative (positive) p(t) will have a positive (negative) impluse of area 2π. The results may be easily extended to waveshapes other than impluses. The click process may be expressed as,

$$p(t) = -2\pi\ \dot{y}(t)\ u[-A - x(t)]\ \delta[y(t)] \tag{4}$$

where $u(x)$ is the unit step function and $\delta(x)$ the unit impluse function.

The autocorrelation of the output noise is given by

$$R_{zz}(\tau) = E\{z(t+\tau)\ z(t)\} \tag{5}$$

$$= \frac{1}{A^2}\ R_{\dot{y}\dot{y}}(\tau) + R_{gp}(\tau) + R_{pg}(T) + R_{pp}(\tau).$$

The first term is the parabolic spectrum gaussian noise term, the second and third terms are the cross-correlation terms and the last term is the autocorrelation of the spike process. The cross correlation term has the form

$$R_{gp}(\tau) = E\{g(t+\tau)\ p(t)\} = R_{pg}(-\tau) \tag{6}$$

$$= E\{-\frac{\dot{y}_2}{A}\ 2\pi\ \dot{y}_1\ u(-A - x_1)\ \delta(y_1)\}$$

where the expection is over t and the subscripts 1 and 2 refer to time instants t and (t+τ). By evaluating the appropriate integrals $R_{gp}(\tau)$ is found to be,

$$R_{gp}(\tau) = \frac{\sqrt{\pi}}{2\beta}\ \rho''\ \text{erfc}\ \beta \tag{7}$$

where $\rho'' \triangleq \frac{d^2}{d\tau^2}\ \rho_{xx}(\tau)$ $\quad \rho_{xx}(\tau) = \frac{R_{xx}(\tau)}{N}$

$$\beta = \sqrt{\frac{A^2}{2N}} \qquad N = R_{xx}(0)$$

From Eq. (7) it is seen that the gaussian noise and the click noise decouple as a complementary error function of β, the decoupling is strongly effected by the input filter shape due to the term $\rho''_{xx}(\tau)$; however the two components are indeed uncorrelated for large CNR as is generally assumed.

The autocorrelation of the click process is given by,

$$R_{pp}(\tau) = 4\pi^2 E\{\dot{y}_1\, \delta(y_1)\, u(-x_1 - A)\, \dot{y}_2\, \delta(y_2)\, u(-x_2 - A)\} \qquad (8)$$

The corresponding integrals can be evaluated after rather lengthy manipulations and the autocorrelation takes the form

$$R_{pp}(\tau) = 2\pi\gamma\ \mathrm{erfc}\,\beta\ \delta(\tau) \qquad (9)$$

$$-2\pi\left\{\tfrac{1}{4}\,\mathrm{erfc}^2\,\beta + \sum_{n=1}^{\infty} \frac{\left[\varphi^{(n)}\left(\frac{A}{\sqrt{N}}\right)\right]^2}{n!}\,\rho^n\right\}\left\{\frac{\rho}{\sqrt{1-\rho^2}} + \frac{\rho\rho'^2}{(1-\rho^2)^{3/2}}\right\}$$

where $\gamma = \sqrt{-\dfrac{R''_{xx}(0)}{R_{xx}(0)}}$ = radius of gyration of the band pass filter in rps.

$$\rho \triangleq \rho_{xx}(\tau) \qquad \varphi(x) = \frac{1}{\sqrt{2\pi}} \int_{-\infty}^{x} e^{-\frac{u^2}{2}}$$

$$\varphi^{(n)}(x) \triangleq \frac{d^n}{d\,n}\,\varphi(x)$$

For large CNR only the first term in Eq. (9) is significant, and it should be noted that this is the flat spectrum Poisson shot noise term.

The power spectrum of the click process, $S_{pp}(\omega)$, may be obtained by taking the fourier transform of $R_{pp}(\tau)$ numerically. In Fig. III-2.1 the normalized power spectrum is given for a gaussian shaped filter. The correlation between the clicks produces a dip in the power spectrum around the origin and hence the click power at the output is reduced.

By comparing $S_{pp}(0)$ with the exact power spectrum of the noise output of the FMD as given by Rice[2] we see that for $\omega = 0$ they are identical for all CNR (note that for $\omega = 0$ $S_{zz}(0) = S_{pp}(0)$ since $S_{pg}(0) = 0$). The analysis presented is an extension and elaboration of the FM noise problem as studied by Rice[1]. The decomposition of the FM noise into two components provided an understanding of the FM threshold phenomenon. The analysis presented in this report elaborates, extends and justifies the generally used method of FM noise decomposition.

References.

1. S.O. Rice, "Noise in FM Receivers", chap. 25, pp. 375-424, in "Proceedings, Symposium on Time Series Analysis", M. Rosenblatt (ed.), John Wiley and Sons, Inc., N.Y., 1963.

2. S.O. Rice, "Statistical Properties of Sine Wave plus Random Noise", B.S.T.J., vol. 27, Jan. 1948.

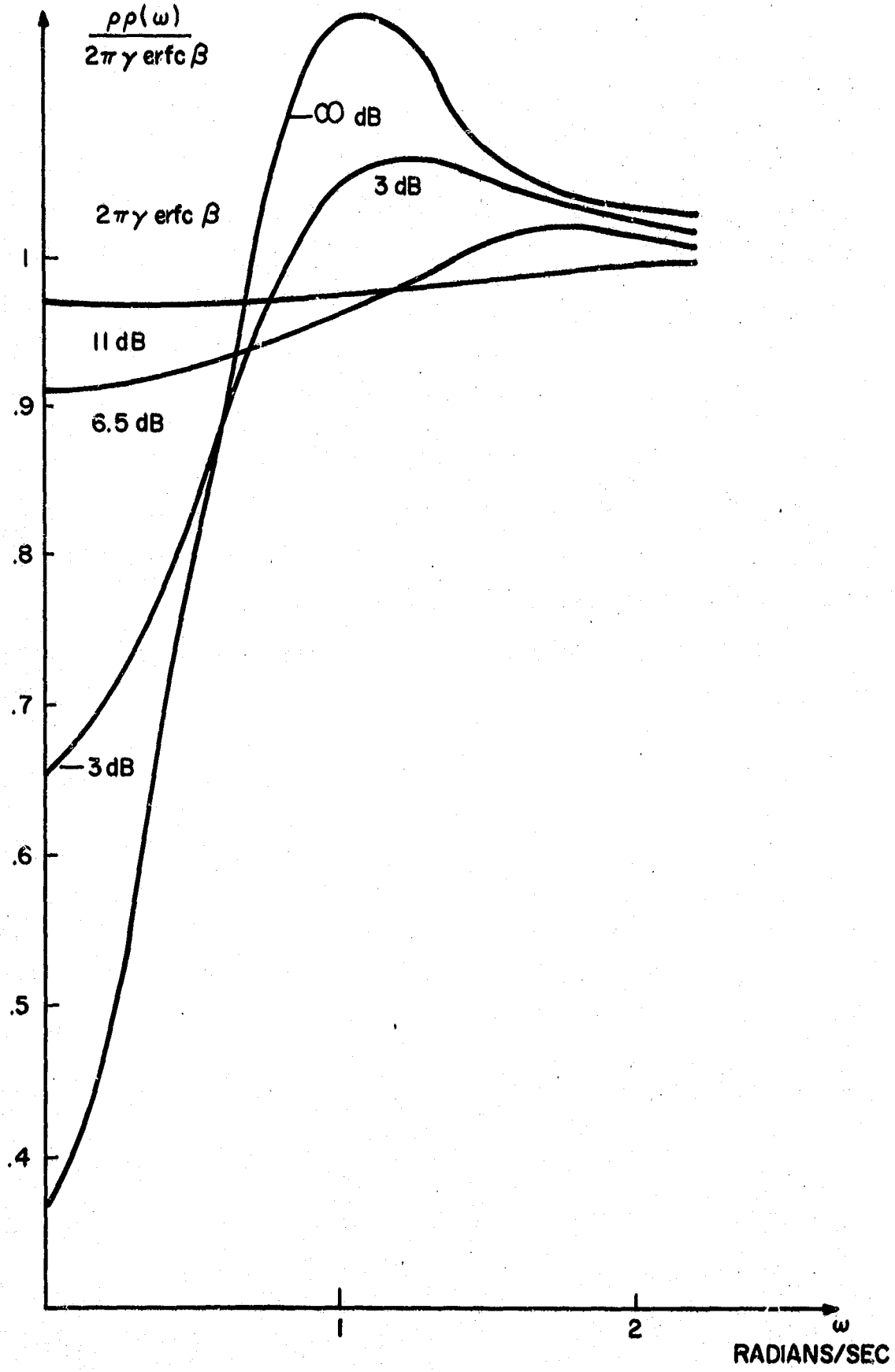

Fig. III-2.1 Normalized Power Spectrum of the Click Process for a Gaussian Shaped Filter

3. FM Multipath Interference.

Although frequency-modulation communications systems contain interference-suppression capability greater than that of amplitude-modulation systems of comparable power, FM systems are not entirely immune to such interference. Interfering noise, unrealted transmitters, or echoes of the desired signal can produce interference in the demodulated information. Such factors can result in degradation of system performance.

Interference in AM systems results in such effects as noise in the audio output, beat notes, or reception of two signals simultaneously. Random noise interference in FM systems may cause effects at the output of the receiver that are similar to the familiar AM noise. As noise intensity increases, eventually sudden, isolated "clicks" are heard at the speaker. This phenomenon, which has beed treated extensively in the literature, may be the limiting factor with respect to noise performance of the system. When unwanted signals generated by other transmitters or even by echoes of the desired signal are received, other effects also peculiar to FM occur. When spurious echoes of the desired signal are received, a "multipath" transmission situation is said to exist. In this, case, the transmitted signal arrives at the receiver via two or more distinct paths.

The importance of FM interference due to multipath transmission was first recorded by M.S. Crosby in the 1930's. Echo interference was observed of sufficient severity for Crosby to conclude that "on circuits where multipath transmission is encountered, frequency modulation is impracticable". Crosby continued his research and developed a simplified theory which maintained that two-path interference could be considered a beat note between the interfering signal. This approach is a useful way of viewing the problem.

In this report we are concerned principally with the effect of a delayed attenuated echo of a modulated FM signal upon the demudulated output. The chief effect of such interference is to creat a (Crosby) "beat note." Since the signals are frequency modulated and randomly phased, however, the instantaneous frequence of the desired and interfering signals in constantly changing; and the frequency of the interference "beat note" must change as well. In addition, because of the properties of the FM demodulator or discriminator, strong harmonics of the beat frequency are also observed.

If the modulation of the two received signals is changing very slowly with time, the beat note character of the interference is readily observed. Over a short period of time, the two signals appear as unmodulated sinusoidal radio-frequency carriers, with the frequency of each signal determined by the value of its respective (approximately constant) modulation signal. Thus, over a short period of time, the interference between two modulated signals is similar to that produced by two carriers of different frequency. Because of this similarity, the case of interference between unmodulated carriers was studied in detail.

It will be seen that the severity of interference between two signals depends strongly upon the relative strength of the carriers of the two signals when modulation is absen, or, alternately, upon the relative signal amplitudes. In particular, if the interfering signal should become nearly as strong as the desired signal, the resulting interference tends to obliterate the desired information if the multipath time spread is appreciable. If the interfering signal does in fact become even stronger than the desired signal, the interference signal modulation will be the information signal extracted by the receiver. When the interfering signal is a delayed

echo of the primary signal, the "capture effect" results in a corresponding delay of demodulated signal. If the echo delay is comparable to the period of the modulation signal, the interference can be severe.

A principal purpose of this report is to determine the severity of the interference as a function of the various parameters involved, such as the delay time, interfering signal strength, and modulation. It is proposed to use two criteria for measuring the interference severity. The first is the number of interference pulses that occur in some convenient time interval such a s period of the modulation signal. The other criterion is the mean-square power of the interference. It is shown that the audio bandwidth of the demodulated interference may be much greater than that of the desired signal. Thus, filtering of the interference and signal will reduce the interference-to-signal power ratio significantly. The amount of this reduction will be determined for certain cases.

Three different types of modulation are studied. The first, which has been mentioned, consists of different but constant (i.e., DC) modulation on the two signals, and is equivalent to the reception of signals from two unmodulated transmitters of different frequency . The second case to be considered to that of sinusoidal-modulation two-path, in which a single modulation frequency is applied and a spurious, additive, delayed echo of the desired signal is received. The sinusoidal-modulation case, is in a sence, a "worst-case" choice, for the instantaneous frequency deviation of the RF signal is near its peak for a large proportion of the time. The final case is that of random modulation of Gaussian density, again received in addition to a delayed, attenuated echo of the modulated signal. Because of the mathematical complexity involved, only the average number of interference pulses or "spikes" will be determined for this case.

Experimental confirmation of certain results are also offered. Since most of this work requires the delaying of FM signals to produce a bipath effect, a delay line of suitable delay (e.g., 1 msec) operating at a suitable frequency (e.g., 1 MHz) was required. Electronic delay lines commercially available at low cost cannot provide such features. This problem was solved by use of the Brooklyn Polytechnic Institute water tank channel simulator[1]. In this system, the large distances involved in actual information transmission are simulated conveniently in the laboratory by transmission of ultrasonic waves through water. Distances of several hundred kilometers can readily be simulated with this system.

A block diagram of the experimental setup appears in Fig. III-3.1. A sinusoidally-modulated FM signal was produced by varying the driving current of an astable multivibrator with the appropriate sinusoidal signal. The RF signal, which was at a frequency of approximately 1 MHz, was then split into two paths. One path included about one meter of water transmission, and produced a delay time of about 0.6 msec. Crystal tranducers were used to transmit and receive the signal in the water tank, and a high-gain amplifier and limiter were used in conjunction with the receiving transducer. The second RF transmission path was simply a bypass of the water tank delay line. The direct and delayed signals were added and filtered by a single-tuned stage. A commercial frequency meter-discriminator and a commercial bandpass filter served as the discriminator. In order to allow observation and measurement of the interference without the modulation information signal, a provision was made to add the (pre-modulation) sinusoidal information signal back on to the discriminator output. Variable gain and phase controls were included in this path, so that the demodulated sinusoidal information signal could be completely cancelled. The final

output could be observed visually with an oscilloscope, or it could be analyzed with an RMS voltmeter or frequency analyzer. Several oscillograms of experimental observations are included in this report. An oscillogram of an experimental simulation of this interference is shown in Fig. III-3.3. In this case the relative signal strength was $\rho = 0.78$.

In Fig. III-3.3 it may be seen that the interference waveform varies greatly for differing values of ρ. In a real situation, one could not predict the values of ρ in davance. For this reason, a statistical approach to the problem seems advisable. To illustrate this approach, the density function of the interference will be calculated if ρ is assured random with some (known) density function. The interference may then be considered a (nonstationary) random process. The density function will of course be a time function: what is most interesting is the value of the density function at some point in time. This is the random interference process at that instant. Thus, it is possible to obtain a density function of the distribution of, for example, the peaks or the valleys of the interference pulses. The distribution $f_\rho(\rho)$ of the interference strength, ρ, will be assumed to be Rayleigh:

$$f_\rho(\rho) = \frac{\rho}{a^2} e^{-\frac{\rho^2}{2a^2}} U(\rho)$$

Here, $U(\rho)$ is the unit step function at $\rho = 0$.

The probability density of the interference $\omega_i(\rho, t)$

$$\omega_i(\rho, t) = \omega_d \rho \frac{\rho + \cos \omega_d t}{1 + \rho^2 + 2\rho \cos \omega_d t}$$

is, following the familar theory of probability density functions,

$$f_{\omega_i}(\omega_{ij} t) = \sum_j \frac{f_\rho(\rho_j)}{\left| \frac{2\omega_i(\rho)}{2\rho} \right|_{\rho = \rho_j}}$$

The $\rho_j(\omega_{ij}t)$ are those ρ for which $\omega_i(\rho_{ij}t) = \omega_i$, that is, the inverse with respect to ρ of the function $\omega_i(\rho_j t)$. The subscript j indicates that where may be several solutions for each value of ω_i. It also serves to distinguish the parameter ρ_j, which is dependent upon ω_i, from the parameter ρ. ρ has the same significance as does ρ_j except that it is an independent variable.

It is necessary first to solve for the ρ_j. The quadratic formula may be applied if $\rho \neq 1$. In this case,

$$\omega_d \rho_j [\rho_j + \cos \omega_d t] = [1 + \rho_j^2 + 2\rho_j \cos \omega_d t]\ \omega_i$$

or

$$\rho_j^2(\omega_d - \omega_i) + \rho_j(\omega_d - 2\omega_i) \cos \omega_d t - \omega_i = 0$$

Now apply the quadratic formula and solve for ρ_j:

$$\rho_j = \frac{-(\omega_d - 2\omega_i) \cos \omega_d t \pm \sqrt{(\omega_d - 2\omega_i)^2 \cos^2 \omega_d t + 4\omega_i(\omega_d - \omega_i)}}{2(\omega_d - \omega_i)}$$

From Fig. III-3.4 it may be seen that there are limits on the values that the interference waveform may assume over the sample space of ρ. For example, when $\omega_d t = 0$, there is no value of ρ which results in a negative value of ω_i. The discriminant of the above solution for ρ_j must be positive in order to assure a real value for $\omega_i \Omega$. Requiring the discriminant to be positive yields an amplitude restriction for the ensemble of waveforms $\omega_i(\rho_j t)$ as ρ is allowed to vary. This restriction is

$$(\omega_d - 2\omega_i)^2 \cos^2 \omega_d t + 4\omega_i (\omega_d - \omega_i) \geq 0$$

Group these terms with respect to ω_i, obtaining

$$\omega_i^2[4 \cos^2 \omega_d t - 4] + \omega_i \cdot \omega_d[4 - 4 \cos^2 \omega_d t] + \omega_d^2 \cos^2 \omega_d t \geq 0$$

If $\cos^2 \omega_d t = 1$, then the inequality reduces to

$$\omega_d^2 \geq 0$$

which is of course always true. Otherwise, note that

$$4 \cos^2 \omega_d t - 4 = -4 \sin^2 \omega_d t$$

divide both sides of the inequality by this quantity to obtain

$$\omega_i^2 - \omega_i - \omega_d^2 \frac{\cos^2 \omega_d t}{4 \sin^2 \omega_d t} \geq 0 .$$

Application of the quadratic formula yields

$$\frac{\omega_d}{2} - \frac{\omega_d}{2|\sin \omega_d t|} \leq \omega_i \leq \frac{\omega_d}{2} + \frac{\omega_d}{2|\sin \omega_d t|}$$

$\omega_i(t)$ may assume any value in this range if all values of ρ are permitted. It will also be required that ρ be positive: This yields an additional restriction

$$\rho_j \geq 0$$

Careful inspection of the terms in the formula for ρ_j indicates that the following signs apply in the square root (discriminant root):

	$\omega_i < 0$	$0 < \omega_i < \frac{\omega_d}{2}$	$\frac{\omega_d}{2} < \omega_K \omega_d$	$\omega_d < \omega_i$
$\cos \omega_d t > 0$	No solution	+	+	No solution
$\cos \omega_d t < 0$	+ and -	+	+	+ and -

Here, "+" indicates that the positive root applies, etc. Note that ω_i is restricted to values between 0 and ω_d when $\cos \omega_d t > 0$. The envelope for $\omega_i(t)$, then, obeying all constraints, is

$$\left|\omega_i - \frac{\omega_d}{2}\right| < \frac{\omega_d}{2} \qquad \text{for} \quad \cos \omega_d t > 0$$

or

$$\left|\omega_i - \frac{\omega_d}{2}\right| < \frac{\omega_d}{2\left|\sin \omega_d t\right|} \qquad \text{for} \quad \cos \omega_d t < 0$$

This envelope is shown in Figure 5.

Now that the solutions for the ρ_j in terms of ω_i have been obtained, it is possible to apply the formula

$$f_{\omega_i}(\omega_{ij} t) = \sum_j \frac{f_\rho(\rho_j)}{\left|\frac{\partial \omega_i(\rho)}{\partial \rho}\right|}\Bigg|_{\rho = \rho_j}$$

Thus,

$$\frac{\partial\, \omega_i(\rho_j t)}{\partial \rho} = \frac{\partial}{\partial \rho}\left[\omega_d \rho \; \frac{\rho + \cos \omega_d t}{1 + \rho^2 + 2\rho \cos \omega_d t}\right] =$$

$$\omega_d \frac{\rho + \cos \omega_d t}{1 + \rho^2 + 2\rho \cos \omega_d t} + \omega_d \rho \frac{\left[1 + \rho^2 + 2\rho \cos \omega_d t\right] - 2\left[\rho + \cos \omega_d t\right]^2}{\left[1 + \rho^2 + a\rho \cos \omega_d t\right]^2}$$

$$= \omega_d \frac{2\rho + \cos \omega_d t + \rho^2 \cos \omega_d t}{\left[1 + \rho^2 + 2\rho \cos \omega_d t\right]^2} .$$

Evaluation of $f_{\omega_i}(\omega_{ij} t)$ at $\omega_d t = 0$, $\frac{\pi}{2}$, and π is particularly interesting, that is, at the valleys, peaks, and midway points of the pulse train. This is, in other words, the probability density function of the random variable $f_{\omega_i}(\omega_{ij} t = 0$, etc.). At these times, the functions simplify somewhat. The values of the solution for ρ_j and of the parameters $\left|\frac{\partial \omega_i}{\partial \rho}\right|$ and $\left|\frac{\partial \omega_i}{\partial \rho}\right|_{\rho = \rho_j}$ evaluated at the three points in time $\omega_d t = 0$, $\omega_d t = \frac{\pi}{2}$, and $\omega_d t = \pi$ appear in the following table.

$\omega_d t$ =	0	$\frac{\pi}{2}$	π
ρ_j =	$\frac{\omega_i}{\omega_d - \omega_i}$	$\frac{\sqrt{\omega_i(\omega_d - \omega_i)}}{\omega_d - \omega_i}$	$-\frac{\omega_i}{\omega_d - \omega_i}$
$\frac{\partial \omega_i(\rho_j t)}{\partial \rho}$ =	$\frac{\omega_d}{(1+\rho)^2}$	$\frac{2\rho\,\omega_d}{(1+\rho^2)^2}$	$\frac{\omega_d}{(1-\rho)^2}$
$\frac{\partial \omega_i(\rho_j t)}{\partial \rho}$	$\frac{\omega_d}{(\omega_d - \omega_i)^2}$	$\frac{\omega_d}{2(\omega_d - \omega_i)^2} \cdot \sqrt{\frac{\omega_d - \omega_i}{\omega_i}}$	$\frac{\omega_d}{(\omega_d - \omega_i)^2}$

The value of $f_{\omega_i}(\omega_{ij}\, t)$ at these three time points may be written in terms of the echo strength probability density, $f_\rho(\rho)$:

$$f_{\omega_i}(\omega_{ij} t = 0) = \frac{\omega_d}{(\omega_d - \omega_i)^2} f_\rho\left[\frac{\omega_i}{\omega_d - \omega_i}\right] \text{ for } 0 < \omega_i < \omega_d; \text{ zero elsewhere.}$$

$$f_{\omega_i}(\omega_{ij}\, \omega_{dt} = \tfrac{\pi}{2}) = \frac{\omega_d}{2(\omega_d - \omega_i)^2} \sqrt{\frac{\omega_d - \omega_i}{\omega_i}} \; f_\rho\left[\frac{\sqrt{\omega_i(\omega_d - \omega_i}}{\omega_d - \omega_i}\right] \text{ for}$$

$0 < \omega_i < \omega_d$; zero elsewhere.

$$f_{\omega_i}(\omega_{ij}\, \omega_d t = \pi) = \frac{\omega_d}{(\omega_d - \omega_i)^2} f_\rho\left[\frac{-\omega_i}{\omega_d - \omega_i}\right] \text{ for } \omega_i < 0 \text{ and } \omega_i > \omega_d;$$

zero elsewhere.

It is now assumed that ρ is Rayleigh distributed, i.e.

$$f_\rho(\rho) = \frac{\rho}{a^2}\, e^{-\frac{\rho^2}{2a^2}}\, U(\rho).$$

It is well known that a Rayleigh distribution of multipath strength frequently is encountered for long-haul radio transmission systems. A typical value of $a = 0.25$ will be assumed. With this choice, the probability that a value of ρ greater than unity will occur is e^{-8} -- a very small number. Still, the density is appreciable over most of the range $0 \leq \rho < 1$. With $a = 0.25$, the density of ρ is

$$f_\rho(\rho) = 16\,\rho\, e^{-8\rho^2}$$

for simplicity, ω_i will be normalized in terms of ω_d. Let $x = \frac{\omega_i}{\omega_d}$. The density of $\omega_i(t,\rho)$ at the three points in the cycle of interference is then easily found to be

$$f_x(x; t = 0) = \frac{1}{(1-x)^2} f_\rho\left[\frac{x}{1-x}\right] = \frac{1}{\omega_d} \frac{x}{(1-x)^3} 16 \exp\left[\frac{-8x^2}{1-x^2}\right] \qquad 0 \le x > 1$$

$$f_x(x; \omega_d t = \tfrac{\pi}{2}) = \frac{1}{2(1-x)^2} \sqrt{\frac{1-x}{x}}\, f_\rho\left[\left[\frac{x}{1-x}\right]^{\frac{1}{2}}\right] = \frac{8}{(1-x)^2} \exp -8\,\frac{x}{1-x} \qquad 0 \le x < 1$$

$$f_x(x; \omega_d t = \pi) = \frac{1}{(1-x)^2} f_\rho\left[\frac{-x}{1-x}\right] = \frac{16x}{(x-1)^3} \exp -8\left(\frac{x^2}{1-x}\right) \qquad x < 0 \text{ and } x > 1$$

These functions are plotted in Fig. III-3.6, along with some representative members of the interference ensemble. The density of ρ is also shown.

Note that for $\omega_d t = 0$ and π, $f_x(x)$ has a Rayleigh-like density shape, with the distributions occuring above and below the $x = 0$ axis, respectively. At $\omega_d t = \frac{\pi}{2}$, however, $f_x(x)$ is quite different. At this point the ensemble waveforms are "clustering" near $x = 0$. This is reflected in a nonzero value for $f_x(0^+)$. Note also that there is a small but finite value of $f_x(x; \omega_d t = \pi)$ for $x > 1$. This reflects the small chance of ρ being greater than unity, in which case the interfering signal "captures" the receiver and $x > 1$, that is, $\omega_i > \omega_d$. Compare with Fig. III-3.4. If the density function for ρ had been weighted more heavily toward large ρ, the value of $f_x(x)$ for $x > 1$ would become approciable.

Detailed Analyses have been carried out for both deterministically modulated and randomly modulated FM. The detail will be available in a forthcoming report. In this report we shall only present the results of both the experimental and the theoretical work. In Figs. III-3.7 and 8 are

shown the effects of multipath as the demodulated sinusoidal-modulated FM.' because of the random relative phase, the distribution of positive and negative "multipath-spikes" (as distinguished form noise-induced spikes) is disturbed statistically. Figs. III-3.9 and 10 show the comparison between experiment and theoretical results which were obtained by averaging over a uniform distribution of phase ϕ. The total RMS interference shown in Fig. III-3.11 again shows excellent agreement between theoretical model and experimental results.

For random modulation, the expected spike density was calculated and is shown plotted in Fig. III-3.12 vs. $f_a \Delta t$ for both uniform and Gaussian modulation specta. A typical experimental observation of spike density for random gaussian modulation is shown in Fig. III-3.13.

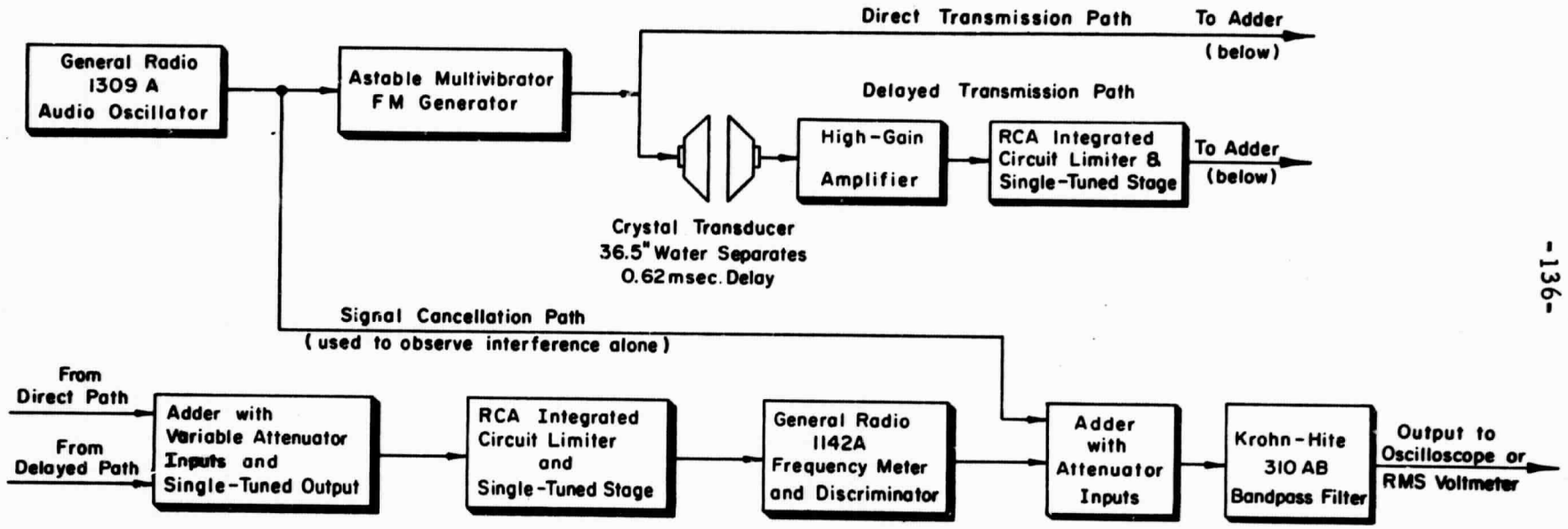

Fig. III-3.1 Block diagram

$$e_1(t) = A \cos \omega_c t$$

$$e_2(t) = \rho A \cos (\omega_c + \omega_d) t$$

$$e_r(t) = e_1(t) + e_2(t)$$

$$= A_r(t) \cos (\omega_c t + \theta(t))$$

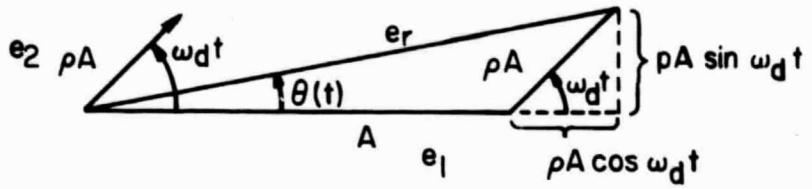

Fig. III-3.2 Phasor diagram of addition of unmodulated carriers

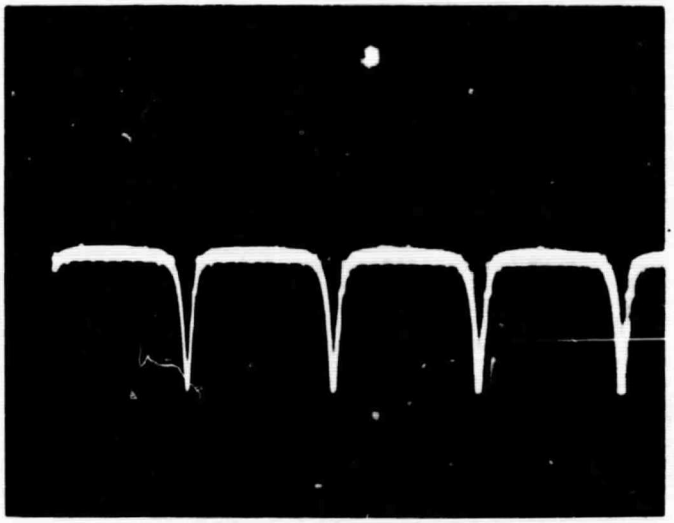

Fig. III-3.3 Unmodulated carriers interference.

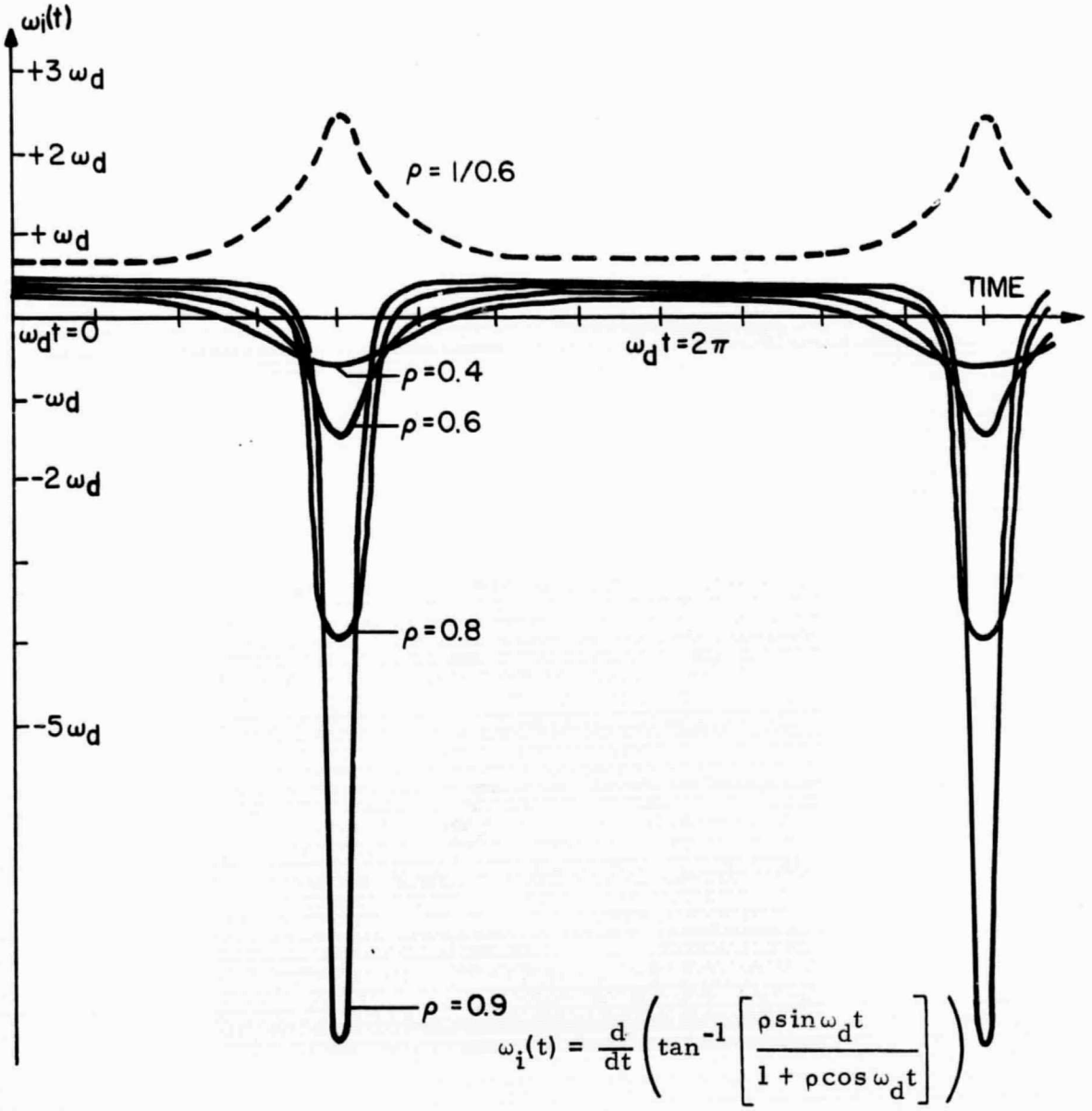

Fig. III-3.4 Demodulated interference $\omega_i(t)$ resulting from simultaneous reception of two unmodulated carriers. Various values of relative carrier amplitude (ρ). ω_d is radian frequency difference between carriers.

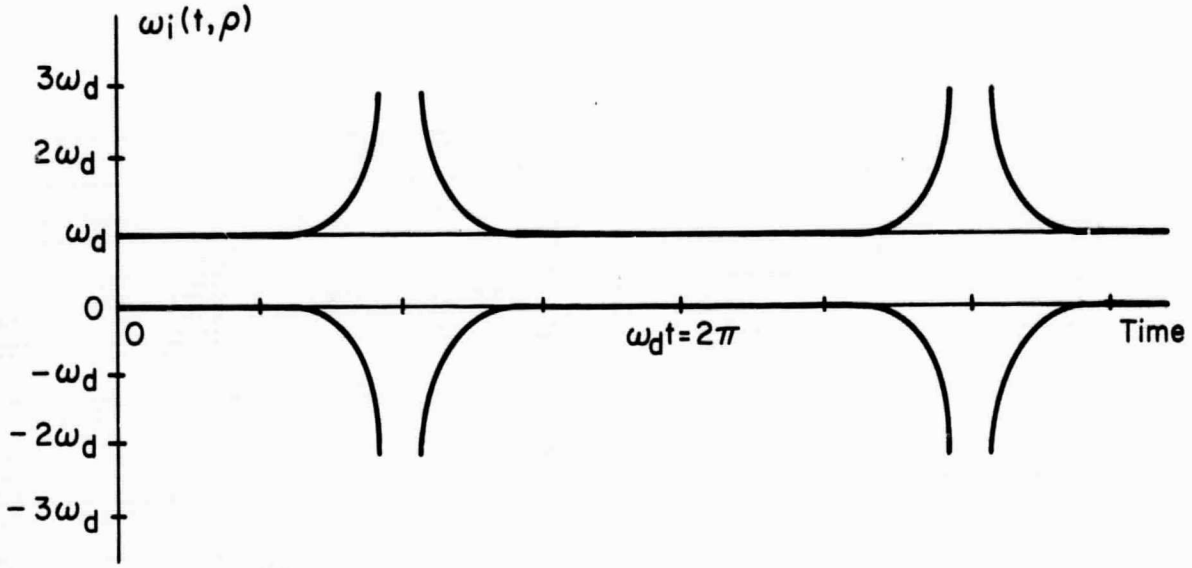

Fig. III-3.5 Envelope of Ensemble of Waveforms $\omega_i(\rho, t)$ Produced by Allowing ρ to Vary Over All Positive Values.

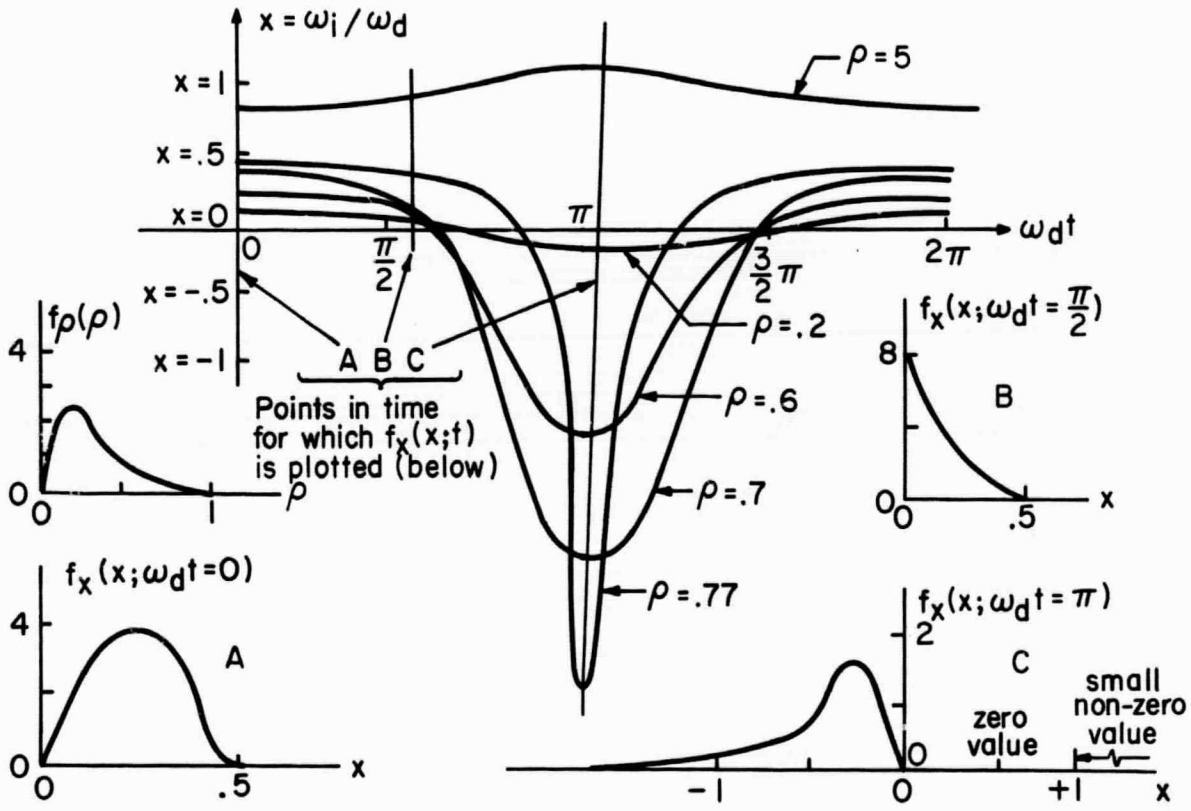

Fig. III-3.6 Density Function of Normalized Interference $x = \omega_i/\omega_d$ for ρ with Rayleigh Density, Plotted for Three Points in x(t) Time Cycle.

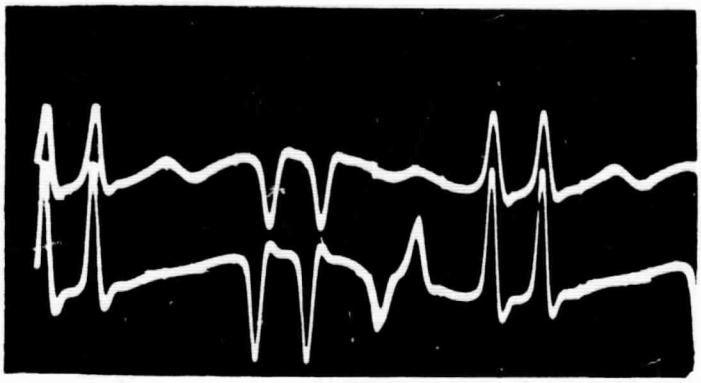

Fig. III-3.7 Demodulated signal plus interference.

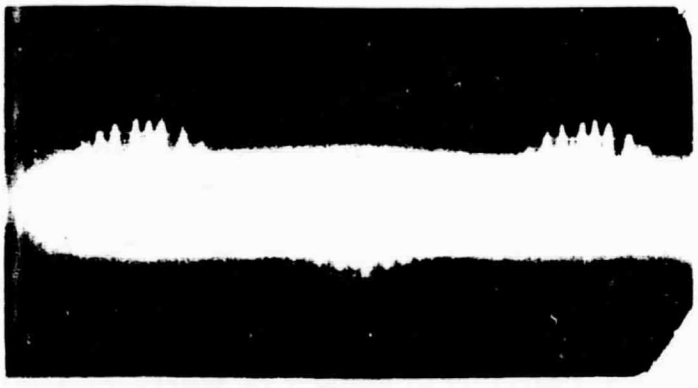

Fig. III-3.8 Sinusoidal envelope of interference.

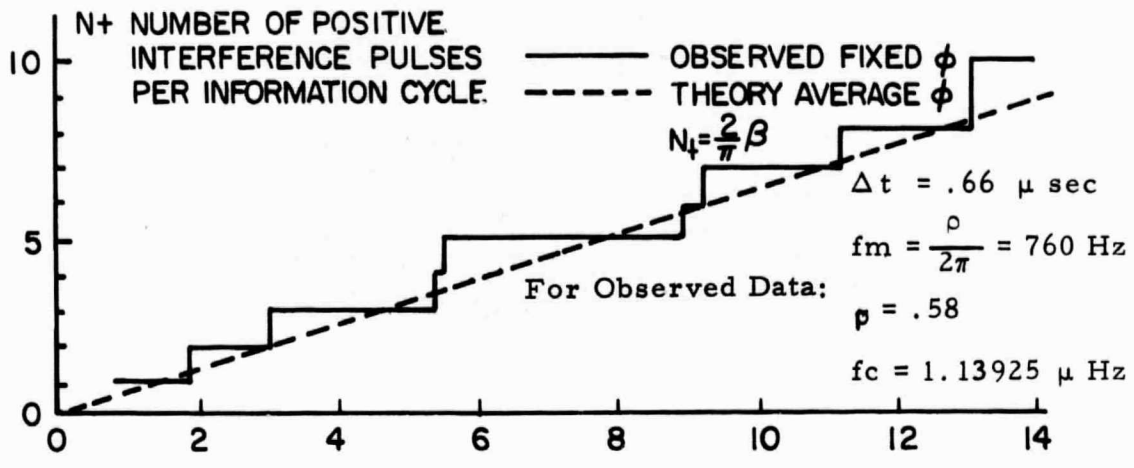

Fig. III-3.9 Variation of number of pulses with β.

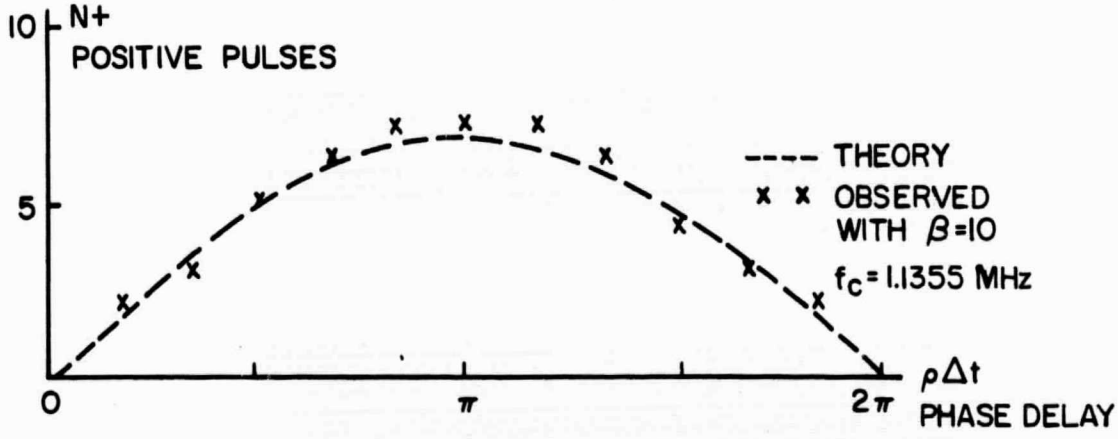

Fig. III-3.10 Variation of number of pulses with ρΔt.

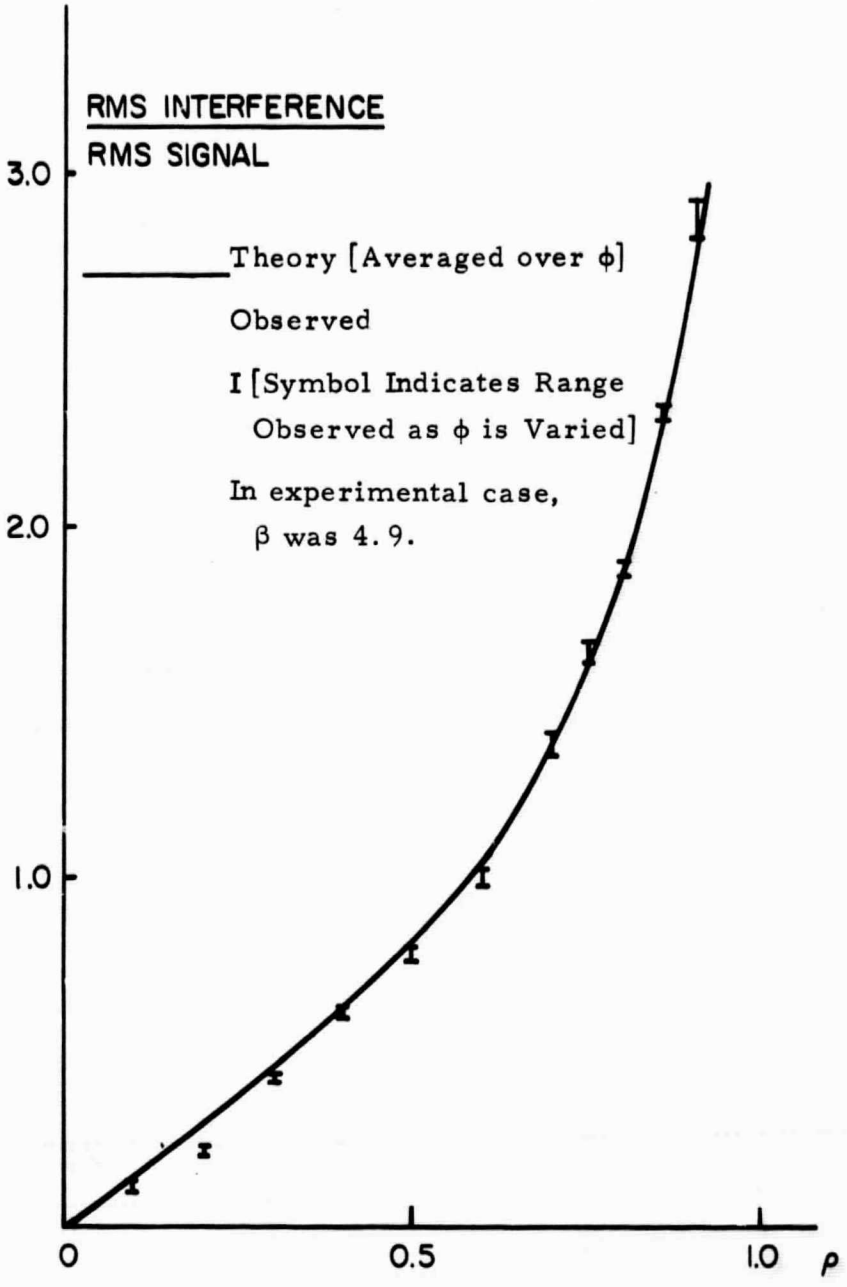

Fig. III-3.11 Interference-to-signal RMS ratio as a function of relative echo strength (ρ).

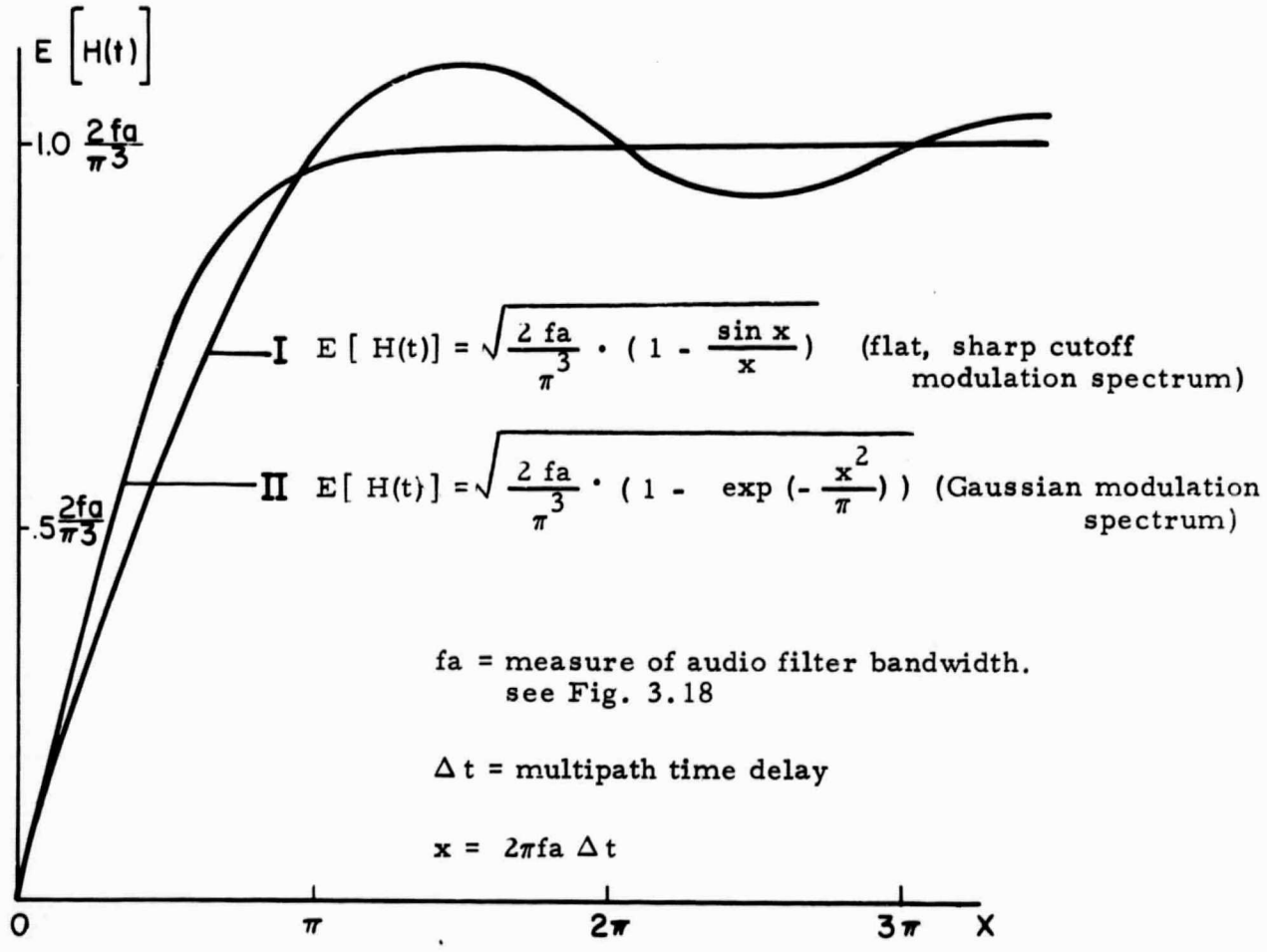

Fig. III-3.12 Expected pulse density for two Gaussian modulation signals

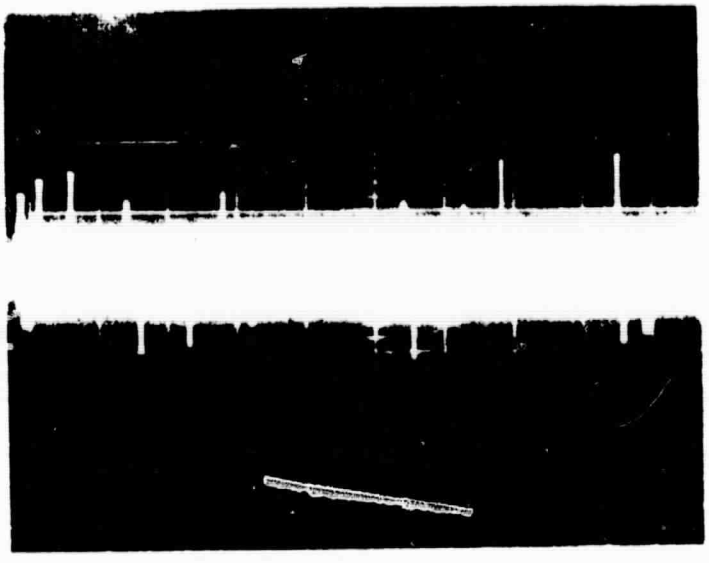

Fig. III-3.13 Interference resulting from random Gaussian modulation.

IV. SINGLE CHANNEL PHASE-SHIFT KEYED COMMUNICATIONS

Introduction. - Practical binary phase-shift keyed (PSK) communication systems require a partially coherent reference signal at the receiver. Two major classes of PSK systems may be identified, according to the technique used to obtain the reference signal: transmitted reference (TR) and single channel (SC). Although SC systems are potentially superior, they are difficult to analyze and have an inherent mark-space ambiguity problem.

Four differentially encoded SC PSK systems have been studied, including Decision Feedback (DF), Squaring (SQ), and a variation of SQ called Absolute Value (AB). In addition, a new Maximum Likelihood (ML) SC system, which is optimum under certain restrictions, is derived and studied. Error counts are obtained for these PSK systems using Monte Carlo simulation on an IBM 360/50 digital computer. Analytical bounds on the average probability of error, P(E), are derived which indicate that these systems all achieve comparable performance. This is in contrast with results which have been published previously.

Partially Coherent PSK Systems. - The degree of radio frequency (RF) coherence which can be established between transmitter and receiver of a communication system greatly influences the performance attainable. Assuming that the signal amplitude and the baud timing, or bit sync, are known at the receiver, we can write the RF signal receiver in the baud $[0, T]$ as

$$v(t) = s_i(t, \theta) + n(t), \quad t \in [0, T],$$

where the subscript i indicates that $s_i(t, \theta)$ is the signal corresponding to message m_i, $i = 1, 2$. $n(t)$ is white Gaussian noise with one-sided power

spectral density N_0. θ is the RF phase, assumed to be constant over the baud, which may be known with various degrees of accuracy depending on the particular communication system. The accuracy with which the value of of θ is known at the receiver determines the degree of RF coherence and thereby the minimum average probability of error P(E) which can be achieved.

Two important signal parameters are the energies of the two possible received signals, E_i, and their mutual correlation coefficient, ρ:

$$E_i = \int_0^T s_i^2(t, \theta)\, dt$$

$$\rho = (E_1 E_2)^{-\frac{1}{2}} \int_0^T s_1(t, \theta)\, s_2(t, \theta)\, dt.$$

If the actual value of θ is known accurately at the receiver, the system is termed coherent. It is known that the best signal set for such a system, in the sense of mimimum P(E), consists of a pair of equal energy anticorrelated ($\rho = -1$) signals. Phase shift keyed sinusoids, defined by

$$s_1(t, \theta) = C \cos(\omega_0 t + \theta)$$

$$s_2(t, \theta) = C \cos(\omega_0 t + \theta + \pi) = -C \cos(\omega_0 t + \theta),$$

form such a set. With the signal energy E received in each baud and the signal-to-noise ratio R defined as

$$E = \frac{C^2 T}{2} \qquad R = \frac{E}{N_0},$$

it can be shown that the mimimum P(E) attainable is

$$P(E) = \frac{1}{2} \operatorname{erfc} \sqrt{R}. \tag{1}$$

The receiver which attains this P(E) is the standard correlation detector.

In practical communication systems the received phase is not known with perfect accuracy. Often, however, an estimate $\hat{\theta}$ of θ is available, and systems using such an estimate are called partially coherent. When the estimate is good, and the signals are properly chosen, partially coherent systems may attain a P(E) close to the lower bound (Eq. 1). Unfortunately, the problem of overall system design, including signal specification and receiver design, is quite complex. The difficulty is that the phase estimate is usually derived at the receiver by special processing of the signals received over several bauds. Thus considerations of receiver complexity, signal structure, and channel characteristics all interact. The procedure which has led to many useful partially coherent systems is to postulate a "reasonable" signal set on the basis of the method to be used by the receiver to derive the phase estimate, and then to seek the parameter values which yield the best operation. Since anticorrelated signals are generally superior when a good phase estimate is available, the best choices are usually modifications of the simple coherent PSK system discussed above. These systems usually fall into one of two catergories, transmitted reference and single channel, although combinations of the two are also possible.

Single Channel Systems. - Transmitted reference (TR) systems transmit a reference signal to the receiver through a channel separate from the data channel. Thus the transmitted signal is a combination of a normal PSK signal and a signal to be used only for RF phase synchronization. The major disadvantage of TR systems is that the available power at the transmitter must be shared between these two signals. In single channel (SC) systems a normal, fully modulated PSK signal is transmitted. The phase estimation portion of the receiver processes this PSK signal in some nonlinear manner in order to remove the modulation. The various SC systems

differ in the nature of this nonlinear processing. The great advantage of SC systems is that the entire transmitter power is used for both data transmission and phase synchronization. Thus SC systems are potentially superior to TR systems.

It is appropriate at this point to introduce the mathematical model used in this study of SC systems and to note the two assumptions involved. First, the carrier frequency ω_0 is assumed to be known accurately at the receiver. Second, the quality of the phase estimate obtainable in actual systems is limited by the rate of change of received phase, caused by channel variations, oscillator phase jitter, etc. This limitation is incorporated into a simple model by postulating a constant received phase, but a limited allowable measurement time. This measurement time is taken as qT, extending over q bauds of duration T. The waveform available at the receiver for the decision on the data transmitted for $t \in [0, T]$ may therefore be represented as

$$v(t) = m(t)\, C \cos(\omega_0 t + \theta) + n(t), \qquad t \in [-qT, T], \tag{2}$$

where m(t) represents the modulation, and takes on the values ± 1 in each baud independently and with equal probability. Some receivers also store the last q decisions.

Although the model (2) is simple, two major difficulties are encountered in the study of SC systems. The first involves the nonlinear processing of the signal performed by the receiver in order to construct a partially coherent reference waveform. Such processing makes it extremely difficult to obtain results analytically. For this reason, Monte Carlo simulation on a digital computer is useful in studying system performance. The second difficulty encountered in SC systems is the "mark-space ambiguity" prob-

lem. In a simple SC system there is no way of determining the absolute sense of the signal received in each baud. That is, even though in low noise the bauds during which a 1 was transmitted can be distinguished from those during which a 0 was transmitted, it is impossible to determine which of these two groups of bauds actually corresponds to the 1 signal. In most SC PSK receivers, this mark-space ambiguity takes the form of two farily stable average phase values of the derived reference, separated from each other by π radians. Even if the correct reference sense is established at the beginning of the transmission, noise may cause loss of synchronism and eventual reference reversal during the transmission, inverting the decoded message. Several techniques are available for dealing with this problem, the simplest of which is differential data encoding. In this scheme data of 1 is represented by no phase change from the signal transmitted in the previous baud, and data of 0 by a phase change of π radians. Since the presence or absence of a phase transition between bauds can be detected equally well using a reference with phase near θ or $\theta + \pi$, there can be no inversion of the data with this technique. However, in a low error rate system where adjacent decisions are approximately independent, differential encoding almost doubles P(E) over that given in (1) above.

Results for Various SC Systems. - Since the SC systems studied are difficult to analyze exactly, and also because they are basically discrete, Monte Carlo simulation on an IBM 360/50 digital computer was found to be a useful tool. Differential data encoding was used in all of the simulations. The systems studied include Differential (D) PSK, Decision Feedback (DF) PSK, Squaring (SQ) PSK, and a variation of SQ-PSK called Absolute Value (AB) PSK. In addition, a new Maximum Likelihood (ML)SC system, which is optimum in a restricted sense, is derived and simulated. The results

are summarized below; details are contained in Ref. 1.

We first establish a performance bound for differentially encoded SC PSK systems as follows. A SC system is operating ideally when its derived reference is noiseless. Then the probability p of incorrectly identifying the sign of the signal received in each baud is given by:

$$p = \frac{1}{2} \operatorname{erfc} \sqrt{R}.$$

Since the reference is perfect, successive decisions are independent, and since differential encoding is used, an error occurs when a wrong detection is followed by a correct one or vice versa. Therefore, the minimum average error probability is given by

$$P(E) = p(1 - p) + (1 - p)\ p = \operatorname{erfc} \sqrt{R}\ (1 - \frac{1}{2} \operatorname{erfc} \sqrt{R}). \tag{3}$$

We now consider Differential (D) PSK which is the simplest and in certain ways the basic SC PSK communication system. In D-PSK, the signal received during the previous baud serves as the partially coherent reference for the present decision. Analytical results are available[2] for various error probabilities in D-PSK:

$$P(E) = \frac{1}{2}\ e^{-R}$$

$$P(E_{j+1}/E_j) = \frac{1}{2\pi} \int_0^{\pi} \operatorname{erfc}^2 (\sqrt{R} \cos \varphi) \tag{4}$$

$$\{1 + \sqrt{R}\pi \cos\varphi\ e^{R \cos^2 \varphi} [1 + \operatorname{erf} (\sqrt{R} \cos \varphi)] \}\ d\varphi$$

$$P(E_{j+2}/E_j) = \frac{1}{2}\ e^{-R}$$

The D-PSK system was simulated on the digital computer, and the error counts were compared to the analytical results above. The excellent agreement obtained indicated the accuracy of the simulation technique. In addition, it was proven that all of the other SC PSK systems studied reduce

to D-PSK for the special case of q = 1. Thus (4) provides an upper bound on the P(E) of any of these systems for $q \geq 1$. The lower and upper bounds given by (3) and (4) differ by approximately 1 db. in SNR, so we expect all of the SC PSK systems to achieve comparable performance. The simulation results support this conclusion.

In Decision Feedback (DF) PSK, combination with the reference of the signal received during the present baud is delayed until a decision about which signal was transmitted is made. This decision is then used as if it were correct to modify the present signal before it is combined with the reference. Since usually P(E) is small, the large majority of received signals are combined in the correct way. The error counts from the DF-PSK simulation are shown for three values of q in Fig. IV-1, along with the bounds on P(E) derived above. It is clear that even for medium values of q the system is operating close to its theoretical limit (Eq. 3).

Another major class of SC PSK systems uses the Phase Doubling (PD) technique. If φ_i is the phase error due to noise in the i^{th} baud, the received phase is

$$\psi_i = \theta + \varphi_i \quad \text{or} \quad \theta + \varphi_i + \pi,$$

depending on the modulation. In either case, the phase doubler output has angle

$$2\psi_i = 2(\theta + \varphi_i), \quad .$$

which is independent of the data. These angles from q bauds are combined to give the phase

$$\theta' = 2(\theta + \varphi'),$$

where φ' represents the total error due to noise. θ' is then halved to obtain the final phase estimate θ:

$$\theta = \theta + \varphi' \ .$$

Two details of this technique demand further attention. First, the q angles $2\psi_i$ can be combined in many ways. Two particular methods which were studied are weighting each angle as the square of the signal amplitude in the corresponding baud (SQ-PSK), and weighting proportional to the magnitude, or absolute value, of the signal amplitude (AB-PSK).

The second and most important consideration is that the procedure of halving the phase θ' is analogous to taking the square root of a complex number, and therefore, the final phase estimate $\hat{\theta}$ has two possible values separated by π radians. A rule must be established for choosing one of these two values. A satisfactory rule is to choose the value $\hat{\theta}$ which is closest to the $\hat{\theta}'$ derived for the previous decision. This choice gives good results for all values of q, and can be shown to be optimum for q = 1, since PD-PSK is equivalent to D-PSK under these conditions.

The PD-PSK systems described above were simulated on a digital computer. The error counts for SQ-PSK are shown in Fig. 2, and for AB-PSK in Fig. IV-1. Little difference is discernible between these results and those for DF-PSK in Fig. IV-1. Proakis et al.[3], on the other hand, have found on the basis of a similar digital computer simulation that DF-PSK is consistently superior to SQ-PSK. Apparently, they simulated a poor SQ system, since their experimental P(E) for q = 1 is significantly higher than the upper bound (4) derived above.

The final system investigated is called Maximum Likelihood (ML) PSK. This system was derived in the following way. Assume that the differentially encoded PSK signal (2) is available, but past decisions made by the receiver are not remembered. ML-PSK is the receiver which attains the smallest possible P(E) for the decision about the latest possible (at t = 0) phase transition. This is accomplished by applying a maximum à posteriori decision rule to the received signal. The ML receiver is quite complicated,

its complexity growing exponentially with q, but it can be implemented. This complexity is reflected in the large amount of computer time used in the simulation. For this reason only two values of q were used, and fewer trials were made for this system than for the others. The error counts are shown in Fig. IV-4. Even for the relatively small q = 5, the experimental P(E) is nearly equal to the theoretical lower bound. Performance is consistently superior to the other SC systems considered, but is not good enough to justify the receiver complexity.

In summary, the simulation results show that the popular SC PSK systems perform similarly. The theoretical lower bound in P(E) for a differentially encoded SC PSK system is approached quite closely for moderate values of q. Furthermore, all of the systems studied reduce to Differential PSK for the special case q = 1.

References.

1. J.F. Oberst, "Binary Phase-Shift Keyed Communication Systems", Ph.D. (E.E.) Dissertation, Polytechnic Institute of Brooklyn, August 1968.
2. J.F. Oberst and D.L. Schilling, "Double Error Probability in Differential PSK", Proceedings of the IEEE (Corr.), June 1968
3. J.G., Proakis, P.R. Drouilhet and R. Price, "Performance of Coherent Detection Systems Using Decision-Directed Channel Measurement", IEEE Transactions on Communication Systems, March 1964, pp. 54-63.

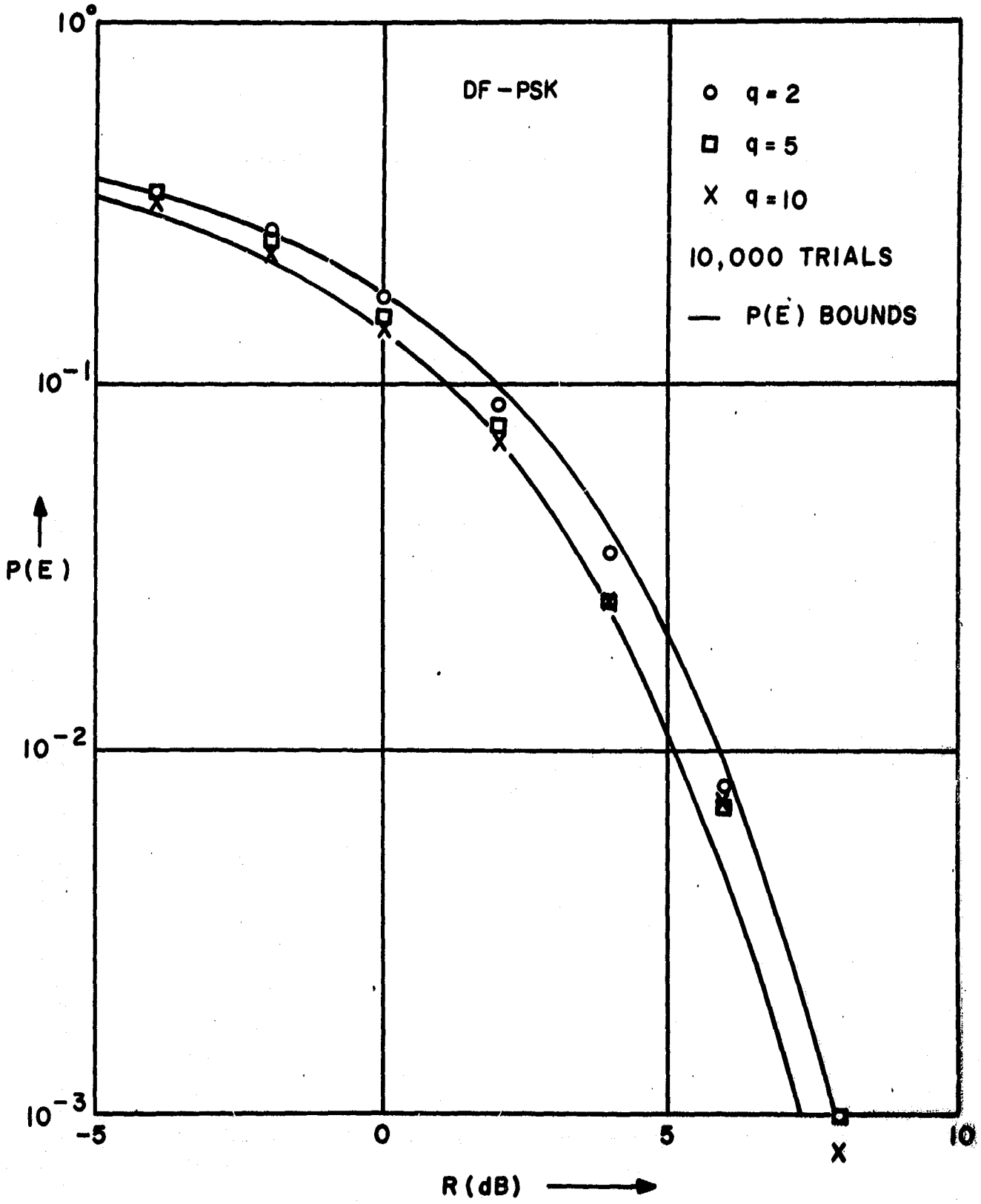

Fig. IV-1 Simulation results for DF-PSK

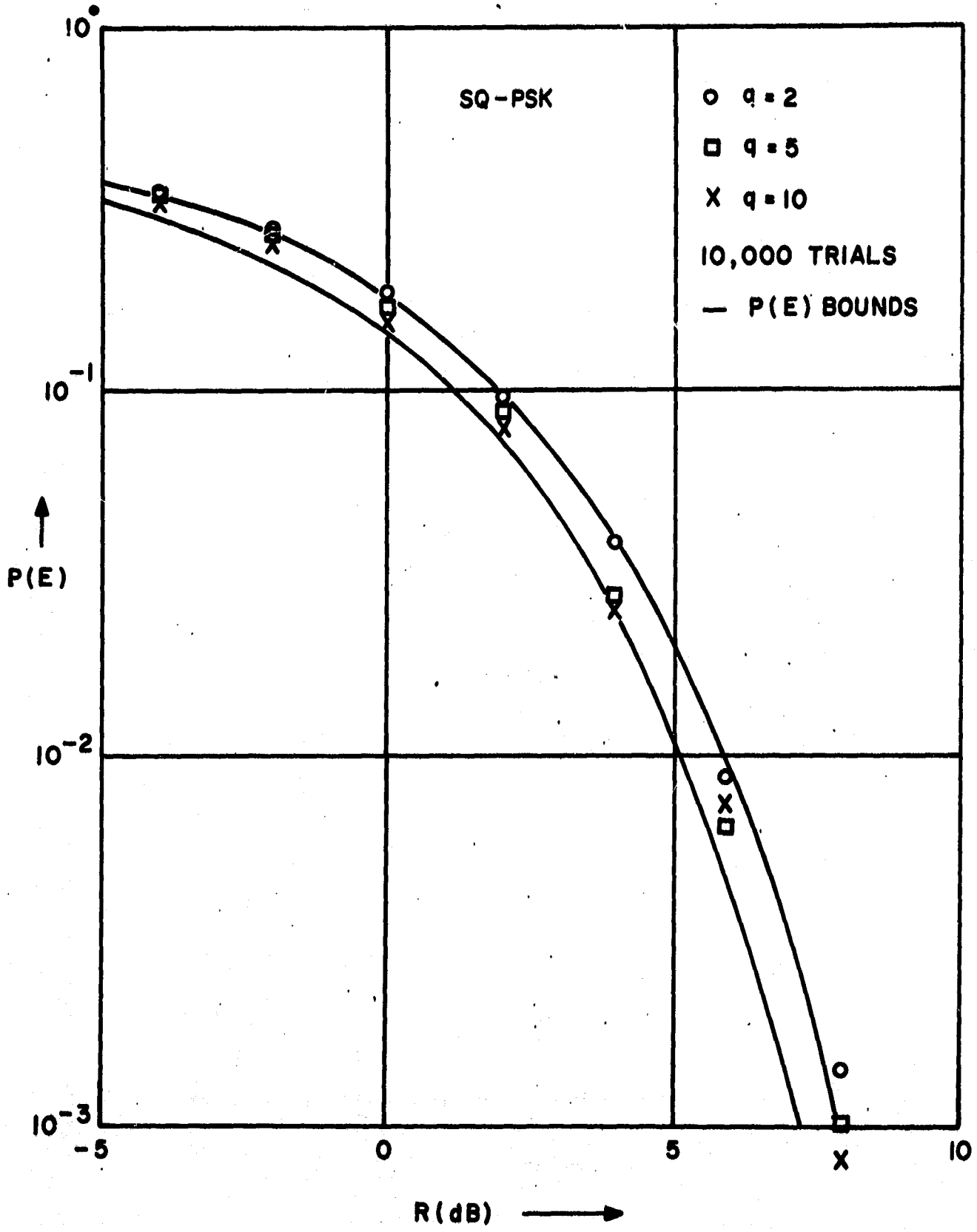

Fig. IV-2 Simulation results for SQ-PSK

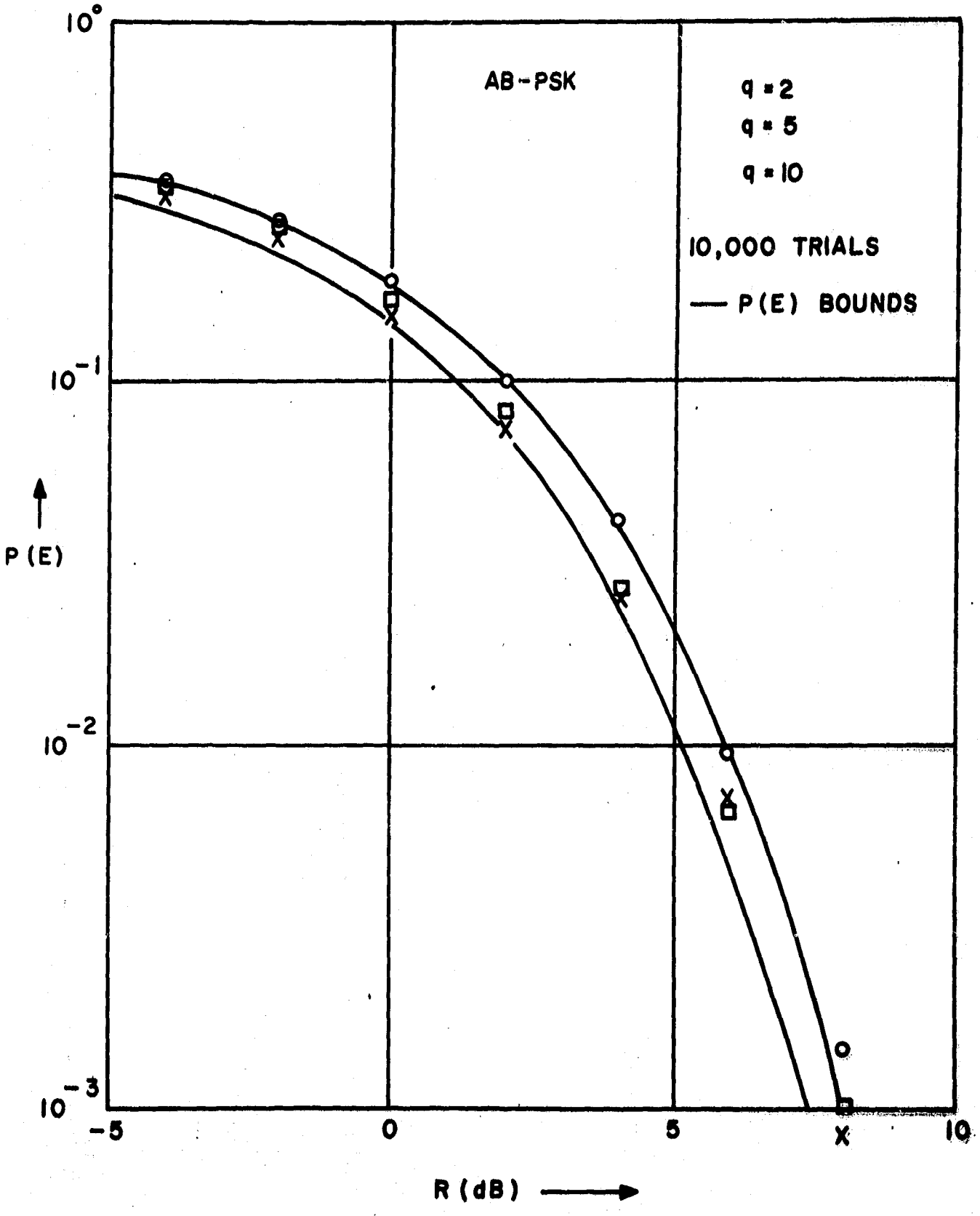

Fig. IV-3 Simulation results for AB-PSK

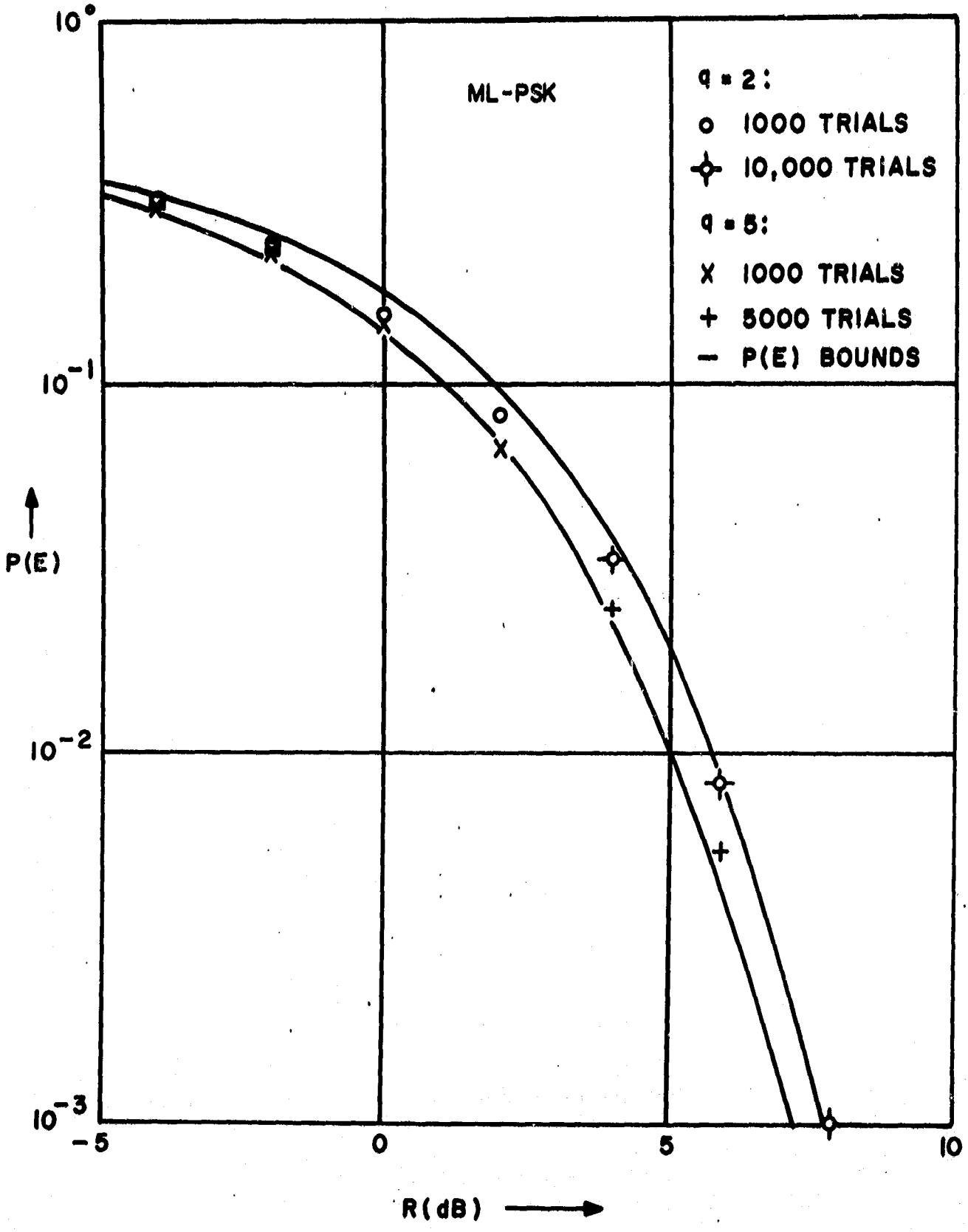

Fig. IV-4 Simulation results for ML-PSK

V. RECURSIVE METHODS IN SIGNAL PROCESSING

1. Derivative Estimates for Recursive Detection.

Introduction. - A recursive approach to signal detection has been proposed using state variable methods to detect known signals in additive, non-stationary, Gaussian non-white noise. This method reduces considerably the computational effort when discrete samples are used. The problem is that the derivatives of the sample are required. These derivatives are not available directly from the sampling process and must be approximated.

Two simple types of derivative estimation have been investigated. One replaces the derivatives, which are random variables, with their expected values. The other method estimates the derivatives by difference equations.

Equations for the signal to noise ratio using these derivative estimation techniques have been derived. The results of this sub-optimum process may then be compared with the optimum process which assumes all derivatives are completely known.

A computer program for finding the optimum and sub-optimum signal to noise ratio for various noise processes and signals has been developed. The results of this program for several signals of interest show the effectiveness of the derivative approximation methods.

It is shown that simple methods of derivative estimation are capable of near optimal results in the proposed recursive detection scheme.

Problem Formulation. - The recursive approach to signal detection developed by Pickholtz and Boorstyn[1] is summarized in this section since it is the basis for the work in this report. This formulation treats the case of discrete time detection of known signals in the presence of additive, Gaussian, non-white noise. It is assumed that the additive noise is generated as the solution of a linear differential equation drive by white noise.

where

$$a_{i,n} = [(\underline{Y}_n - \underline{B}_n \underline{Y}_{n-1}) - (\underline{s}_{i,n} - \underline{B}_n \underline{s}_{n-1})]^T \underline{K}_n^{-1} [(\underline{Y}_n - \underline{B}_n \underline{Y}_{n-1}) - (\underline{s}_{i,n} - \underline{B}_n \underline{s}_{n-1})] \quad (4)$$

$$\underline{B}_n = \underline{C}_{n,n-1} \underline{C}_{n-1,n-1}^{-1} \quad (5)$$

$$\underline{K}_n = \underline{C}_{n,n} - \underline{C}_{n,n-1} \underline{C}_{n,n-1}^{-1} \underline{C}_{n,n-1}^T \quad (6)$$

$$\underline{C}_{n,k} = E[\underline{X}_n \underline{X}_k^T] = E[\underline{X}(n\Delta)\, \underline{X}^t(k\Delta)] = \underline{C}(n\Delta, k\Delta) \quad (7)$$

Now let $s_2(t) = -s_1(t)$ for simplicity. (If this is not true our results are still obtained with $s(t)$ replaced by $s_2(t) - s_1(t)$ and simply derived bias terms added to the likelihood ratio). Then

$$\theta_n = \theta_{n-1} + 2[(\underline{s}_n - \underline{B}_n \underline{s}_{n-1})^T \underline{K}_n^{-1} (\underline{Y}_n - \underline{B}_n \underline{Y}_{n-1})] \quad (8)$$

and

$$\theta_0 = 2\underline{s}_0^T \underline{C}_{0,0}^{-1} \underline{Y}_0 . \quad (9)$$

Eqs. (8) and (9) define the structure of the optimum digital processor.

To evaluate the performance of this receiver we note that the probability of error is a monotonic function of the signal to noise ratio defined as

$$\gamma_n = \frac{E[\theta_n]}{\mathrm{Var}[\theta_n]} \quad (10)$$

It is easily shown from (8) that

$$E[\theta_n] = E[\theta_{n-1}] + 2[\underline{s}_n - \underline{B}_n \underline{s}_{n-1})^T \underline{K}_n^{-1} (\underline{s}_n - \underline{B}_n \underline{s}_{n-1}) \quad (11)$$

$$E[\theta_0] = 2\, \underline{s}_0^T \underline{C}_0^{-1}\, \underline{s}_0^T ,$$

and after some computation that

$$\mathrm{Var}\, \theta_n = 2E[\theta_n] \quad (12)$$

Hence

$$\gamma_n = \frac{1}{2} E[\theta_n] \tag{13}$$

There is a considerable simplification when the noise, X(t), is assumed to be stationary. In this case

$$\underline{B}_n = e^{\underline{A}\Delta} \tag{14}$$

$$\underline{K}_n = \underline{C}_0 - e^{\underline{A}\Delta}\, \underline{C}_0\, e^{\underline{A}^T\Delta} \tag{15}$$

$$\underline{C}_{0,0} = \underline{C}_0 \tag{16}$$

It should be noted at this point that the optimum digital processor must know the complete state vector $\underline{Y}(t)$ at each sample point. Y_n can be found by direct sampling. However, the derivatives $\dot{Y}_n, \ldots Y_n^{(k-1)}$ are not available and must be estimated. This means a digital processor which samples Y(t) at intervals of Δ will yield sub-optimal results. The accuracy to which the derivatives of Y_n can be estimated will determine how close the results will approach the optimum.

Derivative Estimation. - There are many approaches which can be used to recover derivatives from a sampled signal. Unfortunately all have limitations and these limitations become severe when higher order derivatives are required. The advantage of the proposed recursive detection scheme was that it greatly simplifies the digital computations. If a complicated method of estimating the derivatives of Y(t) is required, the advantages of this method may be defeated. For this reason, we shall investigate the suitability of those methods of derivative estimation which require a minimum of computation, hoepfully finding a method that for a suitable class of signals will yield results approaching the optimum.

Another factor to be considered is, how well does the method of derivative estimation lend itself to analysis? It is desirable to find the S.N.R. of the sub-optimal process analytically in order to avoid the problems of simulation.

One very simple method is to estimate the derivatives of Y(t) by the derivatives of E[Y(t)] = s(t). Obviously this is a crude, but easily implemented system since s(t) is completely known.

A more promising approach is to use a difference equation technique to estimate the derivatives of Y(t). A first order difference equation is relatively easy to implement. Higher order difference equations may have merit, but the increased computational effort would probably soon reach a point of diminishing return.

With these factors in mind, it was decided to attempt to find analytical expressions for the sub-optimum S. N. R. for the two methods of derivative estimation described above. For simplicity we consider stationary noise where $s_2(t) = -s_1(t) = s(t)$. These analytic expressions have been found for two types of estimates 1) using the expected values and 2) using a difference equation or recurrence method. The details of the derivations will be available in a forthcoming report.

Results. - In order to evaluate the effectiveness of the derivative estimation techniques several test cases were run. Several common pulse type signals were chosen for evaluation. It was assumed that $s = s_1 * -s_2$. The constants of the differential equation establishing the noise process were varied to yield narrow band, matched and wide band noise. The differential equation is second order and describes a filter which has flat response out to the cut off frequency and then rolls off at 40db per decade. In the matched case, the -3db point of the noise filter is at the -3db point of the signal frequency spectrum. Narrow band noise has a bandwidth of 0.2 of the signal bandwidth. Wide band noise has a bandwidth of 5 times the signal bandwidth.

n_0 was selected to give values of γ_n with a order of magnitude of 10 which corresponds to probabilities of error in the range of interest. The resulting S.N.R. for all cases is a linear function inversely proportional to n_0.

The results for several cases of interest are contained in the following tables.

In the tables the following notations are used.

n_0 = whose noise power spectral density of the defining colored noise

a_0, a = coefficients of the second order noise defining equation

γ_n = the signal to noise ratio at the end of n steps in the recursive procedure.

Conclusions. - These results indicate that near-optimal results can be obtained using either derivative estimation method. Of the two methods, the difference equation method yields more predictable results. In general, the difference equation technique yields results which appear to converge to the optimum as samples increase. The expectation method, however, often shows deterioration as samples increase. The optimum number of samples for this method varies considerably with the signal and noise characteristics.

As would be expected, the optimum as well as sub-optimum processes yield best results when the samples are taken at points which maximize the difference between s_1 and s_2, or in our case the maxima of s. In these cases the sub-optimum processes give near optimal results, even for few samples.

Those cases which depend on sample points where $s_1 = s_2$ show rather poor performance. It is also significant that good results are often obtained in cases where the derivatives approximated by the difference equation could not possibly be meaningful due to the large sample interval.

These observations lead to the conclusion that errors in derivative approximation do not adversely affect the S.N.R. in those cases where meaningful information is available at the sample point in distinguishing s_1 from s_2. Where this information content is not available (i.e. points where $s_1 = s_2$) both optimum as well as sub-optimum processes give poor results.

Utilizing the Markov property of the noise, a difference equation for the optimum test statistic is derived in state vector form. The test statistic is generated recursively by means of a first order difference equation. This formulation is applicable to non-stationary as well as stationary noise. The detection scheme is illustrated in Fig. V-1.1.

It is assumed that one of two completely known signals, $s_1(t)$ or $s_2(t)$ is received in additive, zero mean, Gaussian, non-white noise, X(t). X(t) is assumed to be generated as the solution of a k^{th} order linear time-varying differential equation driven by zero-mean white noise, W(t) which has spectral density n_0. The system is represented by the following state variables equations in matrix form:

$$\underline{Y}(t) = s_i(t) + \underline{X}(t) \qquad i = 1, 2 \quad t \geq 0 \tag{1}$$

$$\dot{\underline{X}}(t) = A(t)\,\underline{X}(t) + \underline{b}W(t) \tag{2}$$

where

$$\underline{X}(t) = \begin{bmatrix} X(t) \\ \dot{X}(t) \\ \ddot{X}(t) \\ \cdot \\ \cdot \\ \cdot \\ X^{(K-1)}(t) \\ X(t) \end{bmatrix}, \quad A = \begin{bmatrix} 0 & 1 & 0 & 0 & \cdots & 0 \\ 0 & 0 & 1 & 0 & \cdots & 0 \\ 0 & 0 & 0 & 1 & \cdots & 0 \\ \cdot & \cdot & \cdot & \cdot & & \cdot \\ \cdot & \cdot & \cdot & \cdot & & \cdot \\ \cdot & \cdot & \cdot & \cdot & & \cdot \\ -a_0(t) & -a_1(t) & -a_2(t) & -a_3(t) & \cdots & -a_{k-1}(t) \end{bmatrix}, \quad b = \begin{bmatrix} 0 \\ 0 \\ 0 \\ \cdot \\ \cdot \\ \cdot \\ 1 \end{bmatrix}$$

$a_i(t)$ are the coefficients of the noise generating differential equations. Using the Markov property of Y(t), the logarithm of the liklihood ratio of the first $t = n\Delta$ seconds of data, θ_n is found by the difference equation

$$\theta_n - \theta_{n-1} = \tfrac{1}{2}(a_{2,n} - a_{1,n}) \tag{3}$$

2. Further Theoretical Results.

The major (preliminary) results of theoretical importance insofar as recursive technique is concerned have been in fact incorporation of more extensive noise models for the detection problem. For example, noise generated by a white process passing through a system with numerator dynamics. E.g.

$$\frac{d^n Y(t)}{dt} + \sum_{K=0}^{n-1} a_K \frac{d^K Y(t)}{dt} = \sum_{\ell=0}^{n-1} b_\ell \frac{d^\ell w(t)}{dt} \qquad (1)$$

where w(t) is white.

In this instance, one cannot choose derivatives of the observations (or of the noise) to form a state vector of the system because these would contain white noise and its derivatives which is clearly unacceptable in a realization. We have therefore chosen as a state vector for the system (1) so that this is avoided. With this choice (1) can be represented as:

$$\dot{\underline{x}}(t) = A(t)\,\underline{x}(t) + \underline{b}\,w(t)$$
$$y(t) = \underline{C}^T \underline{x}(t)$$

where $\underline{x}(t)$ is the state.

The transistion matrix A is

$$A = \left[\begin{array}{c|cccccc} 1 & 1 & 0 & 0 & \cdots & 0 \\ -a_{n-1} & 0 & 1 & 0 & \cdots & 0 \\ 0 & 0 & 0 & 1 & \cdots & 0 \\ \vdots & \vdots & \vdots & \vdots & & \vdots \\ -a_1 & & & & & 1 \\ \hline -a_0 & 0 & 0 & 0 & \cdots & 0 \end{array}\right]$$

and the observation matrix is

$$\underline{C}^T = [1\ 0\ 0\ \ldots\ 0]$$

The essential feature of the new approach is the formation of an estimate of the state

$$\underline{x}(t) = E[\underline{x}(t) \mid y(\tau),\ \tau \underline{c} t]$$

and the proof that this is Markov. The estimate may be formed by a Kalman-Bucy filter once the estimate is generated, the recrusive algorithm proceeds as before. A block diagram of the process is shown in Fig. V-2.1.

VI. HIGH RATE PCM - NOISE EFFECTS

Because of the increasing importance of Pulse Code Modulation in the field of communication, it was desired to construct a high speed system for use as an experimental tool. The initial goal was for a system consisting of an A-to-D and a D-to-A converter with a sampling rate of two words/microsecond. This would allow a maximum modulation signal bandwidth of 1mHz.

Each word was to contain five bits (32 levels) which would produce adequate fidelity for most applications. A design was generated incorporating several single bit encoders in series. This design was built completely with intergrated circuits and performed satisfactorily although the sampling rate criteria had to be reduced by an order of magnitude, down to one sample every five microseconds.

To show that the equipment could be useful as a good approximation to an ideal PCM system, relevant data was taken in the presence of additive white Gaussian noise. The data was plotted on graph paper and the system was shown to adhere closely to predicted results indicating that it can serve as a model in future experiments.

Fig. VI-1 shows a Block diagram of the PCM system and Fig. VI-2 indicated the experimental setup. The theoretical output carrier to noise ratio was calculated and is compared to the experimental in Fig. VI-3. The levelling off of the curve at high CNR is due to residual quantization noise, which for five bits is approximately 30 db. The equipment will now be used for further, in depth, work on PCM and related areas.

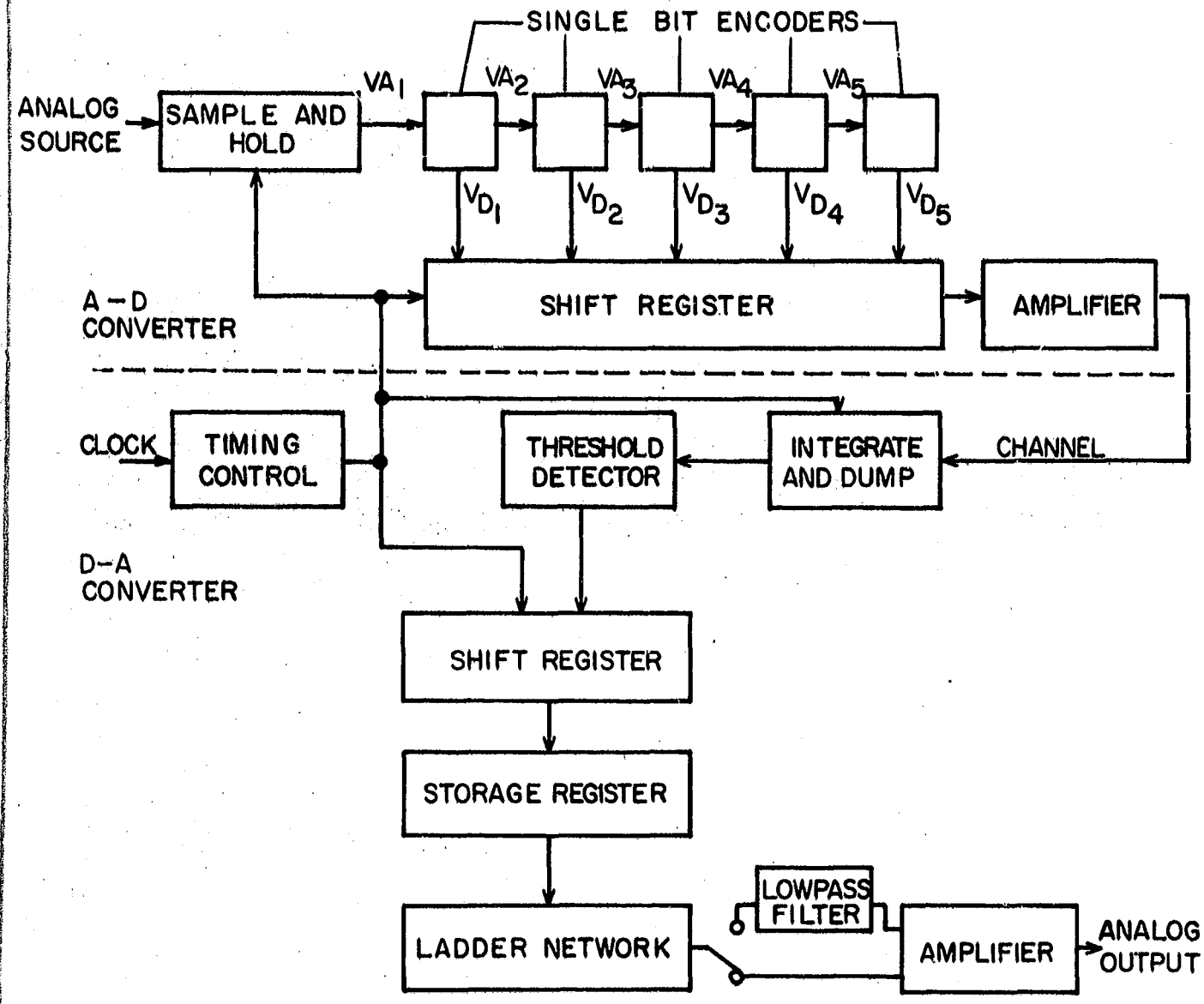

Fig. VI-1 Block diagram of PCM system

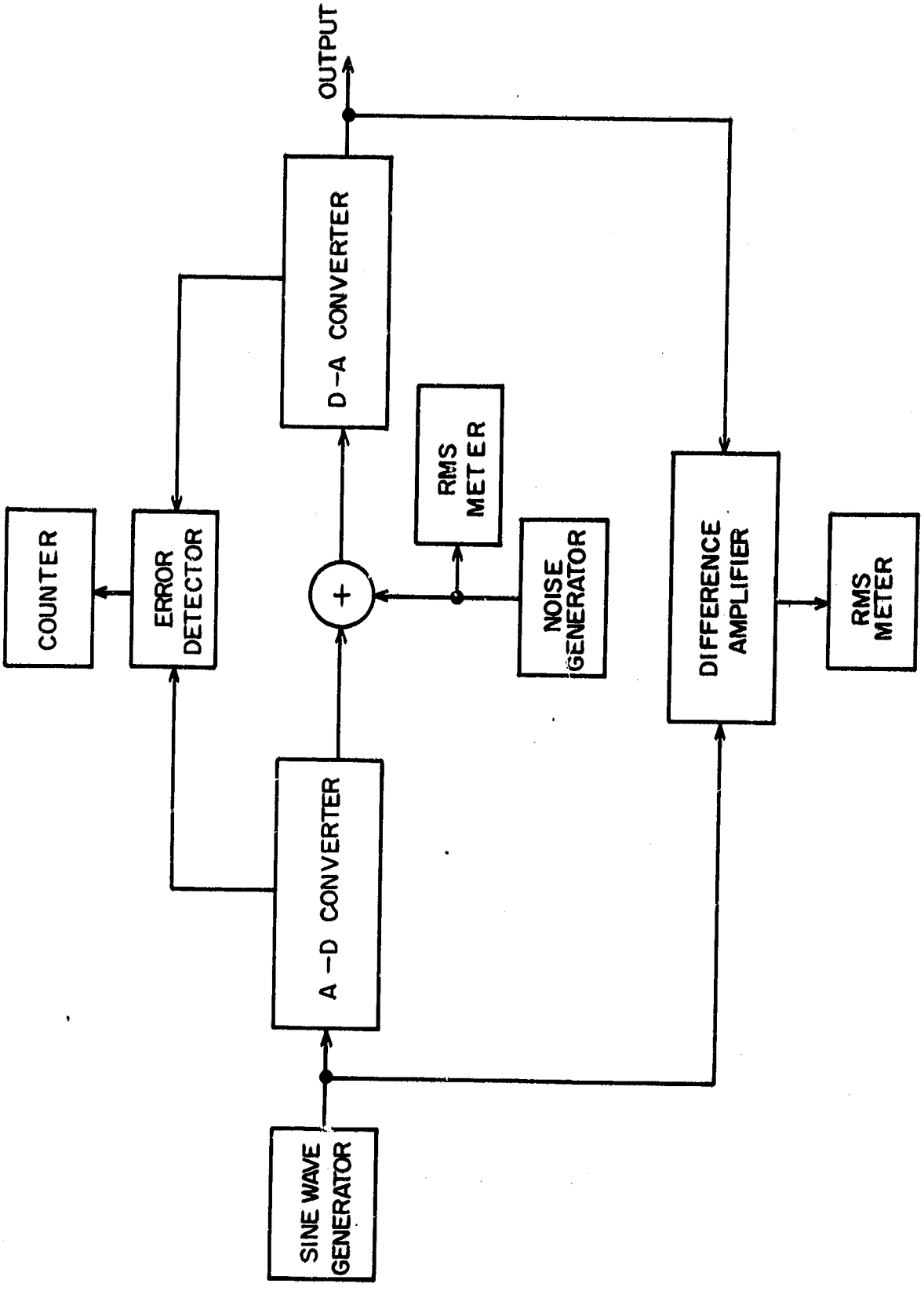

Fig. VI-2 Experimental setup

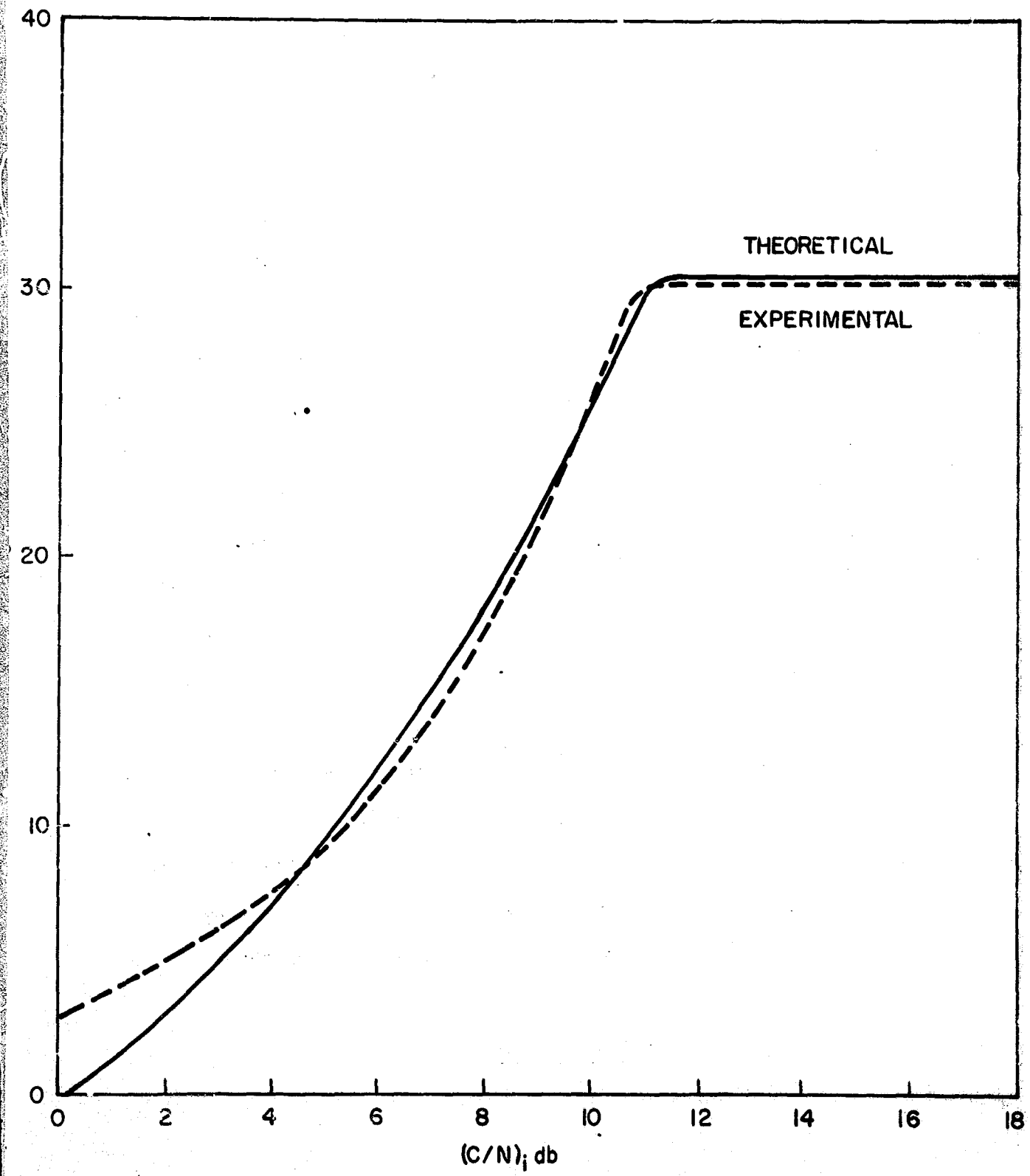

Fig. VI-3 Output signal-to-noise ratio vs. carrier-to-noise ratio.

VII. NEW AND CONTINUED RESEARCH

1. Frequency Demodulation with Feedback.

The "most-likely" noise techniuqe used to determine the threshold and the spikes occurring per second in a PLL has been applied to the FMFB. This program will be continued. The programs goal is to determine the threshold and spike behavior of the FMFB and compare the FMFB with the PLL. In addition the results will be compared to the original FMFB results obtained by Schilling. The basis of this comparison will be equal distortion. One result obtained to date is that the FMFB when operating with gain G = 0 or with infinite gain responds as an FM discriminator. Thus, a gain exists which results in a minimum number of spikes/second. Experimental results will be obtained to supplement the theory.

Hess has shown that theoretically the frequency demodulator with feedback or FMFB should lie midway between the phase locked loop (PLL) and the frequency locked loop (FLL). This means that one limiting form of the FMFB is equivalent to a PLL while another limiting form is equivalent to a FLL. To date most commercial FMFB's have been constructed so as to fall near the PLL end of this range. It is proposed to construct a FMFB capable of being operated at any desired point within the range. This will serve not only to confirm the existance of the postulated FMFB-FLL boundary (the FMFB-PLL boundary has been confirmed by Cassara) but also to explore the previously unreached portions of the FMFB's regions of operation. On the basis of these explorations plus existing theoretical work upon the FLL and the PLL it is hoped to derive a reasonable design theory for the FMFB.

2. Spike Correction in the PLL and FMFB.

The PLL and FMFB outputs indicate a significant increase in the spike

rate for small deviations of carrier frequency from the center of the IF filter. To reduce this increase we will use spike correction techniques to shift the IF filter resonance.

3. Quantized Frequency Locked Loop-Fading Signals.

The second order quantized frequency locked loop (QFLL) reported upon herein will be extended to attempted use as a threshold extending or error reducing detector of fading analog, video, and binary FM systems. The PIB water tank fading channel simulator will be used as a source of controllable fading for these experiments.

Experiments to date with real filtering of noisy binary FM signals ($\beta = 2$) have shown improvements (reductions) at 10^{-5} error rate in the required CNR of 4.5dB through the use of the QFLL over an ideal discriminator alone. In conjunction with proper equalization it is hoped that for fading binary signals at least the same gain will be possible.

4. Quantized 2nd Order Phase Locked Loop.

Based upon the gains realized through the quantization of the amplitude information in the Frequency Locked Loop it is proposed to extend the concept of amplitude quantization to the 2nd order phase locked loop employed as an FM demodulator. The circuitry to perform this quantization has already been developed for the frequency locked loop.

The expected benefits from the quantization are the ability to linearize the phase detector and to reduce the modulation induced clicks (clicks of the second kind). Since with large deviations these signal induced clicks make up a large majority of the total number of clicks it is hoped to achieve a siginificant increase in output S/N for high Δf, below threshold operation.

5. Single Sideband FM.

SSB/FM is currently being investigated to determine if threshold im-

provement techniques can be applied. SSB-FM can be approximated so that one sideband is attenuated rather than eliminated. In this case the bandwidth of the signal can be effectively reduced.

6. Bandwidth Compression.

Bandwidth compression techniques are being studied. The response of bandwidth compressed signals in the presense of noise is to be computed. Some new bandwidth compression devices will be investigated to determine the degree of compression possible and the output SNR.

7. Digital Operations Upon Video Signals.

A series of programs have been written for the PIB PDP8 computer that in conjunction with PIB developed interface equipment allow the transfer of 100 x 100 picture elements from a 35 mm slide to storage in digital form in the tape storage of the PDP8 and subsequent reconversion of the stored digital signal into a picture form.

An additional set of programs allow non-linear processing, digital and analog error introduction, and various types of redundancy reduction operations to be performed upon the digital signals.

These signal processing capabilities will now be used to study the relative errors distortions introduced in video signals transmitted in both analog and digital forms as well as the effect of noise and/or fading upon various redundancy reduction schemes.

8. Recursive Techniques.

Several simulations are now being seen on the recursive techniques developed. Various random number generators with correlated samples have been produced at the algorithm will be tested as if in an actual communications environment.

Further work is being carried forward on direct digital instrumentation

of demodulation methods and for the processing of signals other than for detection such as array processing, data compression and adoptive conditioning and equalization of signal.

Computer programs have been written for simulation and preliminary results are positive.

VIII MASTERS THESES AND DOCTORAL DISSERTATIONS MASTERS THESES

The following Masters Theses of June 1968 were partially supported by this grant:

1. Altman, T., Effects of Noise on PCM
2. Bobsin, J., FM Multipath Interference
3. Dalileo, R., Phase Locked Loops
4. Ergul, F., TV Signals through a Noisy FM Channel
5. Glassman, C., SNR in a Real Limiter
6. Kunzinger, F., Field Effect Transistors
7. Mason, C., Digital Narrowband Filter
8. Refi, J., SNR in an FM Discriminator with Non-Ideal Limiting
9. Schroeppel, E., Diversity Combining
10. Schulman, R ., A study of the Behavior of the Phase Locked Loop
11. Stell, D., Computer Compression of TV Signals
12. Tulunay, E., Antimultipath Modulation Techniques

Ph.D. Dissertations

The following Ph.D. Dissertations of June 1968 were partially supported by this grant:

1. Guida, A., Optimum FM Receivers
2. Milstein, L., Nonparametric Detection
3. Oberst, J., Single-Channel PSK Synchronization
4. Osborne, P., Threshold of the Phase Locked Loop
5. Tepedelenlioglu, N., First Order Analog Frequency Locked Loop
6. Unkauf, M., Second Order Quantized Frequency Locked Loop

IX PAPERS PUBLISHED

1. D. L. Schilling and J. Kuhar, "SNR for Bandbass Limiters", IEEE Transaction of the AES, February 1968.

2. D. L. Schilling and P. Osborne, "Threshold Performance of Phase Locked Loop Demodulators", ICC Convention, 1968.

3. D. L. Schilling and J. Oberst, "Double-Error Probability in DPSK", Proceedings IEEE, June 1968.

4. D. L. Schilling and E. Nelson, "Response of an FM Discriminator to a Digital FM Signal in Randomly Fading Channels", IEEE Transactions on Comm Tech, August 1968.

5. D. L. Schilling and P. Osborne, "Expected Number of Spikes in Phase Locked Loops", ITC 1968.

6. D. L. Schilling and J. Oberst, "Performance of Binary PSK Communication Systems", ITC 1968.

7. D. L. Schilling and J. J. Refi, "Output SNR of an FM Discriminator with NON-Ideal Limiting", ITC 1968.

8. R. I. Pickholtz and R. R. Boorstyn, "A Recursive Approach to Signal Detection", IEEE Transactions on Information Theory Vol IT-14, No. 3 May 1968, pp 445-451.

9. D. T. Hess, "Equivalence of FM Threshold Extension Receivers", IEEE Transactions on Communication Technology, Vol COM-16, No. 5 October 1968, pp 746 - 748.

10. D. T. Hess, "Cycle Stepping in a First Order Phase-Locked Loop", IEEE Transactions on Communication Technology, Vol COM-16, No. 2 April 1968, pp. 255-260.

11. D. T. Hess and K. K. Clarke, "Quantized Second Order Frequency Locked Loop", Convention Record of the Eascon Conference, Washington, D.C., September 1968, pp. 193-197.

12. K. K. Clarke and D. T. Hess - Patent Application "Frequency Demodulator for Noise Threshold Extension" - filed with the U.S. Patent Office, August 15, 1968.